EXPERIMENTAL AND NUMERICAL CHARACTERIZATION OF BONDED JOINTS USING REVERSIBLE ADHESIVES

By

Suhail Hyder Vattathurvalappil

A DISSERTATION

Submitted to
Michigan State University
in partial fulfillment of the requirements
for the degree of

Civil Engineering – Doctor of Philosophy

2020

ABSTRACT

EXPERIMENTAL AND NUMERICAL CHARACTERIZATION OF BONDED JOINTS USING REVERSIBLE ADHESIVES

By

Suhail Hyder Vattathurvalappil

Structural joining of dissimilar materials has recently been recognized as one of the primary challenges limiting the wide acceptance of composite materials in mass-produced vehicles. Joints are considered the 'weak-links' in a structure as they experience complex stress distributions during load transfer and have direct implications on the safety of resulting structural components. This study aims at developing a computational materials design approach of integrating experiments and numerical simulations to better understand the behavior of bonded joints using novel 'reversible adhesives (RA).'

Thermoplastic adhesives reinforced with conductive nanoparticles allow for selective heating of thermoplastics through coupling with electromagnetic (EM) radiations via non-contact methods. This allows for increasing the adhesive temperature above processing temperatures in a short duration which upon cooling forms a structural bond. Hence this process is attractive as it enables quick assembly, removal and re-assembly of joints without the need to heat the entire component. Hence, the term "reversible adhesive (RA)" was coined to indicate the ability of these adhesives to be dis-assembled and re-assembled by selective heating.

RA consisting of Acrylonitrile Butadiene Styrene (ABS) polymer reinforced with conductive nanoparticles, namely ferromagnetic nanoparticles (FMNP - Fe₃O₄), and short carbon fibers (SCF) were developed using melt-compounding. Detailed thermo-mechanical characterization was performed on both the polymer nanocomposites and resulting joints. Also, the effect of repeated EM exposure on degradation of the RA was explored. Surface preparation

studies to enhance structural joint performance was also performed. Lastly, a computational materials-based approach, wherein integration of multi-scale simulations and experiments was developed to explore these novel materials beyond the experimental matrix.

Results indicated that the percolation limit of FMNP to ensure melting and flow during EM exposure was 8 wt.%, and the flow time decreased with increase in FMNP content. ABS adhesive with 16 wt.% FMNP showed good balance of stiffness and strength relative to other concentrations. RA with 16 wt. % FMNP can be heated to its processing temperature of 240°C within 20 seconds under EM heating (200KHz, 1KW). The drawbacks of using Fe₃O₄ nanoparticles as reinforcements (aspect ratio ~1) to enhance mechanical properties was overcome through addition of high aspect ratio short carbon fibers. The results from thermal degradation study of RA indicated that longer exposure to induction heating reduces the overall mechanical properties. However, repeated heating of RA within the processing temperature only effects the ductility as it loses the toughening agent butadiene within ABS. Bonded joints without O₂-plasma surface treatment led to interfacial failures whereas induction-bonded joints with both O₂-plasma and substrate preheating had 15% higher peak loads relative to oven-bonded joints. Finally, a multi-scale computational approach was developed and implemented to explore the design space beyond the experimental matrix and to provide an insight into nano-scale behavior and the local phenomena that cannot be experimentally measured. This work also addresses the limitations and challenges associated with RA. Overall, the integrated experimental and numerical approach such as the one presented in this work creates a benchmark for RA development and can be extended to other thermoplastics, to fully exploit the benefits of these reversible polymers for a wide range of applications.

Copyright by SUHAIL HYDER VATTATHURVALAPPIL 2020 This thesis is dedicated to my parents, sister and to my wife for their continuous prayers and sacrifices

ACKNOWLEDGEMENT

In the name of Allah, the Most Gracious and the Most Merciful

All thanks and praise be to almighty Allah, the lord of the world, the master of day of judgement, the knower of unseen for the successful completion of this thesis. I thank Allah for all the opportunities, trials and strength that have been showered on me to finish writing this thesis.

Personally, I must thank my advisor Professor Mahmoodul Haq. It is his passion for 'structural joining and tailorable materials' that provided the driving force behind my research. He always encouraged me to get trained in all the available facilities related to composite materials at Michigan State University even though some of them were not related to my research. This helped in my overall training and helped me to realize potential paths forward and improvements in my current research. Through my relationship with Professor Haq, I travelled to several technical conferences throughout the United States and presented my work to some of the top scientists in this field. I published this work in a number of esteemed journals both as a first author and as a coauthor. Most notably, I investigated novel reversible adhesives for structural joining technique under careful guidance and tutelage of the leading scientist of structural joining's – Professor Mahmoodul Haq.

I must also acknowledge the members of my thesis committee: Prof. Alfred Loos of the department of mechanical engineering, Prof. Lawrence T Drzal of the department of chemical engineering and material science, and Prof. Weiyi Lu of the department of civil and environmental engineering. In supplement to my advisor Prof. Mahmoodul Haq, these three helped to guide my research program through their valuable suggestion and feedback.

My deepest gratitude goes to all my family members who supported me through the ups and downs of graduate student life. I could not have done it without you. Special thanks to those who helped to see me through from start to finish – my mother Zaida, my father Hyder Ali, my sister Fathima and my wife Salma.

I offer my special thanks to all my colleagues; Mr. Ben Swanson, Mr. Syed Fahad Hassan, Mr. Saratchandra Kundurthi, Mr. Rajendra Prasath Palanisamy and Mr. Erik Stitt for their motivation and sincere help during the graduate program.

This research has been supported financially through a research agreement from the American Chemistry Council (ACC), Plastics division. I would also like to acknowledge the support and guidance of Mr. Michael Day, Project manager (ACC). Additionally, financial support in the form of fellowship awards and assistantship were obtained from department of civil and environmental engineering and the graduate school of engineering. I am grateful to all the support.

TABLE OF CONTENTS

LIST OF TABLESx	ii
LIST OF FIGURESxi	iii
Chapter 1: Introduction	1
1.1. Motivation	1
1.2. Objectives	3
1.3. Background	6
1.3.1. Structural Joining Techniques	6
1.3.2. Electromagnetic Induction Heating	
1.3.3. Polymer Nanocomposites (PNC) as Structural Adhesives	0
1.3.4. Reversible Adhesives & Heating Techniques of Thermoplastic Polymers	
1.3.5. Micromechanical Modeling of Nano Reinforced Polymers	5
1.4. Method/Approach	9
1.5. Organization	
REFERENCES2	23
·	
Chapter 2: Development of Reversible Adhesives ¹	
2.1. Abstract	
2.2. Introduction	
2.3. Experimental Methods	
2.3.1. Materials	
2.4. Adhesive Processing and Manufacturing	
2.5. Mechanical Testing Methods	
2.5.1. Uniaxial Testing	
2.5.2. Impact Tests	
2.6. Monitoring Adhesive Temperature	
2.7. Results & Discussions	
2.7.1. Adhesive Characterization	
2.7.2. Hybrid Reinforcements	
2.8. Conclusions	
REFERENCES4	-2
Chapter 2. Therma Machanical Degradation of Bayersible Adhesives	15
Chapter 3: Thermo-Mechanical Degradation of Reversible Adhesives	
3.2. Introduction 4	
3.3. Experimental	
3.3.2. Processing and Manufacturing	
3.3.4. Temperature Measurement and Induction Heating	
	55

3.4. Results & Discussions	58
3.4.1. Heating Rate Study	58
3.4.2. Thermal Degradation and Corresponding Mechanical Properties	61
3.4.3. Effect of EM Heating on Reversibility/Repeatability	
3.4.4. Investigation into Void Patterns	
3.5. Conclusions	73
REFERENCES	74
Chapter 4: Reversible Adhesive Bonded Single Lap Joints ¹	
4.1. Abstract	
4.2. Experimental Methods	
4.2.1. Materials	
4.2.2. Adhesive Processing and Manufacturing	80
4.2.3. Manufacturing of Single Lap Joints	
4.2.4. Surface Treatment of Adherents and Adhesive Films	
4.3. Mechanical Testing Methods	83
4.3.1. Uniaxial Lap Shear Tests	
4.4. Monitoring Adhesive Temperature	83
4.5. Results & Discussion	84
4.5.1. Induction Heating: Processing Time and Temperature Measurements	84
4.5.2. Mechanical Testing of Oven Bonded Lap-Joints	86
4.5.3. Effect of O ₂ plasma surface treatment	87
4.5.4. Mechanical Testing of Induction Bonded Joints	88
4.5.5. Effect of Adherent Preheating	89
4.5.6. Oven vs Induction Joints: A Comparison	91
4.6. Conclusions	
REFERENCES	95
Chapter 5: Computational Modeling of Reversible Adhesives	97
5.1. Abstract	97
5.2. Introduction	98
5.3. Experimental Details	100
5.3.1. Materials	100
5.3.2. Manufacturing	101
5.3.3. Tensile Tests	102
5.4. Micromechanical Modeling of Nanocomposites	102
5.4.1. Generalized Effective Interphase Model	102
5.4.2. Development of Representative Volume Element	104
5.5. Results and Discussion.	
5.5.1. Determination of Distribution Functions of Short Carbon Fiber	107
5.5.2. Effect of Interphase Properties	108
5.5.3. Effect of Clustering	
5.5.4. Comparison with Experimental Results	
5.5.5. Hybrid Reinforcements	
5.5.6. Effect of Particle Content	
5.5.7. Effect of Aspect Ratio	

5.6. Conclusion	116
REFERENCES	118
Chapter 6: Multi-Scale Modeling of Bonded Joints Using Reversible Adhesives	123
6.1. Introduction	123
6.2. Finite Element Model	124
6.3. Results & Discussion	125
REFERENCES	127
Chapter 7. Massagement of Drassaging Indused Decidual Strains in Devenible Dand	ad Iainta 120
Chapter 7: Measurement of Processing Induced Residual Strains in Reversible Bondo	
7.1. Abstract	
7.2. Experimental Methods	
7.2.1. Materials	
7.2.2. Adhesive Processing and Manufacturing	
7.2.3. Oven and Electromagnetic Induction Joining Technique	
7.2.4. High Definition Fiber Optic Sensors	
7.3. Results & Discussion	
7.3.1. Cooling Rate Measurements in Oven and Induction Bonded Joints	
7.4. Residual Strain Measurements	137
7.5. Conclusion	139
REFERENCES	141
Chantan & Hasling Detential of Dandad Joints Haing Dayansible Adhasiya	1.42
Chapter 8: Healing Potential of Bonded Joints Using Reversible Adhesive	
8.1. Introduction	
8.2. Experimental Procedure	
8.2.1. Materials	
8.2.2. Processing and Manufacturing	
8.2.3. Testing Methods	
8.2.4. Healing	
8.2.5. Fourier Transform Infrared Testing	
8.2.6. Optical Fiber Temperature Measurement	
8.2.7. Thermogravimetric Analysis	153
8.3. Results & Discussion	154
8.3.1. Healing Efficiency	154
8.3.2. Impact Loading	154
8.3.3. Lap Shear Tests	155
8.3.4. Joint Strength	156
8.3.5. Joint Toughness	
8.3.6. Optimum Healing Time for Electromagnetic Heating	
8.3.7. Fracture Analysis	
8.4. Conclusions	
REFERENCES	
	103
Chapter 9: Summary and Conclusions	
9.1. Summary	
9.2. Research Finding's	168

9.2.1. Development of Reversible Adhesives	168
9.2.2. Bonded Joints Using Reversible Adhesives	169
9.2.3. Thermo-Mechanical Degradation of Reversible Adhesives Subjected	d to EM Heating
	170
9.2.4. Computational Modeling	171
9.3. Research Needs	172
9.3.1. Nanoparticle Dispersion Studies	172
9.3.2. Processing Induced Behavior of Bonded Joints	172
9.3.3. Incorporation of robust failure models in the computational framewor	:k 173

LIST OF TABLES

Table 1-1: Advantages and Dis-advantages of induction heating
Table 1-2: Heating mechanisms in Electromagnetic induction heating
Table 3-1: Advantages and Dis-advantages of induction heating
Table 3-2: Heating mechanisms in electromagnetic induction heating
Table 3-3: Case Studies performed in this work
Table 3-4: Infrared wave numbers and its corresponding chemical compounds[8][32][39] 62
Table 3-5: Fe ₃ O ₄ concentrations along the cross section of IZOD fracture surface
Table 5-1: Specimen compositions investigated, nomenclature used: (ABS/micro-/nano-) 101
Table 5-2: Mechanical properties of matrix (ABS), particles (Fe ₃ O ₄ and SCF) and effective interface
Table 8-1: Percentage variation of average peak load and displacement

LIST OF FIGURES

Figure 1-1: Schematic showing multi-scale components in bonded joints made using reversible adhesives
Figure 1-2: Possible heating modes in a conductive workpiece exposed to EM radiations 9
Figure 1-3: Design parameters of polymer nano composites
Figure 1-4: Schematic of nanoparticle clustering and dispersion in polymer matrix
Figure 1-5 Schematic of reversible adhesive and its presence inside a bonded joint
Figure 1-6: True stress-strain curve of ABS thermoplastic
Figure 1-7: Schematic representation of multi-scale modeling
Figure 1-8: Schematic of homogenization using Representative Volume Element (RVE) 17
Figure 1-9: Schematic of FE homogenization based on experiments
Figure 1-10: Schematic showing approach adopted in the study
Figure 2-1: Temperature measurement of adhesive under induction heating process
Figure 2-2: Representative tensile stress-strain plots for all adhesive configurations in this study
Figure 2-3: Elastic modulus of ABS modified FMNP polymer
Figure 2-4: Effect of FMNP content in ABS on (a) Tensile Strength and (b) Strain to Failure 37
Figure 2-5: Effect of FMNP content in ABS on Impact energy of (a) Notched samples (b) Unnotched samples
Figure 2-6: Fracture surfaces showing FMNP dispersion in ABS for varying FMNP content and a constant mix time of 10 min. The black arrows indicate the scale of one micron
Figure 2-7: Effect of short carbon fiber in ABS/FMNP polymer: (a) Tensile Modulus (b) Tensile strength
Figure 2-8: Effect of short carbon fiber in the strain to failure properties of ABS/FMNP polymer

Figure 3-1: Possible heating modes in a conductive work piece exposed to electromagnetic radiations
Figure 3-2: Schematic molecular structure of acrylonitrile butadiene styrene (ABS) 51
Figure 3-3: Induction heating fixture
Figure 3-4: Temperature measurement of reversible polymer under induction heating process . 55
Figure 3-5: Non-conductive specimen housing molds (a) mold for both tensile and IZOD impact coupons (b) Fixture in its closed position
Figure 3-6: Heating rate of PNC under induction heating process – adapted from [36] 59
Figure 3-7: (a) Sensor fiber along the ABS/Fe ₃ O ₄ sample (b) Temperature distribution along 'sensor fiber-length' within the ABS/Fe ₃ O ₄ (16wt.%) sample at varying time intervals
Figure 3-8: a)Heating rate of ABS+16 wt. % of FMnP when exposed to EM radiation b) TGA of ABS+16 wt. % of FMnP
Figure 3-9: FTIR spectra of reversible PNC's exposed to different temperatures by EM heating
Figure 3-10: Reversible PNC's exposed to different temperatures by EM heating (a) Elastic modulus & Yield strength (b) Strain to failure
Figure 3-11: IZOD impact energy of reversible PNC's exposed to different temperatures by EM heating
Figure 3-12: FTIR spectra of reversible PNC's exposed to 3 heat cycles of bulk temperature 240°C
Figure 3-13: Reversible PNC's exposed to 3 heat cycles of bulk temperature 240 °C (a) Elastic modulus & Yield strength (b) Strain to failure
Figure 3-14: IZOD impact energy of reversible PNC's exposed to 3 heat cycles of bulk temperature 240 °C
Figure 3-15: Effect of induction heating on polymer nanocomposites
Figure 3-16: Flow resistance pattern between two fixed plate inside a mold
Figure 3-17: IZOD impact fracture surface for LA-ICP-MS test
Figure 3-18: IZOD Impact fracture surface of reversible PNCs (ABS +16wt.% FMNP) subjected to EMI heating

Figure 4-1: Single lap joint fixture for oven heating process
Figure 4-2: Single lap joint fixture for induction heating process
Figure 4-3: Temperature measurement of adhesive under induction heating process
Figure 4-4: Heating rate of adhesives under induction heating process
Figure 4-5: Time required for processing FMNP embedded ABS in 'adhesive only (no substrates)' and 'lap-joint assembly' configurations
Figure 4-6: Effect of FMNP content in oven bonded joints (a) Peak Loads and Displacements at Failure (b) Failure surfaces of untreated samples
Figure 4-7: Effect of O ₂ plasma treatment: a) Peak Loads and Failure Displacements, (b) Fracture surface indicating cohesive failure in O ₂ plasma treated samples.
Figure 4-8: (a) Peak Loads and Displacements of induction bonded lap-shear joints with varying FMNP content (b) Typical fracture surface for all induction bonded joints
Figure 4-9: Effect of adherent preheating on lap-joint performance. All joints were O ₂ plasma treated and had constant FMNP content of 16 wt.%
Figure 4-10: Load-displacement curve for Oven and induction comparison. Legend: IB-Induction Bonded, OB-Oven Bonded, PH- preheated, NH- No preheat, PT-Plasma Treated, NP-No plasma treatment
Figure 4-11: Single lap shear test fracture surfaces (a) Induction bonded, preheated and plasma treated (b) Induction bonded joint (no preheat and no plasma) (c) Induction bonded after plasma treatment but no preheat (d) Oven bonded (no plasma treatment) (e) Oven bonded after plasma treated
Figure 5-1: Distribution of elastic modulus of interphase region
Figure 5-2: Methodology for development of finite element model
Figure 5-3: Scanning electron microscopy image of tensile coupon (ABS/SCF/Fe ₃ O ₄) fracture surface
Figure 5-4: Representative volume elements (RVE) and corresponding FE models 107
Figure 5-5: (a) SEM image of ABS/CF tensile fracture surface (b) Histogram of SCF aspect ratio 108
Figure 5-6: (a)Modulus of effective interphase at various interphase thickness (b) Effective tensile modulus polymer nanocomposites

Figure 5-7: Fe ₃ O ₄ cluster (a) cluster models considered for RVE generation (b) Particle cluster observed under scanning electron microscopy
Figure 5-8: Effective tensile modulus of ABS/Fe ₃ O ₄ (a) At Different cluster configurations (b) A different aspect ratio (75 percent cluster)
Figure 5-9: Comparison of experimental and FE results of ABS/SCF and ABS/F polymenanocomposites
Figure 5-10: (a) Strategy implemented for hybrid reinforced polymer composites (b) Compariso of experimental and FE results of hybrid reinforced composites
Figure 5-11: Effect of particle content in ABS/Fe ₃ O ₄ and ABS SCF polymer nanocomposites 11
Figure 5-12: Effect of particle alignment and aspect ratio on tensile modulus
Figure 6-1: Overall approach of multi-scale modeling for bonded joints manufactured using EM heating
Figure 6-2: Finite element model of single lap joint
Figure 6-3: Force-displacement curve of single lap bonded joints manufactured using AB adhesive reinforced with 16wt.% fe ₃ O ₄
Figure 7-1: Electromagnetic Induction machine for single lap joint manufacturing
Figure 7-2: Schematic of the support fixture for cooling and the optical fiber sensor in the adhesiv bondline
Figure 7-3: Schematic of the bonded overlap region. The red arrows indicate varying contractio upon cooling of each constituent in its free state
Figure 7-4: Temperature along the adhesive bondline prior to start of cooling cycle
Figure 7-5: Time-temperature plots for oven and induction bonded joints measured at th geometrical center of the adhesive bondline during the cooling process
Figure 7-6: Axial residual strain along the adhesive geometrical center in oven and inductio bonded single lap joints
Figure 8-1: Schematic (enlarged) representation of Single Lap Joint
Figure 8-2: Experimental Methodology
Figure 8-3: Electromagnetic Induction Heating Setup

Figure 8-4 (a) Representative curves for Force and Energy vs Time (b) Indentation in the uppe substrate (Specimen Top View) (c) Force vs Displacement curve showing the maximum
displacement of the tup
Figure 8-5. Comparison of load and displacement bearing capability in similar joints
Figure 8-6: Representative Load-Displacement Curves for different cases
Figure 8-7: FTIR readings of reversible adhesive exposed to various temperatures by EM heating
Figure 8-8: Fracture surfaces in baseline, impacted and induction healed adhesive joints 161

Chapter 1: Introduction

1.1. Motivation

Structural joining of dissimilar materials has recently been recognized as one of the primary challenges limiting the wide acceptance of composite materials in mass-produced vehicles [1]. Joints are considered the 'weak-links' in a structure as they experience complex stress distributions during load transfer and have direct implications on the safety of resulting structural components [2]. A change in design philosophy wherein the behavior of the joints could be tailored to control the overall structural behavior, allow for light weighting, and meet assembly-line requirements is of immediate interest to automotive industry. This study aims at developing a computational materials design approach of integrating experiments and numerical simulations to better understand the behavior of bonded joints using novel 'reversible adhesives.'

Adhesively bonded joints offer the best route for light-weighting by eliminating fastener weight, and associated stress concentrations due to material discontinuity. Thermoplastic adhesives reinforced with conductive nanoparticles allow for selective heating of thermoplastics through coupling with electromagnetic (EM) radiations via non-contact methods. This allows for increasing the adhesive temperature above processing temperatures in a short duration which upon cooling forms a structural bond. Hence this process is attractive as it enables quick assembly, removal and re-assembly of joints without the need to heat the entire component. Hence, the term 'reversible adhesive (RA)' has been coined to indicate the ability of these adhesives to be disassembled and re-assembled by selective heating.

The induction heating process has been adopted by the composite industry in the last couple of decades, mostly for curing fiber reinforced composites. Most of the conventional non-contact induction heating techniques utilized metallic mesh susceptors embedded within the thermosetting

plastics[3][4]. Similarly, electromagnetic induction has been used for welding of carbon fiber reinforced thermoplastics [5][6][7]. Recent studies have showcased the potential of Electromagnetic Induction (EMI) heating for rapid processing and selective heating of thermoplastics, namely reversible adhesives [8]–[10]. The use of graphene nanoplatelets (GNP) in thermoplastics and the use of variable frequency microwave radiations to activate the adhesives has been reported [2]. Similarly, the use of ferromagnetic particles in thermoplastics and activation using eddy currents/induction heating have also been reported [9], [11]–[14].

Most of the reported work has focused on the effect of nanoparticle concentration on resulting heating times and material properties. Detailed understanding of structure-property relations, effect of multiple cycles of heating and cooling and effect of excessive exposure to EM radiations are not fully reported. Furthermore, the effect of nanoparticle dispersion, and hybridization of nanoparticles and its effect on adhesive and resulting joint properties have not been reported. This leads to a huge design space for this extremely 'tailorable material'. An 'integrated experimental and computational approach,' also known as computational design of materials adapted in this work is to aid in better understanding of this material and to predict the behavior of the adhesive and the resulting joints beyond the experimental data.

The computational methodology for mechanical behavior of heterogeneous materials, specifically the nano-meso-macro continuum scale multiscale modeling of polymer nanocomposites is well documented [15]. Nevertheless, the computational modeling material of thermal degradation due to heating of polymer surrounding the nanoparticles, material (mass) loss due to degradation upon exposure to electromagnetic radiation are non-existent. Also, while the literature on computational modeling of the interaction of carbon fiber composite laminates to EMI

heating [16][17] exists, multi-scale modeling (nano-meso-macro) that incorporates damage induced due to processing and its effects on structural properties are non-existent.

1.2. Objectives

The goal of this study is to develop a realistic computational tool that can predict the performance of bonded joints made using reversible adhesives (RA). This multi-scale computational tool will be experimentally validated at every length (nano, meso and macro) scale, and will be used to identify the optimum material properties for a wide range of applications.

In this study, Acrylonitrile Butadiene Styrene (ABS, CYCOLACTM Resin MG 94, SABIC®), an amorphous thermoplastic polymer was reinforced with ferromagnetic nanoparticles (FMNP) and/or short carbon fibers (SCF) to obtain 'Reversible Adhesives'. ABS was selected for its excellent toughness provided by the polybutadiene phase grafted to the acrylonitrile styrene matrix. Additionally, ABS provides a good balance between cost, mechanical properties, chemical resistance, ease in processing and aesthetics [18]. It is widely used in various domains including automotive, consumer market, electronics and sports industry. FMNP particles and carbon fibers were used as conductive reinforcements as they react with EM radiations to produce resistive/Joule's heating. Although FMNP's do not augment the mechanical properties owing to an aspect ratio of ~1, it's capable of providing additional heating modes such as Neel's effect and Brownian heating(Hysteresis loss)[19]. The short carbon fiber (CF) provides the larger aspect ratios to enhance the strengths and ductility. The hybridization of short CF and FMNP will provide necessary synergy for rapid/selective heating along with enhancement of mechanical properties.

The conductive reinforcements in a thermoplastic polymer act as nano heaters, when exposed to the EM radiations to melt the surrounding polymer. This enable rapid assembly and disassembly of bonded joints. However, the heterogeneities introduced in the material increases the complexity

to characterize and predict the response of bonded joints made using reversible adhesives via EMI heating. The heterogeneities include mechanical and thermal behavior of conductive reinforcements and its morphology and orientation in the thermoplastic polymer. These material level heterogeneities are exacerbated by the thermomechanical degradation introduced due to EMI heating. SEM images of IZOD impact fracture surfaces confirms the presence of voids after EMI heating. The micromechanical model developed in this study will account for these material complexities. These models will be validated by experimental testing to reduce the errors that will be carried to the macro level modeling.

Single lap joints were manufactured using RA via EMI heating. Single lap joints were considered as a macroscopic model due to its simple design and manufacturing easiness. The residual strains developed during the manufacturing was monitored and measured using a high definition optical strain sensor embedded in the bondline to understand it's significance in the lap joint response. A computational model was developed and was validated with the aid of aforementioned experiment to account its effect in the overall joint behavior.

The multi-scale methodology adopted in this study is shown in Figure 1-1. The proposed work focus on developing computational models at each scale and thereby predicting the realistic bond performance. Scanning electron microscopy, atomic force microscopy images were used to model the representative volume elements (RVE) at nano/micro scale. The mismatch of modeling results with experiments can be attributed to the assumptions incorporated in the models. However, it is important to compare with experiments, so that the errors can be arrested in propagating to next levels.

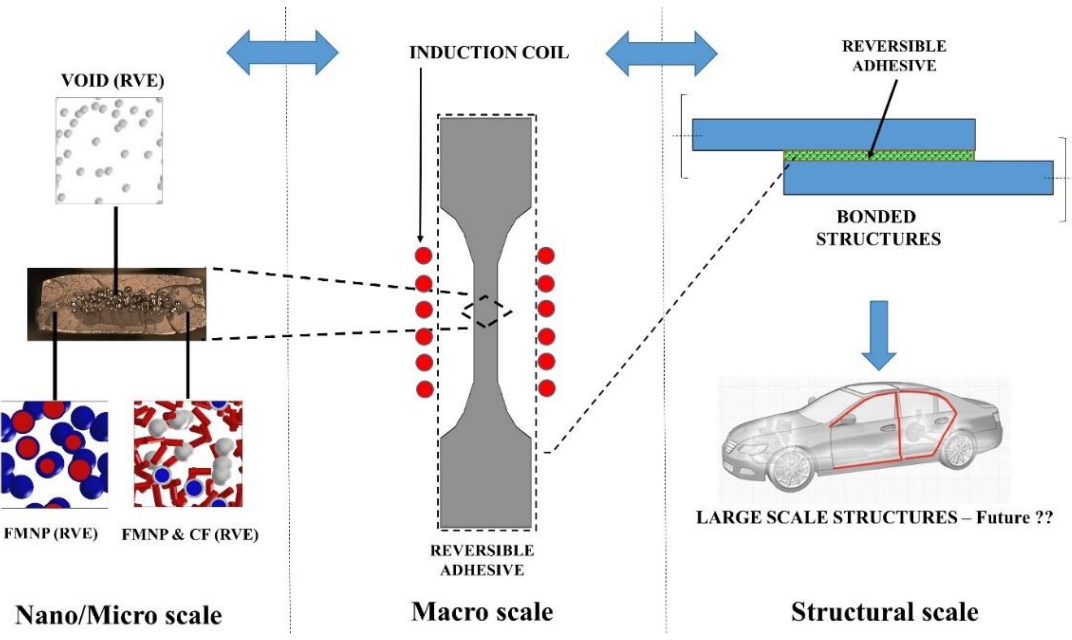


Figure 1-1: Schematic showing multi-scale components in bonded joints made using reversible adhesives

Although the main theme of the work focus on developing the computational model for bonded structures manufactured using EMI heating, experimental investigations were carried out at each length scale to understand the mechanisms contributing to the resulting behavior, and to use the observations and measurements as inputs to the computational model. The computational models once experimentally validated will act as design tools to predict the behavior beyond the experimental matrix studied in this work. Furthermore, the computational tools will provide a launch pad to explore the optimum concentrations of hybrid reinforcement for any application. Overall, the outcome of this work will help in the development of reversible adhesives, bonded joints and crash structures in a rational manner (with a degree of confidence) thereby increasing the safety and reliability of resulting structures.

1.3. Background

1.3.1. Structural Joining Techniques

Structural joining is the critical aspect in vehicle design to facilitate structural integrity and light weighting. An ideal load bearing structure does not contain any joints (monocoque) that could be a possible site of failure. However, manufacturing processes and assembly limits the maximum size of components and joint's have become an inevitable part of the structure. Furthermore, it's almost impossible to manufacture an entire structure such as a car or an airplane out of single material. In addition to comfort, light weighting, aesthetics and economic reasons, another factor that drives the design of automotive vehicles is the environmental emissions. Emissions are directly related to the weight of the structure. Several efforts in light weighting are visible in current automotive segments by the introduction of novel smart materials and joining techniques.

Incompatibility in direct transferability of conventional joining techniques to join composite materials lead to the development of novel joining techniques involving composites material as one of the materials to be joined. Joining can be broadly classified into four main categories. (i) Mechanical fastening (ii) Adhesive bonding (iii) Welding/fusion bonding (iv) Hybrid joining techniques.

Mechanical fastening is one of the most widely used joining techniques due to its simplicity[20]. Unlike the welding process it makes use of additional components such as fasteners or rivets for the joint formation. Although this joining technique can be employed for all the material types, it involves several drawbacks. Some of the detrimental factors involved in using mechanical fasteners are given below:

• Drilling of holes and stress concentration associated with it. (Strong A. Brent: high performance and engineering thermoplastic composites. Technomic Pub., 1993.)

- Weight of the metallic fasteners
- Time and labor requirements for drilling holes.
- Delamination in composite materials occurred during drilling.
- Differential thermal expansion between fasteners and composites.
- Water/foreign particle intrusion between fastener and substrates where complete sealing is desired.

Corrosion

Adhesively bonded joints using thermosetting adhesives is preferable over the mechanical fastened joints as it eliminate the stress concentrations associated with fasteners and results in a uniform load flow over the bonding region. However, bonded joints require surface treatment of the substrates to be bonded prior to the bonding process for following reasons:

- Elimination of contaminants
- Surface wetting
- Chemical functionalization for enhanced bonding
- Increased surface roughness (for mechanical interlocking and enhanced surface area)

Fusion bonding of thermoplastic hot melt adhesive offers potential solutions to replace the mechanical fasteners and thermosetting polymers. In a fusion bonding technique, the polymeric adhesive between the components to be bonded is heated to its viscous/molten state. The molten adhesive is then cooled for the joint consolidation. The three most promising fusion bonding techniques such as thermal welding, friction welding and electromagnetic welding were described in great detail by Ali et.al.[21]. Different physical mechanisms involved in fusion bonding process such as heat transfer, crystallinity and consolidation aspects for modeling purposes play a vital role

in resulting joint behavior [21]. Nevertheless, fusion techniques can cause damage to substrates due to the heat and the mechanical stresses due to fusion techniques

1.3.2. Electromagnetic Induction Heating

It was since the late 1980's, researchers started investigating the induction heating technique for the processing of fiber reinforced polymer composites. Induction heating can be used to process the thermoplastics and thermoset polymer compounds. However, it requires certain conductive susceptor particles/fibers/fabrics embedded within the polymer to transform the electromagnetic energy to heat. The advantages and disadvantages of induction heating is described in Table 1-1.

Bayerl et al [22] summarized the principles of induction heating system with respect to the polymer composites outlining various parametric influences, recent research activities, computational simulation of induction heating, novel ideas and future developments.

Table 1-1: Advantages and Dis-advantages of induction heating

Advantages	Dis-advantages	
Localized heating	High capital investment	
Low operating costs	Restricted to conductive work piece	
Very short heat up times		
Environmentally sound	Work piece shape and size is dependent on	
Reduced energy consumption	coil size and shape	
Optimized consistency		
Improved product quality and productivity		

Induction Heating Mechanism

Electromagnetic induction heating is based on the principles found by Michael Faraday in 1831[23]. According to EM phenomena, a voltage is induced in the conductive work piece when placed in a changing magnetic field. In other words, it describes how an electric current produces magnetic field and how a changing magnetic field produces electric current in a conductor. The possible heating modes produced in a conductive work piece when exposed to EM radiations are shown in Figure 1-2.

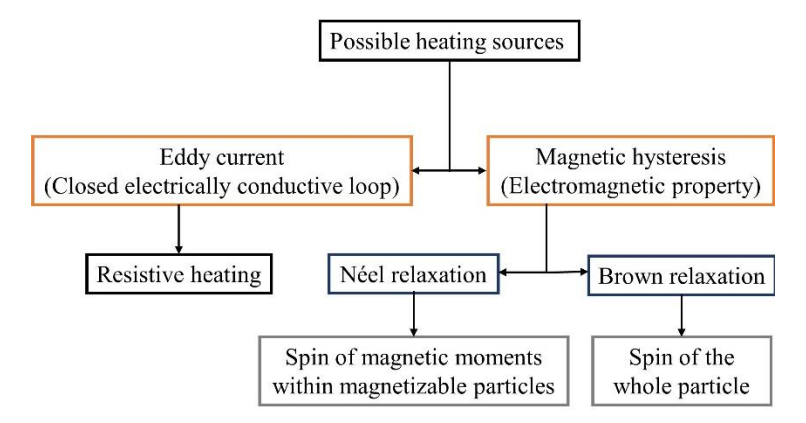


Figure 1-2: Possible heating modes in a conductive workpiece exposed to EM radiations

A typical EMI heating system consists of a power circuit that converts wall outlet 50/60 Hz AC supply to high frequency 10-400 kHz current inside an induction coil to generate a time-harmonic magnetic field within the coil. This field in turn induces eddy currents in any conductive work piece placed in or around the coil (Joule heating) in addition to the magnetic hysteresis losses if the work piece has magnetically susceptibility. These losses are responsible for heat generation within the material bulk volume. The key factors that influence the eddy current and magnetic hysteresis losses as documented in literature are summarized in Table 1-2.

Table 1-2: Heating mechanisms in Electromagnetic induction heating

	Eddy current	Magnetic hysteresis	Reference
	Eddy current	wagnetie Hysteresis	Reference
Precondition for	Closed electrically	Ferromagnetic	[24][5]
induction heating	conductive loop	properties of the	
		susceptor	
Driving mechanism	Induced current,	Magnetization	[24][25][26]
	electric field polarity	reversal (Brown and	
	reversal	Neel relaxation)_	
Heat generation	Resistive and	Friction losses	[26][27][28]
	dielectric heating		
Limitations	Penetration depth	Curie temperature	[24][28]
Side effects	Density increase due	Density increase due	[24]
	to susceptors	to susceptors	
Exemplary susceptors	Carbon fiber fabrics,	Particles of iron,	[29]
	metal grids and metal	nickel and cobalt	
	coated fibers.	alloys, carbon fiber	
		fabrics.	

1.3.3. Polymer Nanocomposites (PNC) as Structural Adhesives

Polymer nanocomposites (PNC) consist of an organic polymer matrix reinforced with nano-scale fillers. The fillers may be of different morphology such as spheres, nanorods, nanotubes, platelets, fibers and so on. Typical size of nanofillers ranges between 0.1nm and 100nm at least in one dimension [30].

Controlled and optimum reinforcement of polymer resins using filler particles can enhance the thermomechanical properties in a desired manner. Design considerations of thermo-mechanical response in PNC depends on several factors as shown in Figure 1-3. Crosby et al.[30] discretized the polymer nanocomposites to three major components namely polymer matrix, nanoscale reinforcements and interfacial materials to enhance the dispersion of fillers/nanoparticles within the matrix.

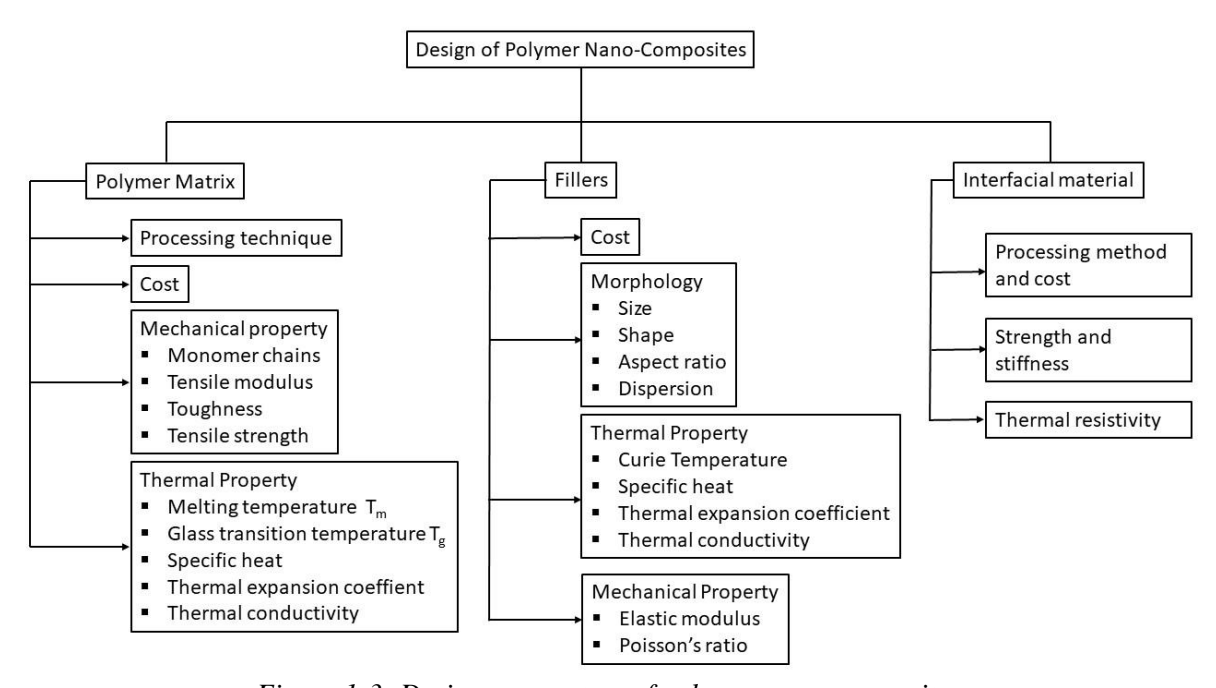


Figure 1-3: Design parameters of polymer nano composites

Dispersion of nanoparticles is a major challenge in the characterization of PNC. Dispersion of nanoparticles in polymer is analogous to dispersing talcum powder in honey. In most cases nanoparticles tend to cluster/attract to other similar particles. This can be attributed to many reasons including the following: 1) Vander Waals force of attraction: - Nano sized materials have high surface area and thereby more surface atoms compared to their bulk counterparts. These atoms in the surface have free valence electrons and make it more active for adsorption with other materials or between each other. 2) Energetics: - Particles with nanoscale dimensions experience smaller levels of repulsion. 3) Magnetic attractions: - Nanoparticles with magnetic susceptibility

can result in clustering. One way to improve the dispersion is to functionalize the nanoparticle such that they repel each other and have affinity to the host matrix. A schematic of the clustering and dispersion of nanoparticles in the polymer matrix is shown in Figure 1-4.

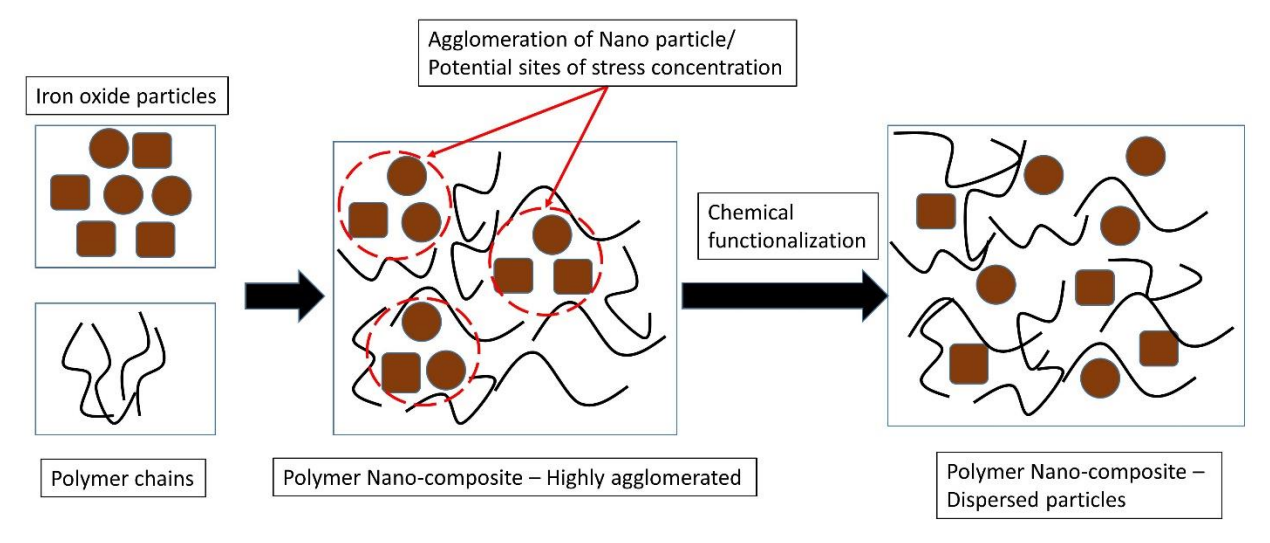


Figure 1-4: Schematic of nanoparticle clustering and dispersion in polymer matrix

1.3.4. Reversible Adhesives & Heating Techniques of Thermoplastic Polymers

Thermoplastic adhesives reinforced with conductive nanoparticles allow for selective heating of thermoplastics through coupling with electromagnetic (EM) radiations via non-contact methods. This allows for increasing the adhesive temperature above processing temperatures in a short duration which upon cooling forms a structural bond. Hence this process is attractive as it enables quick assembly, removal and re-assembly of joints without the need to heat the entire component. Hence, the term "reversible adhesive (RA)" was coined to indicate the ability of these adhesives to be dis-assembled and re-assembled by selective heating.

In general, any thermoplastic polymer can be used as reversible adhesive. However, thermoplastics are generally structurally deficient than thermosets. Furthermore, most thermoplastics are insulators and do not respond to any EM radiations. Hence, they are not commonly used in demanding structural applications. Conventional practice of using thermoset

polymers as adhesives provides good structural bond but also acts as a 'permanent' joint and hinders the disassembly, repair and maintenance of resulting joints. An alternative and effective approach is to design adhesives which are reversible, recyclable and can sustain required structural demands. An effective method of achieving this approach is to disperse conductive particles within a thermoplastic polymer matrix[19], [31]–[35]. Each of these particles can act as 'individual heaters' when exposed to electromagnetic (EM) radiation leading to melting/flow of the surrounding thermoplastic, the extent of which depends upon the EM characteristics of the polymer, nanoparticle type, its concentration, sample geometry, EM coil, EM apparatus (power, frequency) and exposure time[36].

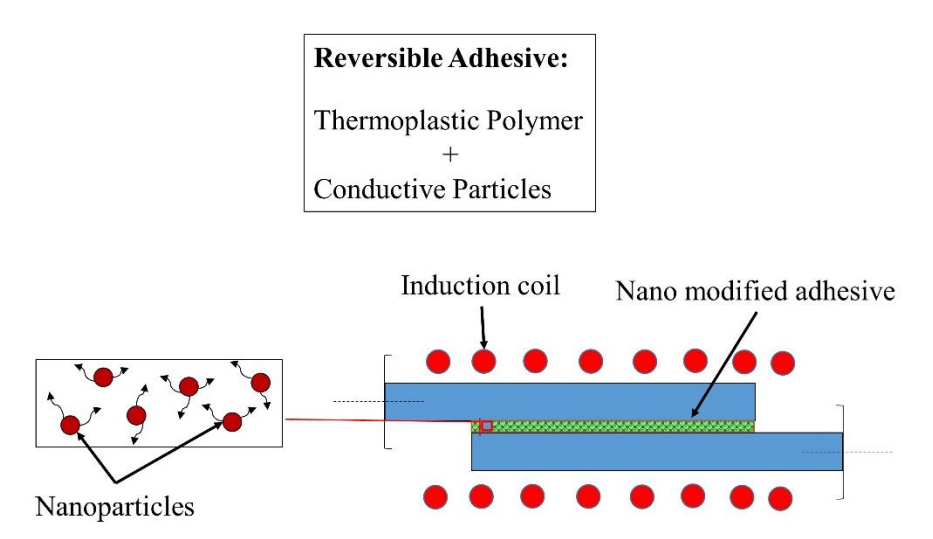


Figure 1-5 Schematic of reversible adhesive and its presence inside a bonded joint

In this work, the term 'reversible adhesive' was coined only for thermoplastic adhesives reinforced with conductive particles. The addition of nanoparticles not only enhances the effective mechanical properties of reversible adhesives but they also interact with the EM radiations to enable rapid heating of the adhesives. This allows for rapid assembly, dis-assembly, and reassembly of bonded joints.

Mechanical Properties of Thermoplastic Polymer

The mechanical properties of amorphous thermoplastics such as ABS (acrylonitrile butadiene styrene) are well documented in the literature. Figure 1-6 shows the true stress-strain response for ABS plastic. The linear elastic behavior for this material (Point A) is only for small strains (≤0.03). This phase of stretching is due to the intermolecular interaction (Van der Waal forces) between the molecular chains wherein it rotates and translate with respect to one another in an elastic fashion.

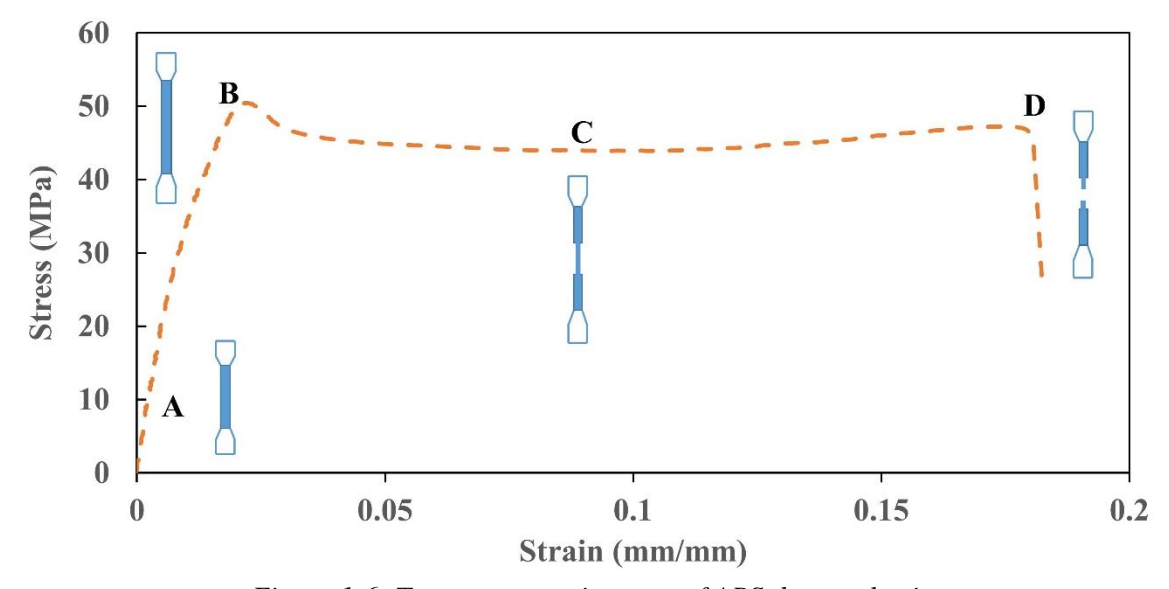


Figure 1-6: True stress-strain curve of ABS thermoplastic

Upon further loading, the stress within the material increases and localized zones will be developed wherein the stresses are large enough to overcome the intermolecular forces to slide or rotate the chains into new positions. The localized zones created in this non-linear visco-elastic phase percolates through the material until the entire material reaches plasticity. At this point the material deforms and flows without any further increase in stress and is called the yield point (Point B).

Beyond the yield point, the stress required for further polymer deformation decreases. This phenomenon is called as strain softening. It indicates that the intermolecular barriers for further

rotation/translation of molecular chains decreases due to localized structural changes. As the load increases, the initially random oriented chains will start to align themselves in the direction of stretching (Point C). Once all the polymer chains reach their maximum extensibility, the strain hardening starts and continues until the material fails (Point D).

1.3.5. Micromechanical Modeling of Nano Reinforced Polymers

Micromechanical modeling of materials is one of the most useful tools in composite/complex/tailorable material analysis. It allows for a deeper understanding of complex materials and phenomena considering the realistic variation in heterogeneities, such as particle sizes (morphology), distribution and material nonlinearities. These micromechanical models can be used to predict effective/homogenized material properties for the one length scale to the next. Hence, multi-scale modeling that links structural behavior to local material behavior can be created. In this work, for micromechanical modeling of reversible adhesives, namely a thermoplastic (ABS) polymer is reinforced with ferromagnetic nanoparticles (Fe₃O₄, FMNP) and short-carbon fibers (SCF). The key micromechanical modeling parameters are as follows.

- Weight/volume fraction of particles.
- Number of inclusions (Dispersion).
- Morphology of nano/micro particles.
- Aspect ratio of the nano/micro particle.
- Interface property between the particles and matrix

The micromechanical models were developed in both Mean Field (MF) Approach and Finite Element (FE) Approach. The homogenized material properties of adhesive were then compared to the theoretical models and experimental data. The goal of this work was to take the homogenized property of micromechanical model into second level of multi-scale analysis,

namely into the lap shear model, to effectively predict the macroscopic behavior such as the distribution of stresses at the bond line thickness as shown in Figure 1-7.

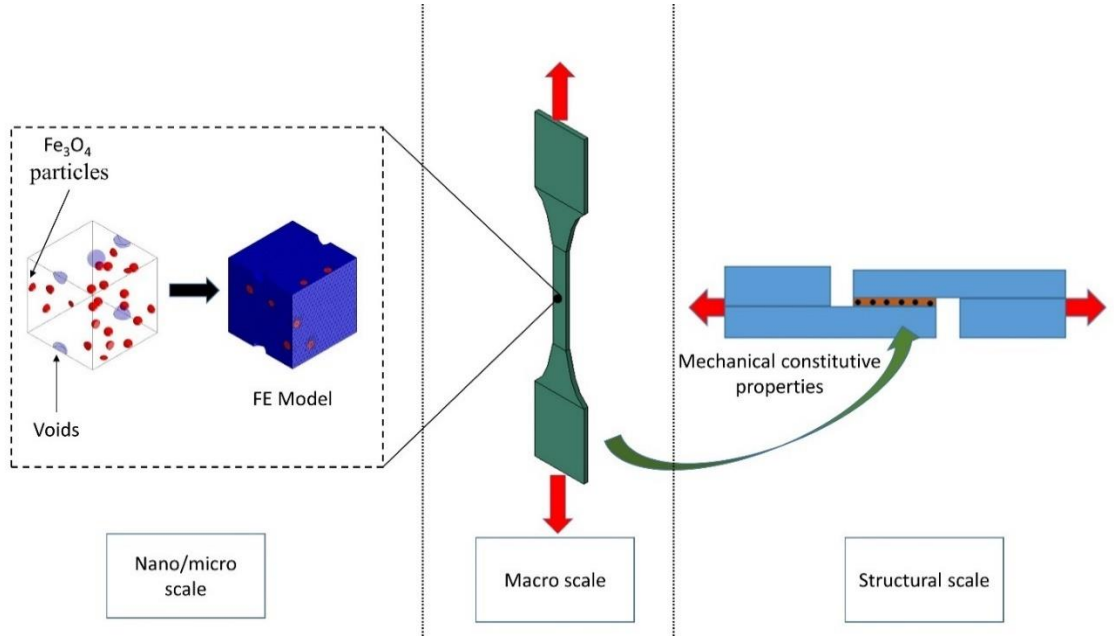


Figure 1-7: Schematic representation of multi-scale modeling

Micromechanical modeling tasks were established in two ways a) Theoretical MF models (ex: Mori-Tanaka model) and b) Representative Volume Element (RVE) studies using FE. The two methods were validated with experiments prior to transfer of information to the next length scale in multi-scale modeling. In both the methods, the RVE was used to represent the heterogenous medium and the volume average properties obtained from RVE was used as homogenized property for macroscale modeling. The schematic of this approach is given in

Heterogenous Medium

Equivalent Homogenous Medium

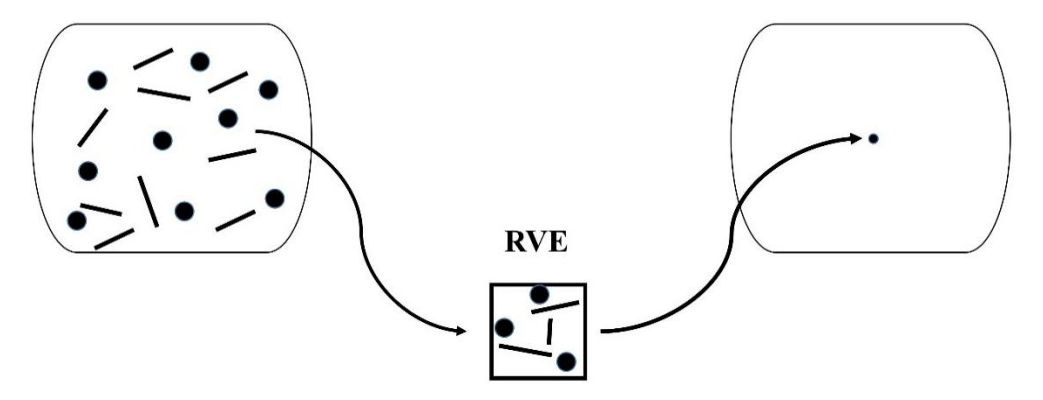


Figure 1-8: Schematic of homogenization using Representative Volume Element (RVE)

At nano/micro scale, the constituents that are present in the polymer nanocomposite are FMNP + SCF in ABS resin. The FMNP used in this work was not surface treated or chemically functionalized to be compatible with host ABS polymer. This was by design to obtain the baseline performance using 'as received' FMNP. Further improvements will only showcase the enhancement of the material. The drawback of using non-functionalized material is it can effect dispersion and cause agglomeration. One technique adopted in this study to improve the dispersion was to increase the mix times in DSM extrusion. The aspect ratio of FMNP's were ~1 and as such the orientation doesn't play any role in augmenting elastic modulus. In the case of short carbon fibers, the fibers were randomly oriented as the orientation and dispersion of SCF cannot be controlled using the DSM extrusion used in this work.

Micromechanical modeling using RVE has been widely applied in polymer nanocomposites to predict the material behavior [37]–[40]. FE based RVE can provide detailed understanding of the phenomena governing the stress-transfer, deformation and failure initiation within the constituents within the RVE. Also, robust plasticity and damage models can ben assigned to realistically model the material behavior. In this work, periodic boundary conditions were assigned to these RVE's as it represents the infinitely repeating subset of the material volume.

Periodicity was assigned in all the three axes to the RVE using commercially available FE software Digimat ® and ABAQUS ®. Once the periodic boundary condition (PBC) equations were assigned to the surface nodes of the RVE using equation constraints in ABAQUS®, an average strain was applied to RVE by introducing a displacement control to the PBC equations. In order to calculate the equivalent homogenized model in macroscale, energy equivalence was enforced between the micro and macro model. This resulting equation is given in Eq. (1) [39]

$$\left(\sigma(X,y):\varepsilon(X,y)\right)_{RVE} = \Sigma(X):E(X) \tag{1}$$

Where $\sigma(X,y)$ and $\mathcal{E}(X,y)$ represent the micro scale stresses and strains, $\Sigma(X)$ and $\Sigma(X)$ are the macro scale stresses and strains. An effective stiffness tensor was calculated based on the strain applied and the average macro stress developed in the RVE. The average macro stresses can be calculated using volume integration of the RVE as shown in Eq. (2)

$$\Sigma(X) = 1/V \int \overline{m} \sigma(X, y) dV \tag{2}$$

The effective stiffness tensor can be calculated $Q^{H}(X)$ can be calculated from based on Eq. (2) and average strain applied as shown in Eq. (3)

$$Q^{H}(X) = (\sum(X))/(E(X))$$
(3)

In this work, the nanoparticle detachment strength was modeled using the closed form solution proposed by Salviato et al.[41]. This model provides a critical debonding stress beyond which the spherical reinforcement de-bond from the matrix.

Reversible adhesives subjected to electromagnetic induction heating (EMI)

One of the drawbacks of EMI heating of polymers embedded with conductive particles is that the polymer surrounding the particle heats up faster than the rest. This can lead to degradation of polymer surrounding the nanoparticle. Also, as the bulk temperature of the polymer increases, low melting point constituents within the polymer may start to evaporate/degrade. This leads to

formation of micro/meso scale voids in the bulk polymer as shown in Figure 1-9. Furthermore, the adhesive coupons after DSM extrusion contain less reinforcements at the edge of the coupon due to skin effect caused due to polymer flow. Hence, the reinforcement concentration is higher in the center of the bulk adhesive coupon relative to its edges.

The average clustering of reinforcement is dependent on its concentration within the ABS polymer. The RVE model can be validated based on the cluster pattern observed in the SEM or by increasing the size of one FMNP to an average size of the cluster. X-ray diffraction technique was used to quantify the concentration of reinforcements in cross section(c/s) of the tensile coupon subjected to EMI heating.

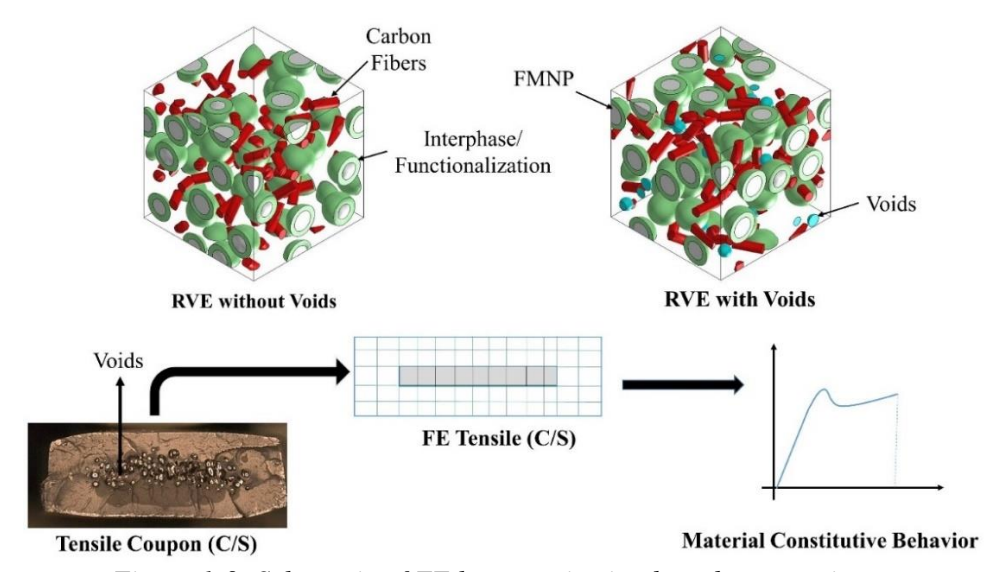


Figure 1-9: Schematic of FE homogenization based on experiments

1.4. Method/Approach

The goal of this study was to understand the potential of reversible adhesives for structural bonding applications and to develop a computational predictive tool that will allow for better design of resulting bonded joints. Detailed experimental characterization aided with electron microscopy measurements were used to develop a computational framework to better understand and predict the behavior of these complex material. A multi-scale model was developed to predict

the structural properties of bonded joints manufactured using EMI heating. The computational model will also account for the significant heterogeneities observed in the nano/micro scale such as morphology, interphase and agglomeration of reinforcements. It should be noted that the study focused on validating the computational models developed in each scale using experiments. A schematic of the overall workflow is shown in Figure 1-10.

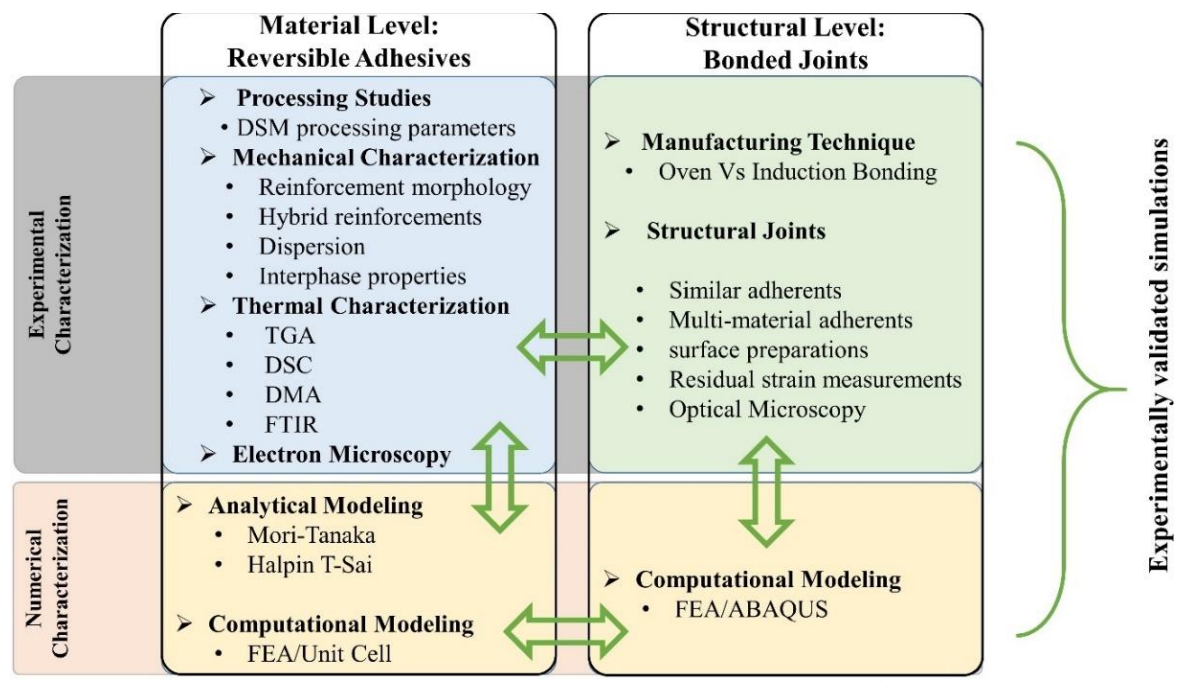


Figure 1-10: Schematic showing approach adopted in the study

The study consisted of following tasks:

I. Processing and Characterization

- a) Mechanical and thermal characterization of reversible adhesives with ferromagnetic nano particles (FMNP) and short carbon fiber (SCF) reinforcements.
- b) Degradation study of the reversible adhesives upon exposure to electromagnetic induction heating using tensile and IZOD impact property characterization.

II. Micromechanical modeling

- a) Develop RVE's for computational modeling that can accurately represent the heterogeneities, such as their morphology, distribution, clustering, interface, voids, and material properties of reversible adhesives with the aid of electron microscopy tools.
- b) Experimental validation of RVE's at material level.

III. Single Lap Joint Manufacturing Using Electromagnetic Induction Heating

- a) Characterization of single lap joints manufactured using electromagnetic induction heating based on varying EMI exposure time, surface treatments and adherent preheating.
- b) Determination of manufacturing induced thermal residual stresses in bulk adhesive material and at the bi-material interface with respect to different cooling times in single lap joints.

IV. Multi-Scale Modeling

a) Homogenized RVE representing the nano/micro scale of the reversible adhesive was used to predict the behavior at macro-scale structural behavior of a single lap joint.

1.5. Organization

The dissertation has been organized into eight chapters. The first chapter introduces the work with a brief background, description of objectives and methods adopted in this work.

- Chapter 2 reports the study on development of reversible adhesives, its processing and characterization.
- Chapter 3 provides the thermo-mechanical degradation study conducted on reversible adhesives subjected to electromagnetic radiations.
- Chapter 4 reports the development of bonded joints manufactured using reversible adhesives and its characterization.

- Chapter 5 reports the numerical and analytical models to predict the mechanical properties of reversible adhesives (material level)
- Chapter 6 provides an overview of the numerical models to predict the structural behavior of bonded joints.
- Chapter 7 reports the manufacturing induced residual strain development in induction and oven bonded joints.
- Chapter 8 reports the healing potential of reversible adhesives on bonded joints subjected to impact loading.
- Finally, chapter 9 provides concluding remarks, research needs and recommendations.

REFERENCES

REFERENCES

- 1-[1] Workshop report, "Light-Duty Vehicles Technical Requirements and Gaps for Lightweight and Propulsion Materials," 2013.
- 1-[2] M. Haq, E. G. Koricho, A. Khomenko, R. Gerth, and L. T. Drzal, "Tailorable Adhesives for Multi-Material Joining, Facile Repair and Re-assembly," in *American Society for Composites 30th Technical Conference*, 2015.
- 1-[3] T. E. Tay, B. K. Fink, S.H.McKnight, S.Yarlagadda, and J. W. Gillespie, "accelerated curing of adhesives in bonded joints using induction heating.pdf," *J. Compos. Mater.*, vol. 33, no. 17, 1999.
- 1-[4] S. Yarlagadda, F. BK, and J. W. Gillespie, "Resistive susceptor design for uniform heating during induction bonding of composites," *J. Thermoplast. Compos. Mater.*, vol. 11, 1998.
- 1-[5] R. Rudolf, P. Mitschang, and M. Neitzel, "Induction heating of continuous carbon-fibre-reinforced thermoplastics," *Compos. Part A Appl. Sci. Manuf.*, vol. 31, no. 11, pp. 1191–1202, 2000.
- 1-[6] L. Augh, J. W. Gillespie, and B. K. Fink, "Degradation of continuous carbon fiber reinforced polyetherimide composites during induction heating," *J. Thermoplast. Compos. Mater.*, vol. 14, no. 2, pp. 96–115, 2001.
- 1-[7] H. Kim, S. Yarlagadda, J. W. Gillespie, N. B. Shevchenko, and B. K. Fink, "A study on the induction heating of carbon fiber reinforced thermoplastic composites," *Adv. Compos. Mater.*, vol. 11, no. 1, pp. 71–80, 2002.
- 1-[8] S. Budhe, M. D. Banea, S. de Barros, and L. F. M. da Silva, "An updated review of adhesively bonded joints in composite materials," *Int. J. Adhes. Adhes.*, vol. 72, no. October 2016, pp. 30–42, 2017.
- 1-[9] E. Verna *et al.*, "Adhesive joining technologies activated by electro-magnetic external trims," *Int. J. Adhes. Adhes.*, vol. 46, pp. 21–25, 2013.
- 1-[10] R. Ciardiello, G. Belingardi, B. Martorana, and V. Brunella, "International Journal of Adhesion and Adhesives," *Int. J. Adhes. Adhes.*, vol. 89, no. December 2018, pp. 117–128, 2019.
- 1-[11] S. H. Vattathurvalappil and M. Haq, "Thermomechanical Characterization of Nano-Fe3O4 Reinforced thermoplastic adhesives and joints," *Compos. Part B Eng.*, vol. 175, no. communicated, 2019.
- 1-[12] S. H. Vattathurvalappil and M. Haq, "Evaluating healing behavior of thermoplastic adhesive

- bonded joints subjected to transverse impact loads," in SPE ANTEC, 2019.
- 1-[13] R. P. Palanisamy, S. H. Vattathurvalappil, O. Karpenko, Y. Deng, and M. Haq, "Process monitoring of Induction-based adhesively bonded lap-joints," in *SPE ANTEC*, 2019.
- 1-[14] T. Bayerl, "Application of Particulate Susceptors for the Inductive Heating of Temperature Sensitive," Institut für Verbundwerkstoffe GmbH, 2012.
- 1-[15] M. Haq, "Hybrid hierarchical bio-based materials: development and characterization through experimentation and computational simulations," 2009.
- 1-[16] B. S, T. D, and F. J, "3-D simulation of induction heating of anisotropic composite materials," *IEEE trans Magn*, vol. 41, pp. 1568–1571, 2005.
- 1-[17] K. HJ, Y. S, S. NB, F. BK, and G. Jr., "Development of a numerical model to predict inplane heat generation patterns during induction processing of carbon fiber reinforced prepreg stacks," *J. Compos. Mater.*, vol. 37, pp. 1461–1483, 2003.
- 1-[18] H. Polli, L. A. M. Pontes, A. S. Araujo, J. M. F. Barros, and V. J. Fernandes, "Degradation behavior and kinetic study of ABS polymer," *J. Therm. Anal. Calorim.*, vol. 95, no. 1, pp. 131–134, 2009.
- 1-[19] T. Bayerl and P. Mitschang, "Heating of Polymer-Polymer Composites By Inductive Means," in *Iccm-Central.Org*, 2011, pp. 1–6.
- 1-[20] V. . Bhandari, *Introduction to machine design*. Tata McGraw-Hill, 2001.
- 1-[21] A. Yousefpour, M. Hojjati, and J. P. Immarigeon, "Fusion bonding/welding of thermoplastic composites," *J. Thermoplast. Compos. Mater.*, vol. 17, no. 4, pp. 303–341, 2004.
- 1-[22] T. Bayerl, M. Duhovic, P. Mitschang, and D. Bhattacharyya, "Composites: Part A The heating of polymer composites by electromagnetic induction A review," *Compos. Part A*, vol. 57, no. 2014, pp. 27–40, 2017.
- 1-[23] M. Faraday, "On the magnetization of light and the illumination of magnetic lines of force c. 1. c. 1," *R. Soc.*, 1846.
- 1-[24] V. Rudnev, D. Loveless, R. Cook, and M. Black, *Handbook of induction heating*. Basel: Marcel Dekker AG, 2003.
- 1-[25] E. C. Stoner and E. . Wohlfarth, "A Mechanism of magnetic hysteresis in heterogenous alloys," vol. 240, 1948.
- 1-[26] L. Néel, "Some theoretical aspects of rock-magnetism," *Adv. Phys.*, vol. 4, no. 14, pp. 191–243, 1955.

- 1-[27] S. Yarlagadda, B. K. Fink, and J. W. Gillespie, "Resistive susceptoruniform heating during induction bonding of composites," *J. Thermoplast. Compos. Mater.*, vol. 11, pp. 321–337, 1998.
- 1-[28] W. Suwanwatana, S. Yarlagadda, and J. W. Gillespie, "Hysteresis heating based induction bonding of thermoplastic composites," *Compos. Sci. Technol.*, vol. 66, no. 11–12, pp. 1713–1723, 2006.
- 1-[29] X. K. Zhang, Y. F. Li, and J. Q. Xiao, "Theoretical and experimental analysis of magnetic inductive heating in ferrite materials," *J. Appl. Phys.*, vol. 93, 2003.
- 1-[30] A. J. Crosby and J. Y. Lee, "Polymer nanocomposites: The 'nano' effect on mechanical properties," *Polym. Rev.*, vol. 47, no. 2, pp. 217–229, 2007.
- 1-[31] S. H. Vattathurvalappil and M. Haq, "Thermomechanical characterization of Nano-Fe₃O₄ reinforced thermoplastic adhesives and single lap-joints," *Compos. Part B Eng.*, vol. 175,107162, 2019.
- 1-[32] S. H. Vattathurvalappil, S. F. Hassan, and M. Haq, "Monitoring Residual Strains in Ovenand Induction-bonded Joints," in *Proceedings of the American Society for Composites—Thirty-fourth Technical Conference*, 2019.
- 1-[33] S. H. Vattathurvalappil and M. Haq, "Experimental and numerical Investigation of Bonded joints subjected to transverse impact loads," in *SPE ACCE*, 2017.
- 1-[34] R. Ciardiello, B. Martorana, V. G. Lambertini, and V. Brunella, "Iron-based reversible adhesives: Effect of particles size on mechanical properties," vol. 232, no. 8, pp. 1446–1455, 2018.
- 1-[35] R. Ciardiello, A. Tridello, V. Brunella, B. Martorana, D. S. Paolino, and G. Belingardi, "Impact response of adhesive reversible joints made of thermoplastic nanomodified adhesive," *J. Adhes.*, vol. 8464, no. January, p. 00218464.2017.1354763, 2017.
- 1-[36] S. H. Vattathurvalappil and M. Haq, "Thermomechanical Characterization of Nano-Fe3O4 Reinforced thermoplastic adhesives and joints," *Compos. Part B Eng.*, vol. 175, no. communicated, p. 107162, 2019.
- 1-[37] Z. Xia, "On selection of repeated unit cell model and application of unified periodic boundary conditions in micro-mechanical analysis of composites," vol. 43, pp. 266–278, 2006.
- 1-[38] S. Li, "Science and Boundary conditions for unit cells from periodic microstructures and their implications," vol. 68, pp. 1962–1974, 2008.
- 1-[39] J. C. Michel and H. Moulinec, "Effective properties of composite materials with periodic microstructure: a computational approach," vol. 7825, no. 98, 1999.

- 1-[40] B. El Said and S. R. Hallett, "Multiscale surrogate modelling of the elastic response of thick composite structures with embedded defects and features," *Compos. Struct.*, vol. 200, no. May, pp. 781–798, 2018.
- 1-[41] M. Salviato, M. Zappalorto, and M. Quaresimin, "International Journal of Solids and Structures Nanoparticle debonding strength: A comprehensive study on interfacial effects," *Int. J. Solids Struct.*, vol. 50, no. 20–21, pp. 3225–3232, 2013.

Chapter 2: Development of Reversible Adhesives¹

2.1. Abstract

In this work, Acrylonitrile Butadiene Styrene (ABS) was selected as the thermoplastic adhesive and reinforced with varying concentration of ferromagnetic nanoparticles (FMNP) through melt processing. The effect of FMNP content on thermo-mechanical properties was experimentally characterized. Results indicate that the percolation limit of FMNP to ensure melting and flow during induction bonding was 8 wt.%, and the flow time decreased with increase in FMNP content. ABS adhesive with 16 wt. % FMNP showed good balance of stiffness and strength relative to other concentrations.

2.2. Introduction

Adhesively bonded joints have become a route for enabling light weighting in automotive applications as they eliminate fastener weight, drilling of holes, associated stress concentrations and delamination, distribute the load over large areas, and can incorporate dissimilar material substrates[1]–[4]. Conventional thermoset bonded joints however, are one-time cure and cannot be disassembled during maintenance and repair. The use of thermoplastic adhesives for bonded joints is promising for re-assembly/ repair, but the energy required to heat the entire adhesive area limits the feasibility of this technique. The heat is generally applied through the adherends and is infeasible in non-metallic adherends, such as fiber reinforced composites. On the other hand, thermoplastic adhesives reinforced with conductive nanoparticles that interact with electromagnetic radiations via non-contact methods such as induction heating, can rapidly heat the

¹ Part of this work has been published in : S. H. Vattathurvalappil, M. Haq, "Thermomechanical characterization of Nano Fe3O4 reinforced thermoplastic adhesives and single lap joints", Composites – Part B, 2019, 175, 107162.

adhesive, allowing it to flow and form a bond upon cooling. Similar process can be used to disassemble or re-assemble the joint.

Induction heating in structural bonding offers several advantages compared to that of the conventional oven bonded joining technique[5]–[7]. This includes rapid processing, repeatability, low energy consumption, smaller space requirements and targeted heating of adhesives without degrading the adherents. A typical induction heating system consists of a power circuit that converts a regular power supply to high frequency 10-400 kHz current inside an induction coil to generate electro-magnetic field within the coil. This field in turn induces eddy currents in any conductive work piece placed around the coil (Joule heating) in addition to the magnetic hysteresis losses if the work piece has magnetic susceptibility.

The induction heating process has been adopted by the composite industry in the last couple of decades, mostly for curing fiber reinforced composites. Most of the conventional non-contact induction heating techniques utilized metallic mesh susceptors embedded within the thermosetting plastics[8], [9]. However, these metallic meshes besides acting as susceptors also behave as a flaw in the bondline, thereby compromising structural integrity. To eliminate the need of any metallic susceptors meshes, few studies [10], [11] have focused on the potential of using magnetic nanoparticles. Bayerl et al [12], [13] used iron oxide particles as susceptors in the thermoplastic adhesive material and claimed that these particles act as reinforcements that elevate the mechanical properties. However, they did not extend the studies to adhesive characterization in bonded joints. Ferromagnetic nanoparticles (FMNP) with diameters around 100 nm have very high curie temperature (temperature at which the permanent magnetic property is lost)[13]–[15] and a potential to produce heating modes such as hysteresis (Kneels effect and Brownian motion) [16], [17] and are considered as a good candidate for repeated heating of thermoplastics. `Verna et al.

[6] studied the behavior of single lap joints with ferromagnetic susceptors in a hot melt thermoplastic adhesive and mainly focused on the thermal response and strength of the lap joints at various concentrations of iron-oxide powder. However adhesive characterization based on tensile and Izod-impact properties were not reported.

The above studies mainly focus on the incorporation and application of nano-particles in hot-melt adhesives using induction heating techniques. However, experimental characterization studies comparing the behavior of joints from oven and induction heating techniques are relatively limited. Mahdi et al.[18] reported a comparative analysis between oven and induction-based heating techniques in woven fabric composite single lap epoxy-bonded joints. A stainless-steel receptor mesh was used to produce the localized heating to cure the two unique epoxy adhesives. Lap-shear strength, flexural strength and Mode-I toughness parameters were compared and the effect of oven or induction curing process was found to be insignificant on resulting properties. One major observation from this work is that the adhesive thickness for induction and oven cured samples was not maintained the same as the steel mesh increased the bondline thickness in the induction heated samples. Despite this difference, the study concluded that there was only a small drop in the shear strength of induction single lap joints. Severijns [19] et al. also compared the bond strength between oven and induction bonded joints with glass fiber reinforced composite adherents and epoxy adhesive. Instead of a mesh, 200µ iron oxide particles with 7.5 volume percent of iron oxide particles were embedded in the epoxy adhesive. The authors compared the lap shear strength of single lap joints and found that the induction heating method increases the strength of the joints by about 6% relative to oven heating. At the time of this manuscript preparation, to the best of our knowledge, the aforementioned are the only reported studies comparing oven and induction based adhesive curing techniques. Furthermore, it should be noted

that it dealt with thermoset epoxies and similar work with thermoplastic adhesive is not reported. Lastly, it should be noted that irrespective of whether susceptible iron-oxide particles or iron-meshes are used, the interaction of susceptors to electromagnetic field is important. Changing the electromagnetic parameters (power, frequency, and current) can change the field strength and thereby change the heating efficiency. For thermoplastic adhesives, the electromagnetic parameters should be selected such that there is proper adhesive flow and wettability to ensure a proper bond. Optimization of electromagnetic parameters to achieve a balance in heating efficiency and structural properties is possible but will require a detailed study on resulting parameters by changing each of the EM parameters which is beyond the scope of this work. In this work, by design, the maximum electromagnetic field offered by the system was used to ensure proper wettability and bonding and the resulting material and joint behavior s compared with oven-bonded joints.

The purpose of this paper is two-fold: a) To experimentally characterize the mechanical behavior of the ABS adhesive reinforced with FMNP particles, and b) To study performance of oven and induction bonded joints manufactured using these adhesives. In this study, tensile properties (modulus, strength, ultimate strain) and Izod impact strengths of the adhesive were characterized with varying concentrations of FMNP and processed at two different mixing times in order to identify an adhesive configuration having the optimum synergy of mechanical properties. Additionally, fiber-optic sensors were used to precisely record the processing temperatures in the adhesive bondline. Three selected adhesive configurations were used to study the behavior of single lap joints. Lastly, the effects of surface treatment and adherent preheating (in induction bonded joints) was studied. The materials used, processing techniques, experimental characterization and the discussion of the results are reported in the following sections.

2.3. Experimental Methods

2.3.1. Materials

This study used Acrylonitrile Butadiene Styrene (ABS) as the thermoplastic adhesive (CYCOLACTM Resin MG 94, SABIC®). ABS was selected for its excellent toughness provided by the polybutadiene phase grafted to the acrylonitrile styrene matrix. Additionally, ABS provides a good balance between cost, mechanical properties, chemical resistance, ease in processing and aesthetics [20] and is widely used in various domains including automotive, consumer market, electronics and sports industry. The processing temperature provided by the ABS supplier is 240°C and was used for all processing in this work. The higher the processing temperature, the better the flow and wettability for joining purposes. The ferromagnetic nanoparticle (FMNP) fillers used were Iron (II, III) oxide (Fe₃O₄, Sigma Aldrich) spherical particles with approximately 50-100 nm in diameter. ABS reinforced with short carbon fibers were purchased from Sigma Aldrich as 3D printing filaments. 15 wt.% of high modulus short carbon fibers were present in MG 94 ABS polymer (CarbonXTM CFR-ABS).

2.4. Adhesive Processing and Manufacturing

A total of six ferromagnetic nanoparticle (FMNP) concentrations in ABS were studied in this work, namely: i) neat ABS (0 wt.%), ii) 4 wt.%, iii) 8wt.%, iv) 12wt.%, v) 16 wt.%. and vi) 20 wt.%. First, the ABS pellets were dried for 3 hours at 80°C to remove any residual moisture. A 15 cc. mini-extruder (DSM Netherlands) was used for processing the ABS/FMNP mixtures. The desired quantity of FMNP powder was dry mixed and fed to the DSM extruder barrel that houses two contra screws rotating at 100 RPM. The barrel temperature was maintained at 240°C (melt temperature) and the polymer was mixed for either 3 min. or10 min.

The molten samples were then collected in a transfer cylinder connected with a piston. The temperature of this transfer cylinder was also maintained at 240°C. This molten samples were then pushed into ASTM closed molds using a pneumatic piston at 100 psi. The mold temperature was kept at 80°C to cool down the sample. Each batch fed to the DSM extruder consisted of 10g of ABS along with the desired weight fraction of FMNP. Further, molten adhesive was collected as discs and cooled to further create adhesive films by compressing it in a Carver press. Steel spacers of 1mm were used along with a temperature of 150°C and a pressure of ~575 kPa. The resulting films were cut into 25.4 mm x 25.4 mm. squares to be bonded with the adherents. The tensile and impact samples were measured for its dimensional compatibility with ASTM standards and no visible effects of shrinkage or voids were observed after cooling process.

2.5. Mechanical Testing Methods

2.5.1. Uniaxial Testing

Tensile tests were carried out on the adhesive coupons having Type-IV dimensions as per the ASTM D638 standards. Tests were conducted at a cross-head speed of 5 mm/min. and a load-cell with maximum capacity of 4.44 kN was used. The elastic modulus, ultimate strength and failure strains were recorded.

2.5.2. Impact Tests

Izod impact tests were conducted on notched and un-notched samples for all adhesives in this study. The dimensions of DSM extruded samples had un-notched dimensions of 63.5 x 12.7 x 3.98 mm, with the width reducing to 9.55 mm in notches samples. The samples were tested using a 5 J hammer and impact resistances were measured according to ASTM 256-10.

2.6. Monitoring Adhesive Temperature

In order to monitor the thermoplastic melting during the induction process, accurate temperature measurements in the adhesive are needed. While several non-contact infrared temperature sensors are available, they only provide surface temperatures [13]. In order to measure the temperature in the adhesive bond-line, a fiber-optic sensor was placed in the bond-line and time-temperature measurements were recorded during the exposure to electromagnetic radiations. Specifically, a distributed fiber-optic sensor (Luna ODiSI-B) which had a diameter of 1.0 mm was used as shown in figure 2-1. This system uses the Rayleigh scattering effect in optical fibers to enable continuous measurement of either temperature or axial strain along the entire length of the fiber. The fiber optic sensors were placed along the center and two edges of the adhesive film. Only the center fiber optic sensor was used to determine the heating rate of the adhesive as the edges have boundary condition that can lead to rapid cooling

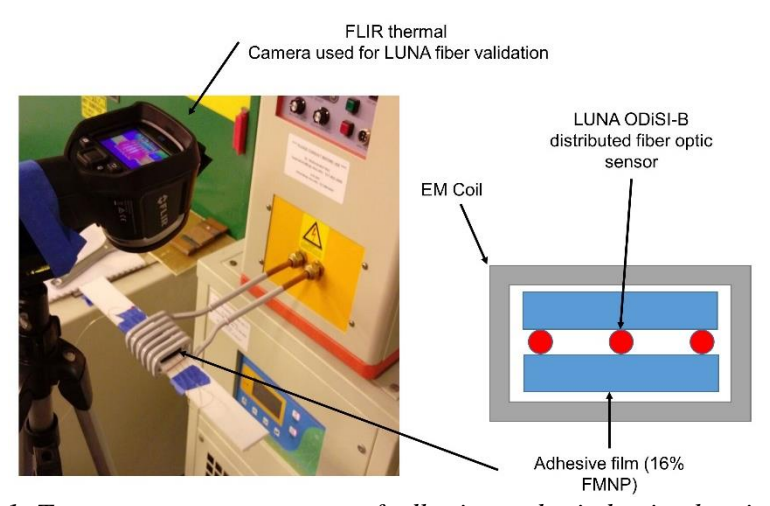


Figure 2-1: Temperature measurement of adhesive under induction heating process

2.7. Results & Discussions

2.7.1. Adhesive Characterization

While long mixing times can facilitate dispersion of nanoparticles, they can also deteriorate the polymer. In this study, tensile and impact samples with 3 min. and 10 min. mix times in the

DSM extruder were studied. Figure 2-2 shows the representative tensile stress-strain plots for all adhesive configurations in this study

The variation of tensile modulus (figure 2-3), tensile strength (figure 2-4 a) and ultimate tensile strains (figure 2-4 b) were recorded as a function of concentration of FMNP and extruder mix-times and compared with neat ABS properties. A drop in elastic modulus was observed with addition of FMNP and as the particle concentration increased the modulus also increased. At 16 wt.% of FMNP an average increase in modulus of ~13% was observed.

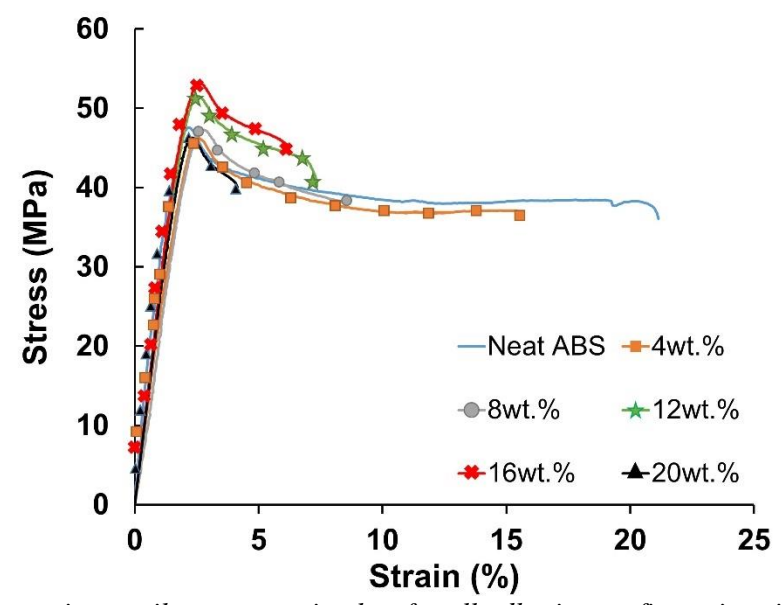


Figure 2-2: Representative tensile stress-strain plots for all adhesive configurations in this study

It should be noted that significant enhancements in modulus were not expected as the morphology of FMNP is nearly spherical with aspects ratio of ~1. In this case, the FMNP acts as a filler that interacts with electromagnetic radiations to facilitate heating and not a structural reinforcement. Similar results have been reported in [13], wherein reduction in modulus due to FMNP addition is reported. Furthermore, as the FMNP content increased beyond 16 wt.%, the modulus dropped. This is attributed to agglomeration of FMNP particles at higher concentrations. The agglomerated particles act as stress-concentrators and locations for onset of failure, thereby reducing the modulus, strength and ductility. The drop in modulus is gradual whereas the drop in

strain to failure is rapid. Hence, FMNP contents beyond 20 wt.% were not pursued in this work. This is confirmed by observations in tensile strengths and ultimate tensile strains as shown in figure 2-4.

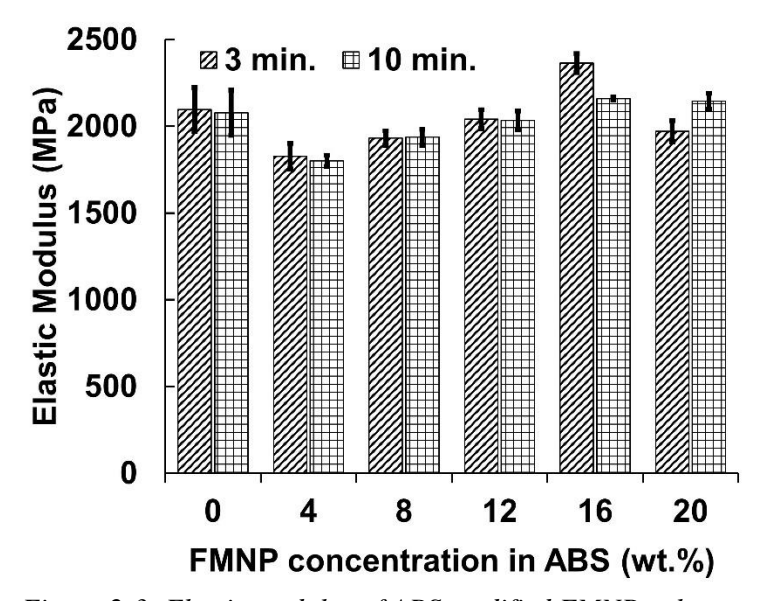


Figure 2-3: Elastic modulus of ABS modified FMNP polymer

The tensile strengths have trends similar to that of elastic modulus and are shown in figure 2-4 a. The ultimate tensile strains decreased with increasing FMNP content as shown in figure 2-4 b. This is attributed to the lack of compatibility or proper adhesion of FMNP to host polymer (ABS). Furthermore, addition of rigid, agglomerated nanoparticles have been shown to reduce ductility of resulting polymers [21]. While, the effect of mixing time on modulus was not significant, consistently higher tensile strengths and ultimate strains were observed with increasing mix time. On average, the tensile strengths for 10 min. mixing time increased by 7-8% relative to similar concentration samples with 3min. mixing time. The increase in ductility and strengths due to increase in mixing time is attributed to relatively better dispersion of FMNP and reduction in the concentration of agglomerated particles resulting in less locations for onset of failures.

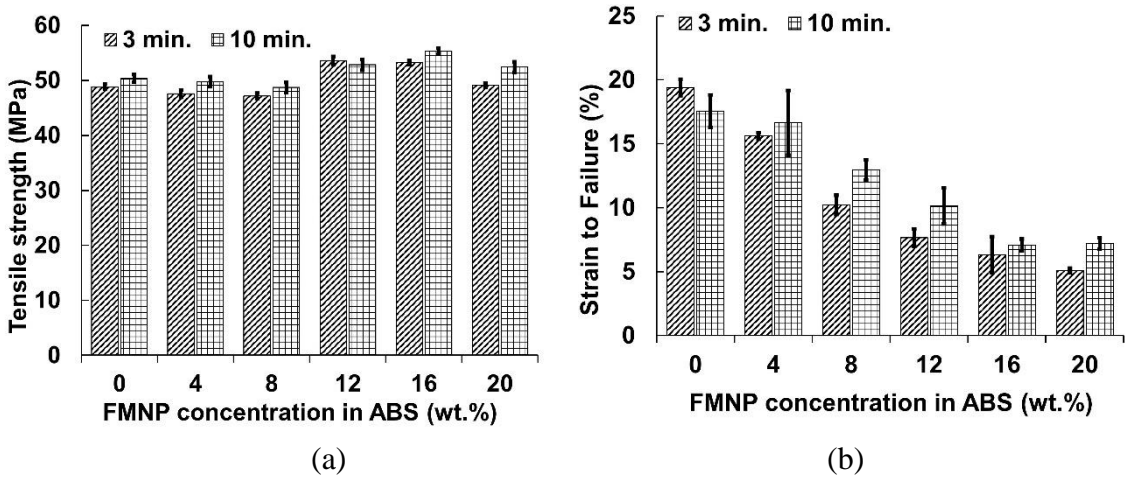


Figure 2-4: Effect of FMNP content in ABS on (a) Tensile Strength and (b) Strain to Failure

Figure 2-5 shows the impact strengths of notched and un-notched samples with varying concentrations of FMNP. It was observed that the average impact strength of the adhesive decreases as the FMNP content increases. The decrease in impact strength is more significant in the samples with 10 minutes of mix time, which is attributed to the polymer chain degradation due to longer exposure to high temperature. Similar degradation has been reported in [22]. On average, the impact strengths of samples with 3-minute mix time relative to similar concentrations at 10 min. mix times samples was 26% greater for neat ABS samples and 10% greater for FMNP reinforced samples. For nano-reinforced plastics, both notched and un-notched Izod tests are commonly performed [23]. In general, the notched tests represent the resistance to crack growth in the presence of a crack/notch, while the un-notched strengths include the energy to create a crack [24]. In this work, a comparison of notched and un-notched impact strengths was performed. Un-notched impact strengths followed similar trends as those of notched tests, but were approximately 5 times higher than that of notched specimens as shown in Figure 2-5 b. Similar to tensile strengths, the decrease in impact strengths with the addition of FMNP is attributed to agglomeration of nanoparticles leading to increased stress concentrations and possible locations for onset of failure[13].

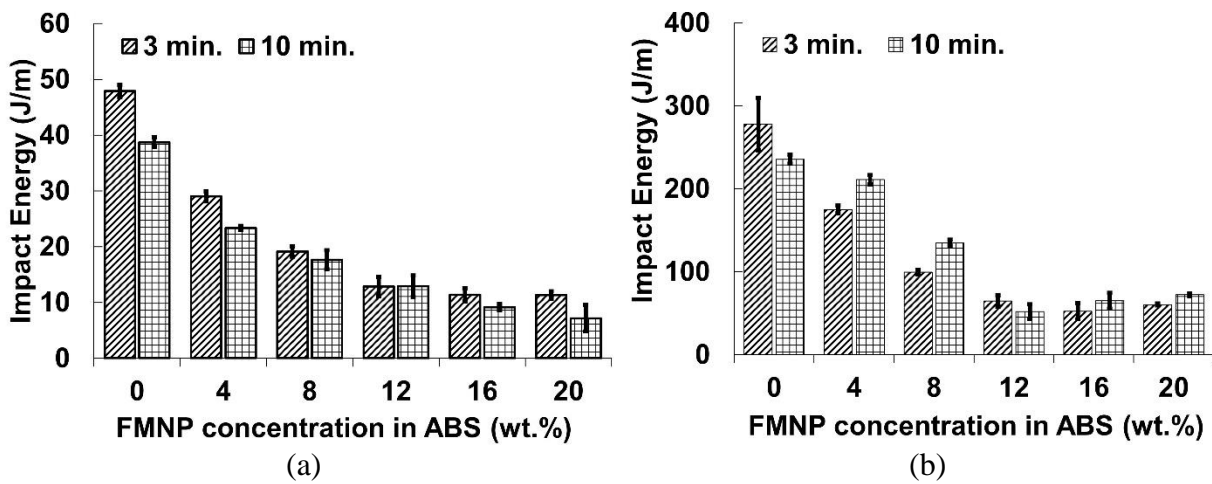


Figure 2-5: Effect of FMNP content in ABS on Impact energy of (a) Notched samples (b) Un-notched samples

Effect of mixing time in the DSM extruder had a direct effect on resulting mechanical properties. Scanning electron microscopy (SEM) images for various concentrations of FMNP are provided in Figure 2-6. The FMNP particles used had an average size of 100nm with random morphology (aspect ratio of 1). As tensile and impact strength results indicate, nano-particle agglomeration was observed, and as expected agglomeration increases with increasing FMNP concentration. While no distinct enhancements in dispersion of FMNP at 10 min. relative to 3min. were observed, the tensile strengths of 10 min. mix adhesives were higher than those of 3 min. mix times. Hence, for all future results in this manuscript, the adhesives with 10 min. mixing time were used.

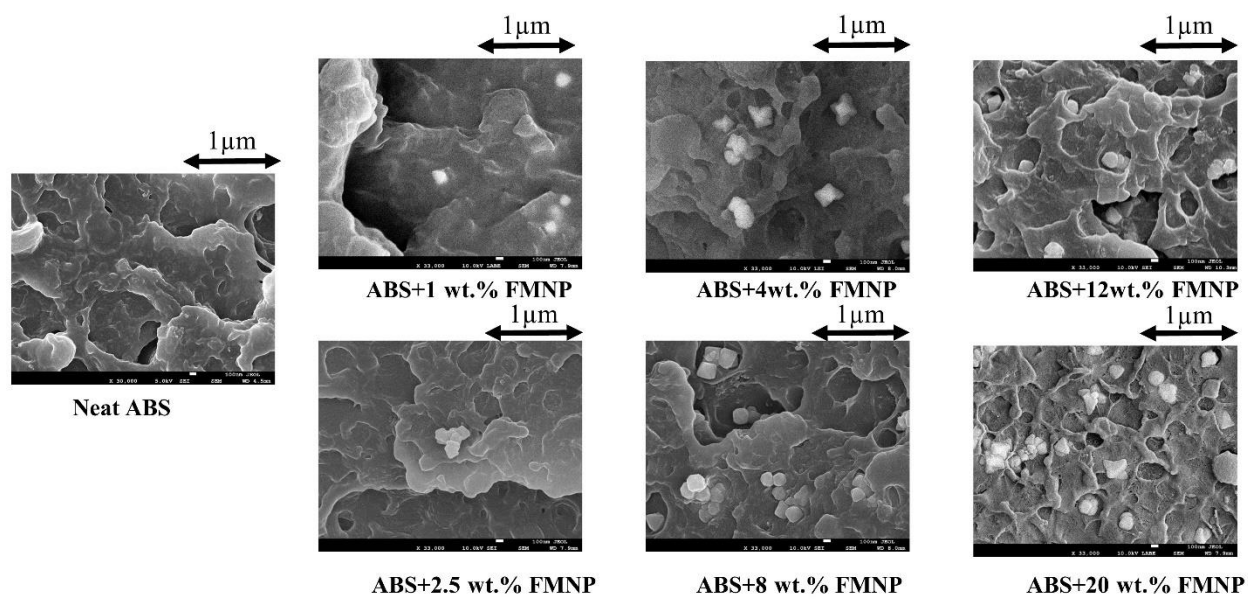


Figure 2-6: Fracture surfaces showing FMNP dispersion in ABS for varying FMNP content and a constant mix time of 10 min. The black arrows indicate the scale of one micron.

2.7.2. Hybrid Reinforcements

Short carbon fibers (SCF) were added as additional reinforcements to enhance the mechanical and EM response of polymer nanocomposites. Figure 2-7 (a) and Figure 2-7 (b) represents the tensile modulus and tensile strength of the ABS polymer reinforced with Fe₃O₄ and SCF. It was evident from these curves that the tensile modulus increased by 40 percent with the addition of SCF. However, any increase in Fe₃O₄ particles to ABS/SCF polymer did not create any additional enhancement in modulus and strength. Short carbon fibers used in this work possess a mean aspect ratio of 4.6 (section 5.5.1) and higher aspect ratios can result in better load carrying capability. According to the shear lag theory, the load transfer between the matrix and reinforcements is achieved through interfacial shear stresses and normal stresses.

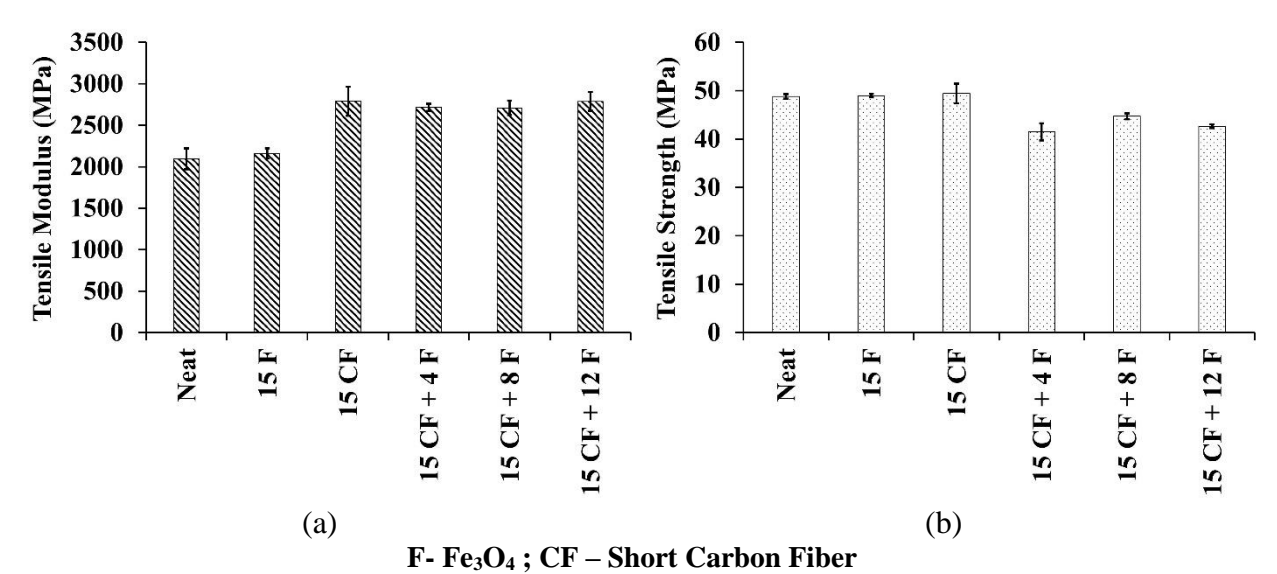


Figure 2-7: Effect of short carbon fiber in ABS/FMNP polymer: (a) Tensile Modulus (b) Tensile strength

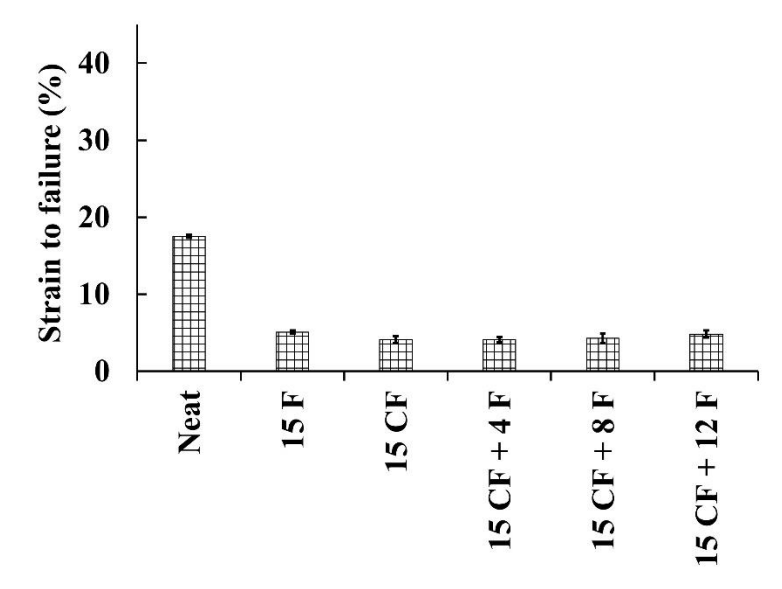


Figure 2-8: Effect of short carbon fiber in the strain to failure properties of ABS/FMNP polymer

Unlike tensile modulus, no significant improvement was observed in strain to failure (Figure 2-8). This can be attributed to multiple factors. Lack of proper adhesion can be one of the factors that results in reduced toughness. Another reason for the premature failure is the coalescence of stress concentrations around the reinforcements. As the number of particles

increases, it results in rapid coalescence of stress concentrations around the reinforcements and lead to premature failure.

2.8. Conclusions

This work studied the influence of ferromagnetic nanoparticles (FMNP) on a thermoplastic adhesive and resulting joint behavior. The adhesive of choice was ABS (acrylonitrile butadiene styrene), although the approach of targeted heating of the adhesive and creation of bonded joints can be easily transitioned to other thermoplastics. With the use of fiber-optic sensors, the minimum concentration of FMNP in ABS to react to induction heating was 8 wt.%. Nevertheless, polymers with lower melting points will require lower concentration and vice versa.

REFERENCES

REFERENCES

- 2-[1] W. Lin and M.-H. R.Jen, "The strength of bolted and bonded single lapped composite joints in tension," *J. Compos. Mater.*, vol. 33, pp. 640–666, 1999.
- 2-[2] J. H. Kweon, J. W. Jung, T. H. Kim, J. H. Choi, and D. H. Kim, "Failure of carbon composite-to-aluminum joints with combined mechanical fastening and adhesive bonding," *Compos. Struct.*, vol. 75, no. 1–4, pp. 192–198, 2006.
- 2-[3] M. Haq, A. Karpenko, Oleksiia Khomenko, L. Udpa, and S. Udpa, "Guided wave inspection of dissimilar material joints using time reversal techniques," *Int. J. Appl. Electromagn. Mech.*, vol. 45, pp. 957–964, 2014.
- 2-[4] S. M. R. Khalili, A. Shokuhfar, S. D. Hoseini, M. Bidkhori, S. Khalili, and R. K. Mittal, "Experimental study of the influence of adhesive reinforcement in lap joints for composite structures subjected to mechanical loads," *Int. J. Adhes. Adhes.*, vol. 28, no. 8, pp. 436–444, 2008.
- 2-[5] S. Budhe, M. D. Banea, S. de Barros, and L. F. M. da Silva, "An updated review of adhesively bonded joints in composite materials," *Int. J. Adhes. Adhes.*, vol. 72, no. October 2016, pp. 30–42, 2017.
- 2-[6] E. Verna *et al.*, "Adhesive joining technologies activated by electro-magnetic external trims," *Int. J. Adhes. Adhes.*, vol. 46, pp. 21–25, 2013.
- 2-[7] R.Ciardiello, G.Belingardi, B.Martorana, and V.Brunella, "Physical and mechanical properties of a reversible adhesive for automotive applications," *Int. J. Adhes. Adhes.*, vol. 89, pp. 117–128, 2019.
- 2-[8] T. E. Tay, B. K. Fink, S.H.McKnight, S.Yarlagadda, and J. W. Gillespie, "accelerated curing of adhesives in bonded joints using induction heating.pdf," *J. Compos. Mater.*, vol. 33, no. 17, 1999.
- 2-[9] S. Yarlagadda, F. BK, and J. W. Gillespie, "Resistive susceptor design for uniform heating during induction bonding of composites," *J. Thermoplast. Compos. Mater.*, vol. 11, 1998.
- 2-[10] S. R. Border J., "Induction heated joining of thermoplastic composites without metal susceptors," in *34th international SAMPE symposium*, 1989, pp. 2569–2578.
- 2-[11] E. Verna *et al.*, "Validation of a New Nano-Modified Adhesive Joining Technology Triggered By Electromagnetic Field, By Testing of a Real Component," no. June, pp. 22–26, 2014.
- 2-[12] T. Bayerl, R. Schledjewski, and P. Mitschang, "Induction heating of thermoplastic materials by particulate heating promoters," *Polym. Polym. Compos.*, vol. 20, no. 4, pp. 333–342,

2012.

- 2-[13] T. Bayerl, "Application of Particulate Susceptors for the Inductive Heating of Temperature Sensitive," Institut für Verbundwerkstoffe GmbH, 2012.
- 2-[14] W. Suwanwatana, S. Yarlagadda, and J. W. Gillespie, "Hysteresis heating based induction bonding of thermoplastic composites," *Compos. Sci. Technol.*, vol. 66, no. 11–12, pp. 1713–1723, 2006.
- 2-[15] T. Bayerl, M. Duhovic, P. Mitschang, and D. Bhattacharyya, "Composites: Part A The heating of polymer composites by electromagnetic induction A review," *Compos. Part A*, vol. 57, no. 2014, pp. 27–40, 2017.
- 2-[16] J. Dossett and G.E. Totten, "Nanoparticle Heating Using Induction in Hyperthermia," *ASM Handbook*, Vol. 4C, Induction Heat. Heat Treat., vol. 4, pp. 4–5, 2014.
- 2-[17] Lucas F M Silva, A.Öchsner, and D. A. Robert, *Handbook od Adhesion Technology*, vol. 53, no. 9. 2011.
- 2-[18] J. W. G. S Mahdi, H-J KIM, B.A.Gama, S.Yarlagadda, "A Comparison of Oven-cured and Induction-cured Adhesively Bonded Composite Joints," vol. 37, no. 6, 2003.
- 2-[19] C. Severijns, S. T. De Freitas, and J. A. Poulis, "On the Assessment of Susceptor-Assisted Induction Curing of Adhesively Bonded Joints," in *11th European adhesion conference*, 2016, pp. 1–4.
- 2-[20] H. Polli, L. A. M. Pontes, A. S. Araujo, J. M. F. Barros, and V. J. Fernandes, "Degradation behavior and kinetic study of ABS polymer," *J. Therm. Anal. Calorim.*, vol. 95, no. 1, pp. 131–134, 2009.
- 2-[21] M. Haq, R. Burgueño, A. K. Mohanty, and M. Misra, "Composites: Part A Bio-based unsaturated polyester / layered silicate nanocomposites: Characterization and thermophysical properties," *Compos. Part A*, vol. 40, no. 4, pp. 540–547, 2009.
- 2-[22] M. D. Wolkowicz and S. K. Gaggar, "Effect of thermal aging on impact strength acrylonitrile butadiene styrene (ABS) terpolymer," *Polym. Eng. Sci.*, vol. 21, no. 9, pp. 571–575, 1981.
- 2-[23] B. Chen and J. R. G. Evans, "Impact strength of polymer-clay nanocomposites," *R. Soc. Chem.*, vol. 5, pp. 3572–3584, 2009.
- 2-[24] A. K. Rana, A. Mandal, and S. Bandyopadhyay, "Short jute fiber reinforced polypropylene composites: effect of compatibiliser, impact modifier and fiber loading," vol. 63, pp. 801–806, 2003.

Chapter 3: Thermo-Mechanical Degradation of Reversible Adhesives

3.1. Abstract—

The reinforcement of conductive nano-/micro- fillers in thermoplastic polymers allows for rapid heating upon exposure to electromagnetic (EM) radiation. This phenomenon has been used to create reversible adhesives that allow bonding/removal of substrates via controlled EM exposure. This process of repeated heating/cooling can introduce extreme thermal and mechanical degradation, which is not fully understood. In this work, ferromagnetic nanoparticles (Fe₃O₄) were embedded in ABS polymer using melt-processing. The resulting polymers were subjected to EM heating with varying exposure time and multiple heat/cool cycles. TGA and FTIR spectroscopy were conducted to understand the extent of thermomechanical degradation. Tensile and Izod impact tests were performed on samples post EMI exposure and compared with control samples (no EMI exposure) to understand the effects of degradation. Results indicate that prolonged exposure to induction heating reduces the overall mechanical properties of the reversible polymer. However, repeated heating of ABS/Fe₃O₄ nanocomposites within the melting temperature only effects the ductility, and is attributed to loss of the toughening agent butadiene. Overall, the study creates a first benchmark for a possible path to control EM heating to prevent thermomechanical degradation of reversible thermoplastics.

Keywords—

Thermoplastic polymer, Ferro Magnetic Nanoparticles (Fe_3O_4), Electromagnetic Induction, Polymer degradation

3.2. Introduction

The increasing use of plastics in mass produced automotive structural applications dictates better characterization and understanding of their long-term behavior, especially if these are applied in safety-critical structural components. Hence, the study of polymer degradation is of paramount importance in enhancing the polymer life by maintaining its original properties. The cause of thermo-mechanical degradation can be attributed to different external factors such as temperature, moisture, mechanical stress, creep, radiations etc. [1]. While many studies have been reported on thermal degradation of thermoplastic polymers under conventional oven heating [2–10], very few studies focused on electromagnetic induction (EM) heating [11–13]. Conductive nano-/micro- particle reinforcements, when embedded within a polymer matrix, can act as individual heaters when exposed to electromagnetic (EM) radiation.

The electromagnetic induction technique offers several advantages over the conventional oven heating such as targeted heating, reduced energy consumption, rapid processing, consistent and optimized product quality and safety[14–17]. Although EM heating was first employed in metallic materials, the concept of applying the similar heating technique in polymer matrix composites was introduced in late 1990's[17]. However, it requires certain conductive susceptor particles/fibers/fabrics embedded within the polymer to transform the electromagnetic energy to heat. The advantages and disadvantages of induction heating is described in Table 1-1.

Table 3-1: Advantages and Dis-advantages of induction heating

Advantages	Dis-advantages		
 Localized heating 	High capital investment		
Low operating costs	Restricted to conductive work piece		
 Very short heat up times 	• Work piece shape and size is		
Environmentally sound	dependent on coil size and shape		
Reduced energy consumption			
Improved product quality and productivity			

The conventional practice of using thermoset adhesives hinders the disassembly and repair of the joints. On the other hand, thermoplastic adhesives facilitate assembly/disassembly for maintenance/repair. But, this will require heating of large areas of bondlines to enable melting of thermoplastics. Hence, reversible adhesives, namely thermoplastics reinforced with conductive nanoparticles allow for rapid heating of the bondline upon exposure to EM radiations [18–22]. However, these conductive thermoplastics can undergo extensive thermo-mechanical degradation during EM processing due to complex heating mechanisms and longer EM exposure times[20][12]. The goal of this paper is to investigate and quantify the extent of thermo-mechanical degradation in these polymers when exposed to EM radiations.

In order to understand the various sources/mechanisms of heating in metallic particle reinforced polymers due to EM heating, a brief background is provided here. Electromagnetic induction heating is based on the principles established by Michael Faraday in 1831[23], and detailed in the Maxwell-Faraday equation (Maxwell's 3rd law) as given below,

$$EMF = -\frac{d\phi}{dt} = \oint E. \, dL \tag{1}$$

where the total EMF around the circuit is equal to integrating the E field around the circuit. The total magnetic flux $\Phi(t) = \int_S B(t) dS$ is given as the sum of magnetic flux density (B) over the area. As such equation (1) can be written as,

$$\int_{S} \nabla \times E. \, ds = \int_{S} \frac{dB(t)}{dt}. \, ds \tag{2}$$

Maxwell's 3rd law states that a voltage is induced in a conductive work piece when its placed in a changing magnetic field. In other words, it describes how an electric current produces magnetic field and how a changing magnetic field produces electric current in a conductor. The possible heating modes produced in a conductive workpiece when exposed to EM radiations are shown in figure 3-1. In this work, the susceptors, namely the conductive nano-/micro-reinforcements within the thermoplastic will act as heat sources for the polymer through one or more of the heating modes described in Figure 3-1.

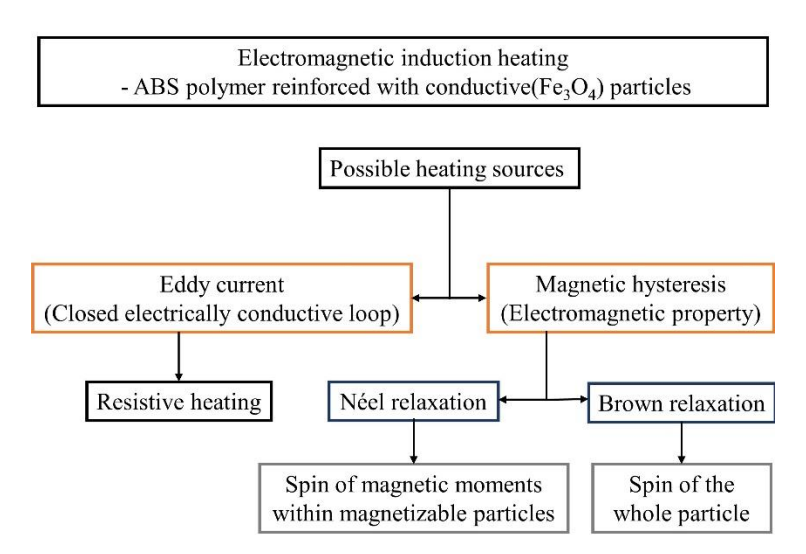


Figure 3-1: Possible heating modes in a conductive work piece exposed to electromagnetic radiations

An EM heating system consists of a power circuit that typically converts 50/60 Hz AC supply to a high frequency 10-400 kHz current inside an induction coil to generate a magnetic field within the coil. This EM field in turn induces eddy currents in any conductive work piece placed in or around the coil (Joule heating). If the work piece has magnetic susceptibility and a large hysteresis, there would be additional energy losses. Together, these losses are responsible for heat generation within the material bulk volume. The key factors that influence the eddy current and magnetic hysteresis losses are presented in table 3-2.

Table 3-2: Heating mechanisms in electromagnetic induction heating

	Eddy current	Magnetic hysteresis	Reference
	·	Ç	
Precondition for	Closed electrically	Ferromagnetic properties	[24][16]
induction heating	conductive loop	of the susceptor	
Driving mechanism	Induced current,	Magnetization reversal	[16][25][26]
	electric field polarity	(Brown and Neel	
	reversal	relaxation) _	
Heat generation	Resistive heating, and	Magnetic hysteresis, and	[26][27][28]
	dielectric heating	friction losses	
Limitations	Penetration depth	Curie temperature	[16][28]
Side effects	Density increase due	Density increase due to	[16]
	to susceptors	susceptors	
Exemplary susceptors	Carbon fiber fabrics,	Particles of iron, nickel	[29]
	metal grids and metal	and cobalt alloys.	
	coated fibers.		

As mentioned earlier, limited studies have been reported on the thermal degradation of thermal polymer composites subjected to EM heating, and its resulting effects on the polymer's mechanical properties[30][13]. Bayerl et al.[13] studied the degradation due to laser, infrared, and induction heating in thermoplastic polymers such as polyether ether ketone (PEEK) and high density polyethylene (HDPE) with ferromagnetic nanoparticles as susceptors. Their study showed that EM heating at a constant power (10 kW) and frequency (450 kHz) reduced the time to reach the polymer melting point with increasing EM exposure times. However, this paper did not

consider the potential causes for the polymer degradation and its effect on mechanical properties. Furthermore, the rate of temperature increase when exposed to EM radiations remains unknown.

In extrinsic heating (infrared, laser, and oven heating), the power input is provided directly on to the surface and the material volume reaches a steady-state temperature through radiation, onvection, or conduction. Masanori et al.[2] studied the thermal degradation of ABS and its constituent monomers under extrinsic heating using TGA-FTIR method. They found that the degradation behavior remains essentially the same in both ABS and in its individual constituents. They also observed that the degradation started in the butadiene phase and proceeded to the styrene acrylonitrile (SAN) phase. Tiganis et al. [8] concluded that thermal oxidation of SAN phase in ABS polymer only resulted in minor degradation compared to the butadiene phase. Furthermore, they concluded that ageing and thermal degradation at lower temperatures (< 120°C) did not affect the bulk polymer and was predominantly a surface phenomenon. However, this behavior might not be replicated in intrinsic heating methods such as EM heating, and hence investigated in this work.

In extrinsic heating methods such as oven heating, the temperature measured at any point will be the same throughout the material volume once the steady state is reached. Conversely, for EM heating, the thermal profile in polymer nanocomposite is governed by many factors such as EM field distribution inside the coil and the workpiece, eddy current percolation paths, surface heat transfer, electric, magnetic, and thermal material properties of the polymer nanocomposite. These factors result in non-uniform temperature fields, as observed in earlier work [31]. One hypothesis is that such non-uniform temperatures within the bulk of the polymer would lead to local degradation in regions of high temperature, while the rest of the polymer reaches processing temperature.

One of the several challenges involved in EMI heating is the temperature monitoring in bulk of the PNC. Degradation during polymer processing can be aggravated by increasing the operating temperature and its exposure time. Although the possibility of thermal degradation of these PNC due to EMI exposure was acknowledged in previous studies [34][12][20], the quantification of its effect on mechanical properties was not documented elsewhere.

In this study, ferromagnetic particles (Fe₃O₄) were used as susceptors in acrylonitrile butadiene styrene (ABS) thermoplastic polymer due to its potential to produce both hysteresis and eddy current modes of heating. ABS, a terpolymer (processed using three different monomers) was selected in this work as it is widely used in automotive, electronics, sports and other consumer markets. Also, ABS provides a good balance between cost, mechanical properties, chemical resistance, ease in processing and aesthetics [32]. ABS polymer contains styrene-acrylonitrile (SAN) copolymer as continuous phase and butadiene as dispersal phase and its chemical formula is depicted in figure 3-2. While polystyrene enhances the ease of processing, polyacrylonitrile improves the thermal stability of the terpolymer [33]. The impact strength of the ABS terpolymer is regulated using the grafted poly butadiene phase.

$$\begin{array}{c} \text{--}\text{CH}_2\text{--}\text{CH}=\text{CH}-\text{CH}_2 \xrightarrow{\text{a}} (\text{CH}_2\text{--}\text{CH}\xrightarrow{\text{b}} (\text{CH}_2\text{--}\text{CH}\xrightarrow{\text{c}}_{\text{c}})^{\text{d}} \end{array}$$

Figure 3-2: Schematic molecular structure of acrylonitrile butadiene styrene (ABS)

The scope of this work is to evaluate and understand the degradation mechanisms of ABS polymer reinforced with Fe₃O₄ nanoparticles upon exposure to EM radiations. The frequency of 200 kHz and 30 A of current were maintained constant in this study. The exposure time was changed and the resulting behavior/degradation was studied. While each of the parameters such as

frequency, power and exposure times could be changed to evaluate their effect on resulting thermomechanical properties, this was considered beyond the scope of this work and hence only degradation at constant power and frequency but varying exposure times was explored. The degradation was characterized by experimentally evaluating the tensile and Izod impact properties along with thermogravimetric analysis (TGA) and Fourier transform infrared spectroscopy (FTIR) studies on EM-exposed and un-exposed (control) samples. The combination of mechanical testing, TGA and FTIR data will be used to understand the heating mechanisms and optimum exposure times to limit thermal degradation of the ABS/Fe3O4 polymers. The details on materials used, the manufacturing processes, experimental results and discussions are provided in the following sections.

3.3. Experimental

3.3.1. Materials Used

The polymer nanocomposite (PNC) configuration used for this study consisted of an amorphous thermoplastic polymer (Acrylonitrile Butadiene Styrene, ABS) and magnetite nanoparticles (Fe₃O₄). ABS (CYCOLACTM Resin MG 94) was supplied by SABIC® corporation and Fe₃O₄ fillers were procured from Sigma-Aldrich®. These Iron (II, III) oxide nano powders were approximately 50-100nm in size with a random morphology having aspect ratio one.

3.3.2. Processing and Manufacturing

The ABS/Fe₃O₄ nanocomposite used in this study was manufactured by an extrusion process using a 15cc mini-extruder. Prior to the extrusion process, ABS pellets were dried for 3 hours at 80°C to remove moisture. The desired quantity of Fe₃O₄ powder was dry mixed with the ABS pellets and fed to the DSM extruder barrel that houses two contra-rotating screws at 100 RPM. The barrel temperature was maintained at 240°C (melt temperature) and the polymer was

mixed for 10 min. The molten samples from the extruder were fed into shaping-die/molds corresponding to ASTM D638 type IV [34] tensile and ASTM 256-10 [35] impact coupons. The mold temperature was maintained at 80°C with a back pressure 0.689 MPa. Each batch fed to the extruder consisted of 10g of ABS and the desired weight fraction of Fe₃O₄ nanoparticles. Between every sample made, a time gap of 3 minutes was maintained to cool down the mold to its original temperature. For this study, the desired weight fraction was 16% of Fe₃O₄. This 16 wt.% was selected from previous studies that reported high heating rate with optimum mechanical properties [20].

3.3.3. Electromagnetic Induction Heating

An induction heating system (Across International -IHG06A1) with maximum oscillating power of 6.6 kW, maximum input current of 30 A, and output frequency of 100 – 500 kHz was used in this work. An induction coil (Across International model: IHHC 2 X 1) having a rectangular cross section with internal dimensions of 25.4 mm. x 50.8 mm. was used, as shown in Figure 3-3. This was selected to ensure that the coil windings were as close to the workpiece as possible, in order to maximize the EM field strength in the polymer. It is to be noted that the heating efficiency depends on the workpiece geometry, power, frequency, and input current to the coil.

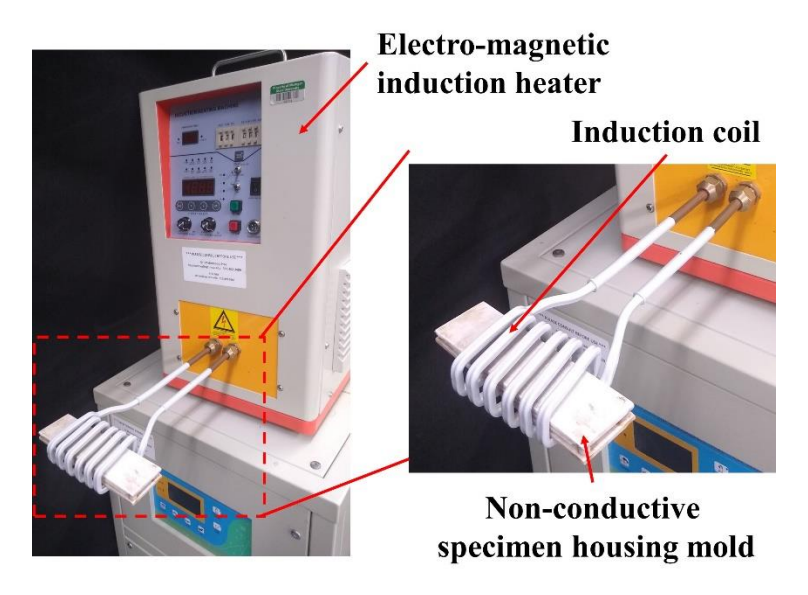


Figure 3-3: Induction heating fixture

3.3.4. Temperature Measurement and Induction Heating

Thermoplastic processing progress was monitored by temperature measurements on ABS/Fe₃O₄ samples. A high definition distributed fiber optic sensor (Luna's ODiSI-B 5.0) was used to measure the temperature. This equipment uses the Rayleigh scattering effect in optical fibers to obtain continuous measurements of either temperature or axial strain along the length of the fiber. The fiber optic sensor was attached to the resulting tensile/Izod impact coupons (Figure 3-4b) prior to placement inside the EM coil (Figure 4-3). This technique provides accurate temperature within the materials relative to other non-contact techniques such as infrared thermography which only provide surface temperatures.

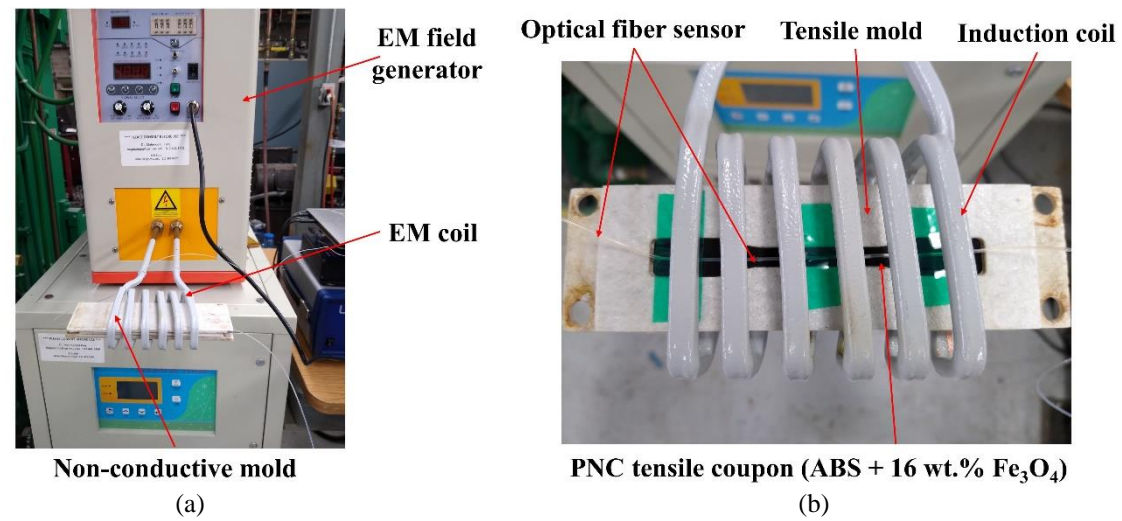


Figure 3-4: Temperature measurement of reversible polymer under induction heating process

3.3.5. Degradation Analysis

Table 3-3 shows the case studies performed in this work. The thermo-mechanical degradation in ABS reinforced with Fe₃O₄ nanoparticles subjected to electromagnetic induction heating was studied in the following manner.

• Heating rate study:

- Obtain the time-dependent heating rate of the ABS/Fe₃O₄ nanocomposite when subjected to electromagnetic heating.
- Thermogravimetric analysis (TGA):
 - Determine the mass loss (as a metric for degradation) of the ABS/Fe₃O₄ nanocomposite as a function of temperature.
- Effect of overexposure to EM heating:
 - The effect of overexposure to EM heating was studied by varying exposure times such that 1%, 2% and 5% mass degradation (obtained from TGA) occurs in the ABS/Fe3O4 polymer.

Table 3-3: Case Studies performed in this work

Material	Parameters		Parameter Studied			
	Mechanical	Thermal				
			Repeatability		High Temperature	
			(3 heat cycles)		Exposure	
ADC			Temper-	EM	Temper-	EM
ABS+	Tensile	• TGA	_	Exposure	-	Exposure
16 wt.% Fe ₃ O ₄	• Izod Impact	• FTIR	ature (°C)	time (s)	ature (°C)	time (s)
10304					315 (1*)	36
			240 (*)	28	350 (2*)	45
					370 (3*)	57

^{* -} Processing temperature of ABS

- Effect of repeated EMI heating on mechanical properties (reversibility):
 - Tensile and impact specimens were subjected to 240°C (processing temperature) using electromagnetic induction for three heat cycles. The resulting material properties for each cycle and resulting fracture surfaces were studied.

• Material Testing:

 Quasi-static tensile and Izod impact tests were performed as per respective ASTM standards to understand the effect of degradation on the mechanical properties.

^{1* - 1%} mass degradation temperature of ABS as obtained from TGA

^{2* - 2%} mass degradation temperature of ABS as obtained from TGA

^{3* - 5%} mass degradation temperature of ABS as obtained from TGA

 Fourier transform infrared spectroscopy (FTIR) and scanning electron microscopy (SEM) were also performed to explain the results observed in mechanical testing, as explained in Section 3.2.

Thermogravimetric Analysis (TGA)

The TGA Q500 from TA instruments was used to obtain high resolution temperature distribution. 20 mg. sample was heated under nitrogen atmosphere from 20°C to 800°C with a ramp rate of 10°C/min to yield the mass loss, onset decomposition temperatures and residues.

Fourier transform Infrared Spectroscopy (FTIR)

FTIR-4600 from JASCO was used to understand the organic materials and its deterioration with respect to different induction exposure temperatures. IR spectra were recorded between a spectral range of $4000 - 400 \text{ cm}^{-1}$ with a resolution of 0.7 cm^{-1} . The samples dimensions used in this study were 5 mm. x 5 mm. x 1.5mm.

Mechanical Property Assessment

Tensile tests were performed as per ASTM D638 standard [] using a cross-head speed of 5 mm./min. on a mechanical screw driven universal testing machine. Izod tests were performed as per ASTM D256 specifications using a TMI impact testing machine. An average of 5 samples were tested for each case. For repeated heating studies, flow/ dimensional instability can occur at temperatures higher than glass transition temperature (T_g). Hence, the samples were enclosed in a non-conductive ceramic housing mold assembly (Figure 3-5) before placement inside the coil for EM exposure. This allowed preservation of the shape of the samples for subsequent mechanical testing.

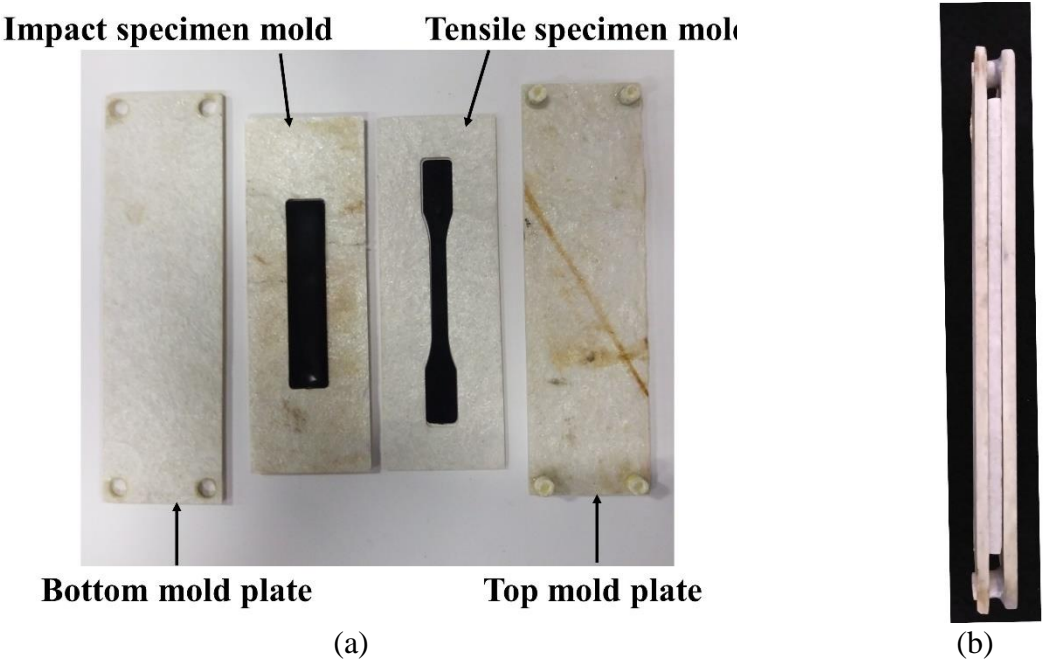


Figure 3-5: Non-conductive specimen housing molds (a) mold for both tensile and IZOD impact coupons (b) Fixture in its closed position

3.4. Results & Discussions

3.4.1. Heating Rate Study

Figure 3-6 illustrates the time required by the ABS films with varying Fe₃O₄ concentrations to reach the processing point under EM exposure (198 KHz and 1.2 KW). It was observed that the time required for PNC processing drastically drops as the Fe₃O₄ wt.% increases. Similar results were reported in [12].

In this work, the ABS reinforced with 16 wt.% Fe₃O₄ was selected as it offered a good balance between tensile properties [20] and heating times. Earlier work focused on heating rate only up to 240°C, and degradation beyond 240°C was not explored. In this work, a high definition distributed fiber optic sensor (described in section 2.4) was used to record the temperature in the ABS/Fe₃O₄ samples during EMI heating.

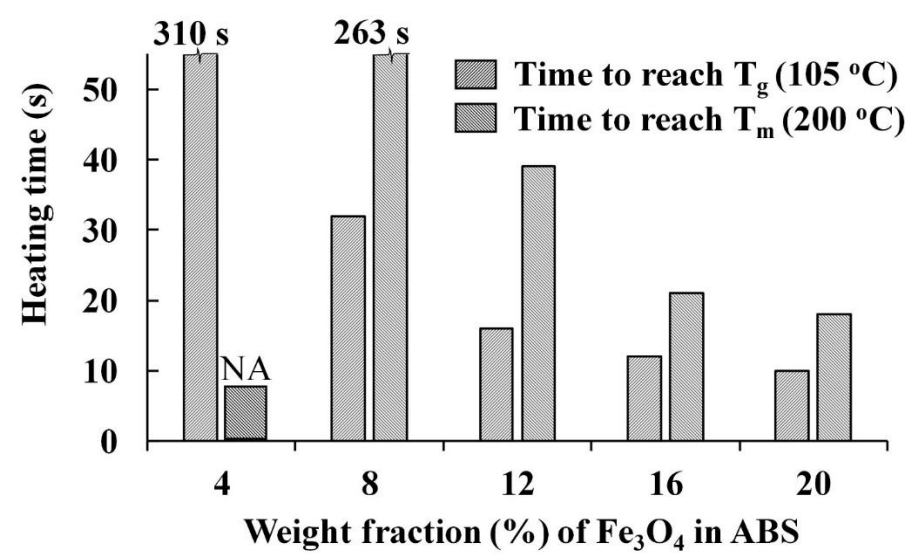


Figure 3-6: Heating rate of PNC under induction heating process – adapted from [36]

In a coil-based induction heating system, as used in this study, the temperature distribution is uneven across the workpiece/polymer nanocomposite housed within the coil. This can partially be attributed to the non-uniform magnetic field strength within the coil, determined by the coil and workpiece geometry. With eddy current also acting as a possible heating mechanism, the associated skin depth effect contributes to non-uniform heating, further increasing the uneven temperature distribution. [11]. The length wise distribution of temperature measured in the tensile and impact coupons is shown in Figure 3-7.

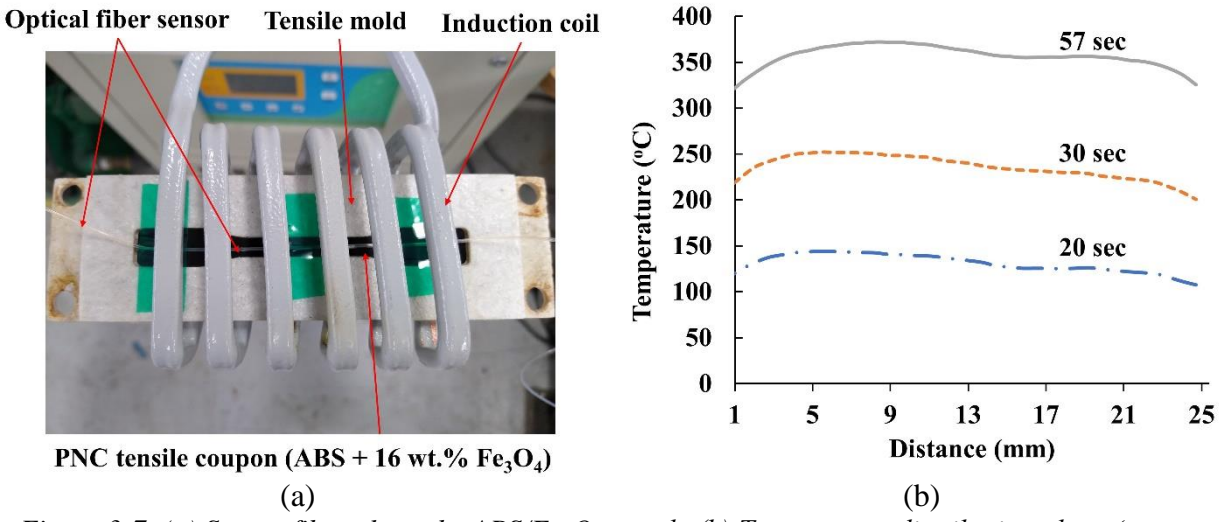


Figure 3-7: (a) Sensor fiber along the ABS/Fe₃O₄ sample (b) Temperature distribution along 'sensor fiber-length' within the ABS/Fe₃O₄(16wt.%) sample at varying time intervals.

The temperature measured in the coupon along the sensor fiber-length at time intervals of 20s, 30s, and 57s are shown in Figure 3-8(a). As expected, the temperature in the adhesive increased with increasing EM exposure time until ~ 320°C. Further exposure to EM radiations reduced the heating rate and reached a maximum temperature of 374°C in 57s. This change in heating rate is shown in figure 8a with a dotted line. This decrease in heating rate could be attributed to either the steady state being achieved with ambient boundary conditions, or due to polymer degradation disrupting the heating mechanisms. To better understand this observation, thermogravimetric analysis was conducted on similar samples (as described in section 2.5.1.)

Figure 3-8b shows the TGA response, and the onset degradation temperature was found to be ~375 °C. The polymer mass rapidly dropped until about 550 °C. The mass degradation levels and corresponding temperatures (1 wt.%, 2 wt.% & 5 wt.%) along with the corresponding EM exposure times were obtained from this test and were provided in Table 3-3. Comparative analysis of TGA and heating rate studies indicate that the PNC film undergoes rapid degradation starting at ~375 °C.

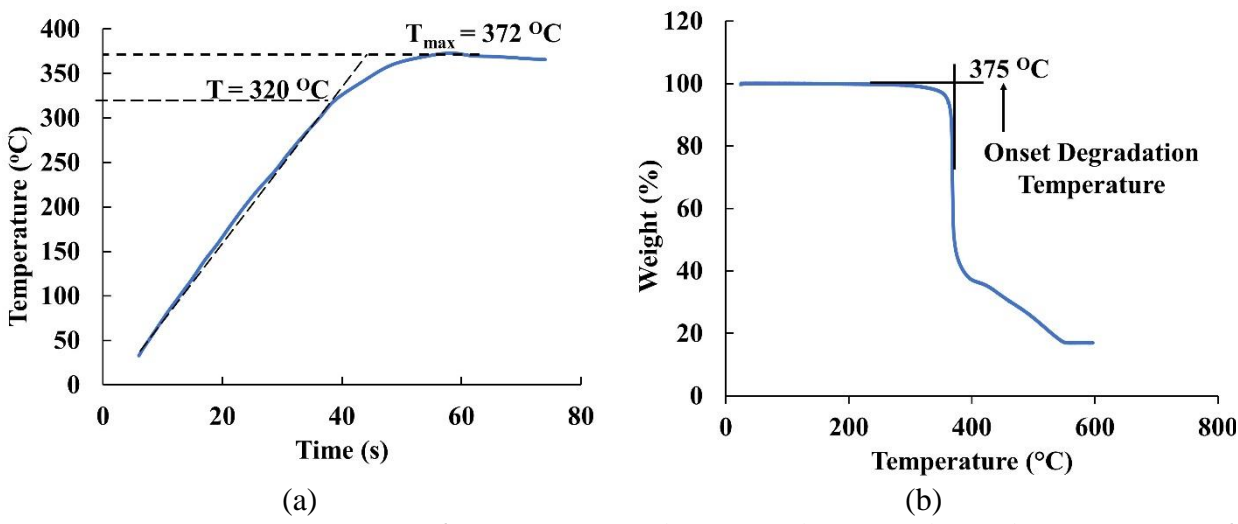


Figure 3-8: a)Heating rate of ABS+16 wt. % of FMnP when exposed to EM radiation b) TGA of ABS+16 wt. % of FMnP

3.4.2. Thermal Degradation and Corresponding Mechanical Properties

It is vital to understanding the mechanisms that control the degradation of ABS polymer to better interpret the Fourier Transform Infrared (FTIR) spectrographs. According to the thermo-oxidative reaction scheme proposed by Shimada and Kabuki [37] for the ABS polymer, the degradation is initiated by hydrogen abstraction by oxygen from the C—H bond in the α-carbon position. This abstraction generates radicals in the presence of oxygen which results in the formation of carbonyl and hydroxide products. The kinetic scheme proposed the formation of polymer radicals and as a result polymer peroxides in further decomposition [37]. This can result in microstructural inconsistencies and act as stress concentrators. Previous studies conducted on styrene acrylonitrile (SAN) and polybutadiene (PB) showed that the its degradation initiated at ~290°C[2], which is lower than the 1% mass degradation temperature observed in TGA (Table 3-3). Hence, the mechanical properties of reversible thermoplastic nanocomposite can be retained only by limiting the thermo-oxidative degradation.

Furthermore, since nanoparticles heat up the surrounding polymer, these particles act as local 'hot spots,' and their temperature can be much higher than the processing temperature of the polymer, even though the average bulk polymer temperature is at its processing point. Also, particle dispersion plays a vital role in the degradation mechanisms. Individual particles may contribute more with hysteresis type of heating whereas agglomerated particles/clusters will introduce Joule/eddy current heating. Hence, it's important to understand and evaluate the thermal degradation of these polymers beyond processing temperatures under EM heating.

Table 3-4: Infrared wave numbers and its corresponding chemical compounds[8][32][39]

IR Spectral bands of ABS polymer					
Wavenumber (cm ⁻¹)	Related molecular component				
702	Aromatic C—H out of plane bending				
911	Deformation of C—H in butadiene units				
966	Deformation of C—H in butadiene units				
1495	Stretching vibration of aromatic ring from Styrene unit				
1600	Stretching of C=C from butadiene				
2237	Acrylonitrile unit C≡N				
2850	Aliphatic C—H stretching				
2920	Aliphatic C—H stretching				
3030	Aromatic C—H stretching				

Fourier transform infrared spectroscopy (FTIR) was conducted (as described in section 2.5.2) to estimate the degradation of chemical constituents of the ABS thermoplastic used in this study. Although FTIR gives a qualitative representation of degradation, it helps to detect the loss of chemical compounds responsible for the deterioration of mechanical properties. Each peak in FTIR corresponds to specific molecular components and structures. Absorption from 4000-1500 wavenumbers corresponds to different functional groups and 1500-400 is often referred to as material finger print[38]. The absorption at this band region due to intramolecular phenomenon is highly material specific. The absorbance peaks of different chemical constituents in ABS polymer is shown in Table 3-4. FTIR spectrograph of ABS/Fe₃O₄ samples studied in this work are shown

in Figure 3-9. The chemical decomposition of the samples was evident from the comparison of absorbance peaks of ABS/Fe₃O₄ samples of varying degradation levels. The absorbance peaks for the samples exposed to 350 °C and 370 °C were reduced by ~75% for all the wavenumbers, suggesting significant degradation at these temperatures relative to control (non-EM exposed) ABS polymer, shown in figure 9 as PT. However, similar peaks revealed a relatively small decline for the samples exposed to 240 °C and 315 °C. This suggests that the degradation can occur even when the measured bulk temperature is at the processing point (240 °C).

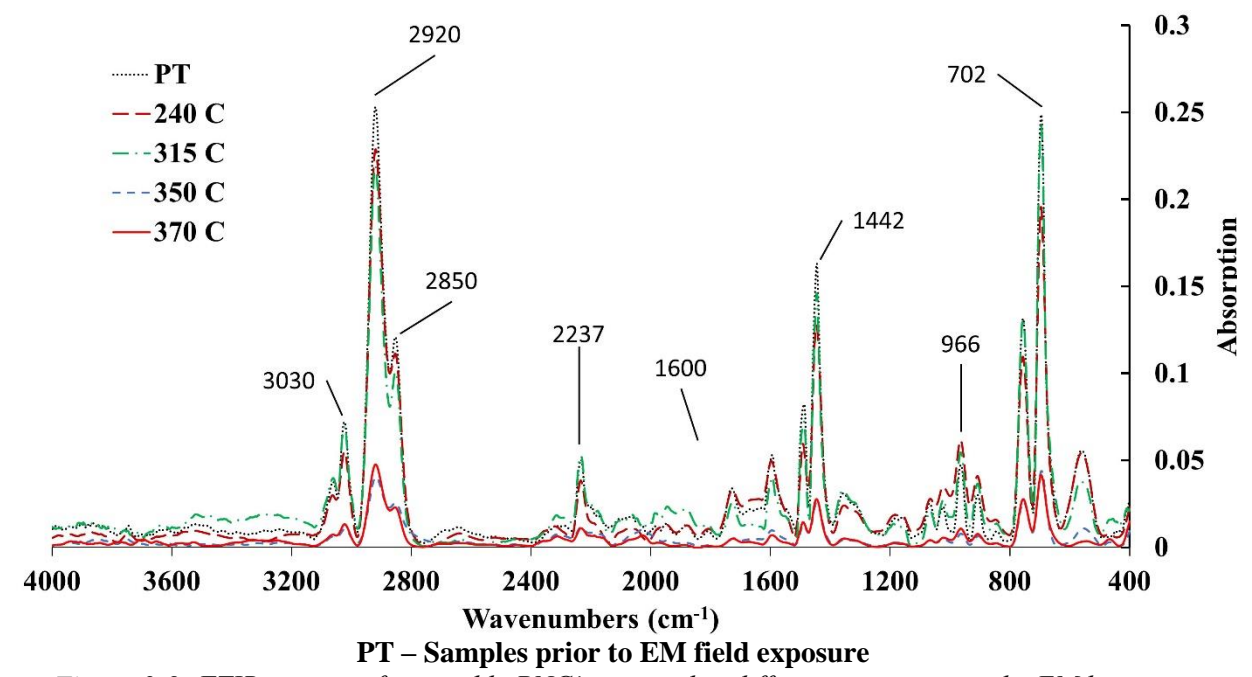


Figure 3-9: FTIR spectra of reversible PNC's exposed to different temperatures by EM heating

The effect of EM heating on mechanical properties of reversible ABS/Fe₃O₄ polymers exposed to EM heating was characterized based on the quasi-static tensile test and IZOD impact tests after EM exposure. This study was performed to understand the capability of reversible ABS/Fe₃O₄ to retain their mechanical properties after exposure to EM radiations. Figure 3-10a shows the average elastic tensile modulus and yield strengths with respect to different degradation levels (average bulk temperature when exposed to EM fields). Despite the degradation revealed in FTIR spectrographs (Figure 3-9), the average tensile modulus and yield strength remained same

until the bulk temperature reached 350 °C. As the bulk temperature of the ABS/Fe₃O₄ approached the onset degradation temperature (375 °C for ABS) of the polymer, the tensile modulus was reduced by 20 % and the yield strength reduced by 10%.

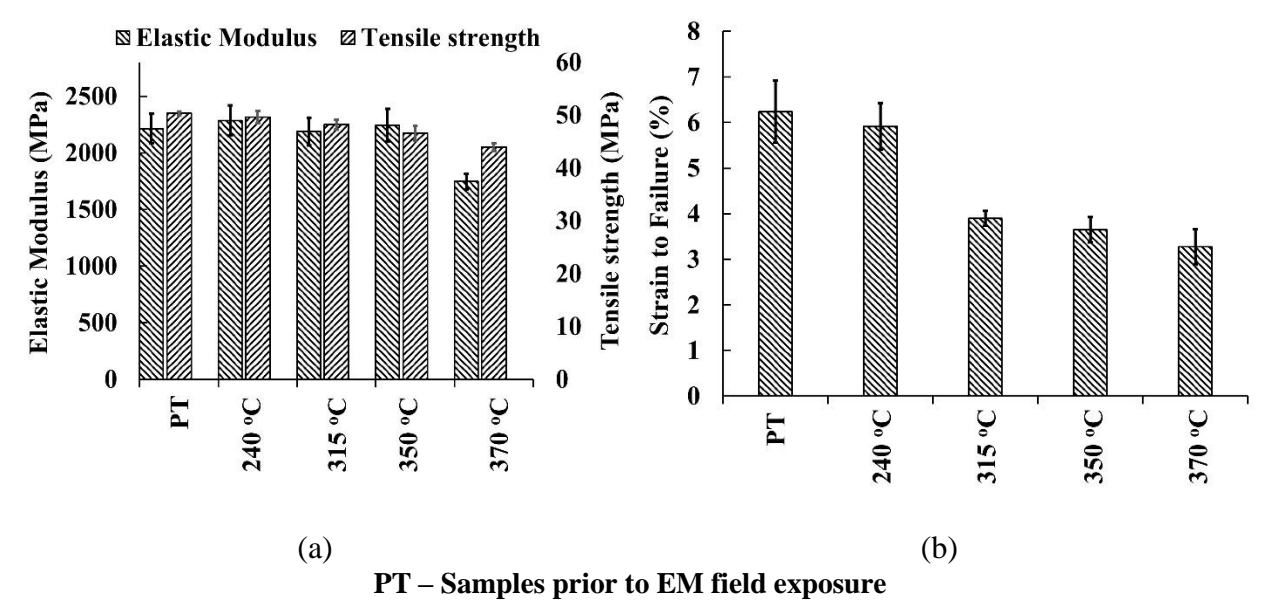
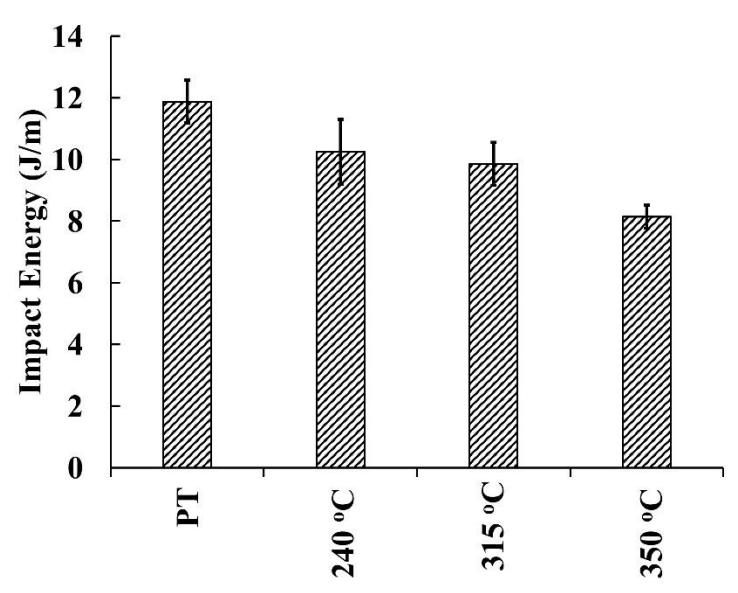


Figure 3-10: Reversible PNC's exposed to different temperatures by EM heating (a) Elastic modulus & Yield strength (b) Strain to failure

Unlike the tensile modulus and yield strength, the strain to failure was reduced in all the samples exposed to EM radiations (Figure 3-10b). Samples exposed to 240°C experienced a slight drop in strain to failure. Further increase in degradation level due to EM exposure reduced the strain to failure by 40% relative to control ABS samples. The drop in ductility/toughness can be attributed to degradation of polybutadiene, which is the monomer widely understood to contribute to the toughness properties of ABS[8]. Overall, the EM exposure affected the ductility of the material significantly compared to its effect on the tensile modulii and yield strengths.



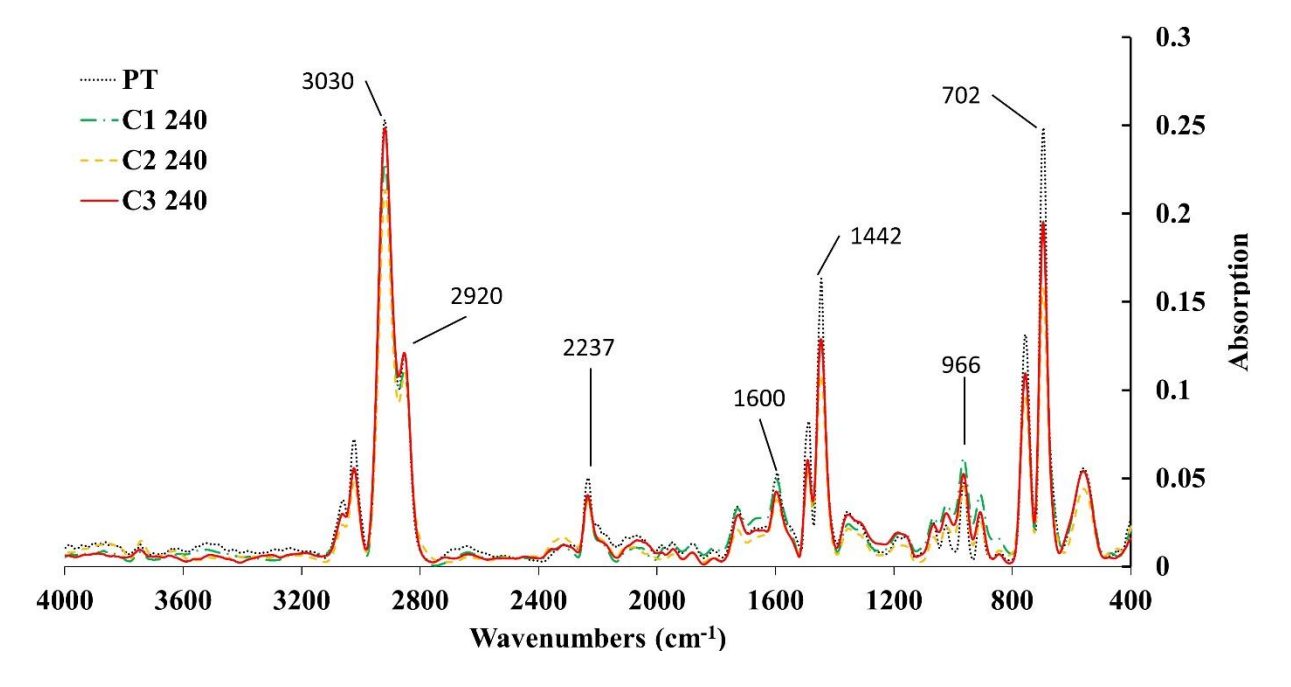
Sample exposed to 370° C was charred and powdered while clamped under IZOD testing machine. Hence not considered for this test. PT – Samples prior to EM field exposure

Figure 3-11: IZOD impact energy of reversible PNC's exposed to different temperatures by EM heating

Similar to tensile tests, IZOD samples were exposed to varying levels of EM radiations followed by testing and the results are shown in Figure 3-11. This test was intended to characterize the impact strength of the EM exposed samples and compare them with pristine un-exposed samples. Impact energy dropped by ~15% for samples exposed to 240°C. As EM exposure and its associated bulk temperature increased, the impact energy also reduced. A maximum reduction of ~33% was observed for EM exposed samples corresponding to degradation bulk temperatures of 350°C. This decrease in impact energy can be attributed to significant degradation in the polybutadiene (PB) phase. Although the major deterioration in mechanical properties are often attributed to the loss of butadiene, the SAN phase can also cause thermo-oxidative and physical ageing in ABS [8][37,40,41]. Further, microstructural inconsistencies such as voids formed during the thermo-oxidative degradation can further lead to brittle failure with no resistance offered for crack propagation.

3.4.3. Effect of EM Heating on Reversibility/Repeatability

The previous section focused on thermal degradation, specifically increasing the bulk temperature of the samples and studying its effect on resulting mechanical properties. In this section, the temperature was maintained a constant (processing point of ABS- 240°C) and repeated EM exposure was to evaluate associated thermal degradation. This study was intended to understand the potential of repeatability/reversibility of the ABS/Fe₃O₄ polymer. The samples were exposed for up to 3 cycles of EM heating. In every cycle, the PNC was heated until the bulk temperature of the polymer reached 240°C, and then allowed to cool to the room temperature before it was exposed to the next cycle of EM heating.



C1, C2 & C3 represents cycles 1, 2, & 3 at temp. – 240 °C; ; PT – Samples prior to EM field exposure

Figure 3-12: FTIR spectra of reversible PNC's exposed to 3 heat cycles of bulk temperature 240°C

The FTIR readings for control (not exposed to EM field) and EM exposed samples (up to 3 heat cycles) are given in Figure 3-12. For all cases of EM exposed samples, a drop in absorbance peak was visible for all wave numbers. While it has been reported that degradation of SAN and butadiene initiates at ~290°C [2], it was observed that the wave numbers 911, 966 and 1600

corresponding to the absorbance spectrum of PB decreased even though the bulk temperature of the polymer did not exceed 240°C. It should be noted that the study in [2] used a uniform convection oven heating to reach 290oC. In this work, the heating due to EM exposure is non-uniform and concentrated around the susceptor particles. While the bulk temperature remains below 240°C, the temperature in the vicinity of the nanoparticles may far exceed 240°C causing degradation of polymer surrounding the particles, thereby supporting the observation in reduction of FTIR peaks relative to control samples.

In order to quantify the effects of repeated EM exposure, mechanical characterization of tensile and IZOD properties were performed. Figure 3-13 (a) shows the elastic tensile modulus and yield strength of the PNC's exposed to EM radiations. The average yield strengths were not significantly affected by repeated EM exposure. The average tensile modulus increased slightly with a maximum of 8% at the end of three EM heat cycles. This increased tensile modulus can be attributed to the degradation of polybutadiene (PB) monomer as indicated by wave numbers 966 and 1600. This results in a loss of ductility accompanied by an increase in stiffness. Thermo-oxidative degradation of PB increases the polymer density by crosslinking and thereby increases the young's modulus[8]. However, EM exposure for longer time/temperature period resulted in significant drop in tensile modulus as shown in Figure 3-10.

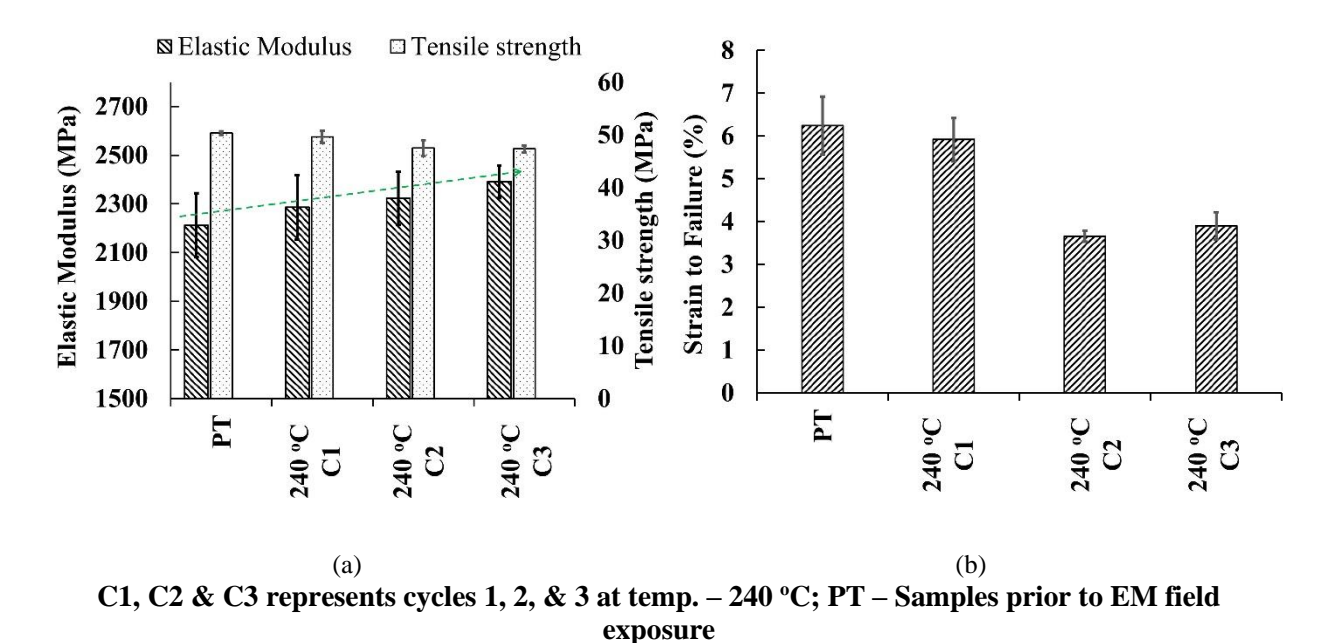


Figure 3-13: Reversible PNC's exposed to 3 heat cycles of bulk temperature 240 °C (a) Elastic modulus & Yield strength (b) Strain to failure

The strain to failure values of PNC's under various EM exposure temperature is given in Figure 3-13 (b). For samples with a single EM exposure, the strain to failure reduction was insignificant. Further exposure to EM field reduced the strain to failure by 40%. This confirms that the toughness property of the PNC reduces upon multiple EM exposure. As explained earlier, the reduction in toughness or strain to failure can be attributed to degradation of PB[42]. Further, thermo-oxidative degradation of the PB phase increases polymer density by cross-linking. This leads to increase in stiffness and brittleness. Similarly, the loss PB and its associated contribution to toughness mechanisms reduces ductility.

Figure 3-14 shows the results of the notched IZOD impact tests for samples with varying EM exposure. The impact strength reduced with increasing frequency of EM exposure. Similar to tensile strains and ductility, the reduction in toughness was expected with increasing EM exposure.

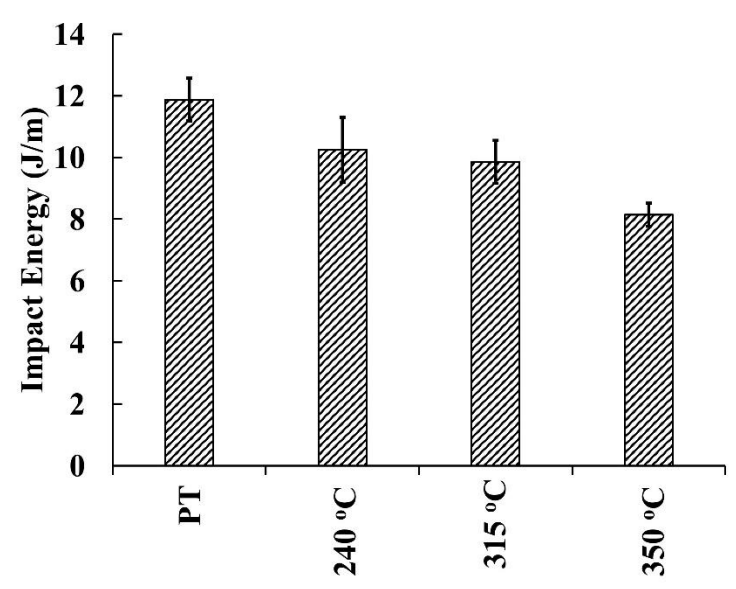


Figure 3-14: IZOD impact energy of reversible PNC's exposed to 3 heat cycles of bulk temperature 240 °C

It was observed that the reversible PNCs can undergo multiple exposure to EMI heating without degrading the elastic tensile modulus and yield strength if the bulk temperature of the polymer does not exceed its processing point (240 °C for ABS). However, this temperature value depends on the thermoplastic polymer used to make reversible PNCs. Polymers with higher processing temperature and glass transition temperatures are expected to tolerate higher exposure time of EM radiations and vice versa. This also depends on the thermal and mechanical property of the polymer to resist damage due to high temperature exposure.

3.4.4. Investigation into Void Patterns

After exposure to EM heating, all the samples studied (tensile and impact) showed a rectangular pattern of voids throughout the cross-section of the samples(Figure 3-15). The void patterns were not observed in oven heated samples exposed to similar temperatures.

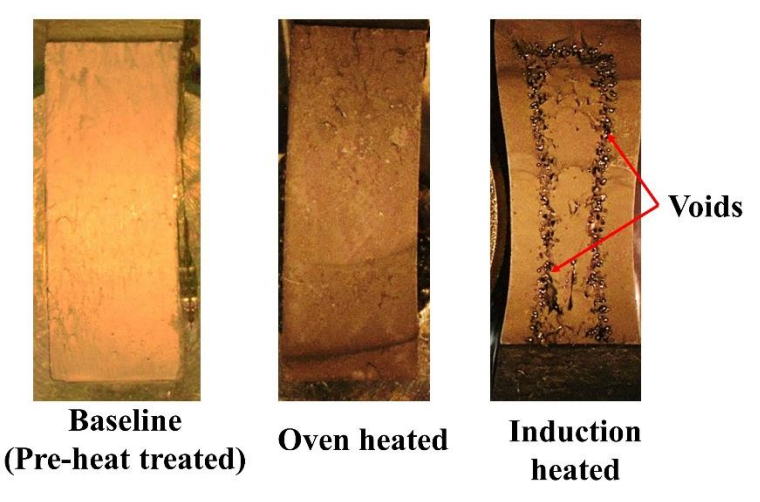
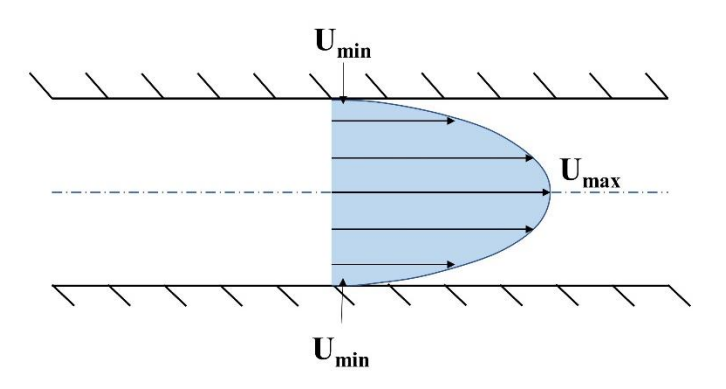


Figure 3-15: Effect of induction heating on polymer nanocomposites

These voids were only produced after the EM processing, and always in a rectangular pattern, with the same distance from the outer walls. This structured distribution of voids indicates a relation to the non-uniform Fe₃O₄ concentrations that arise from molding artifacts. Molded PNCs can contain non-uniformity of reinforcement concentration along the cross section of the sample. This can be attributed to the flow resistance between the mold surface and the molten sample[43][44], as shown in Figure 3-16.



Fluid flow inside a hollow cylinder

Figure 3-16: Flow resistance pattern between two fixed plate inside a mold

Laser ablation inductively coupled mass spectroscopy (LA-ICP-MS) test was conducted to understand the concentration of Fe₃O₄ along the cross section of the extruded samples as shown in Figure 3-17. Three points along the cross section of the IZOD impact fracture surface was

considered for the study. Point 1 represent the edge of the sample, point 2 was taken from the line of voids/degradation and point 3 was from the center of the sample.

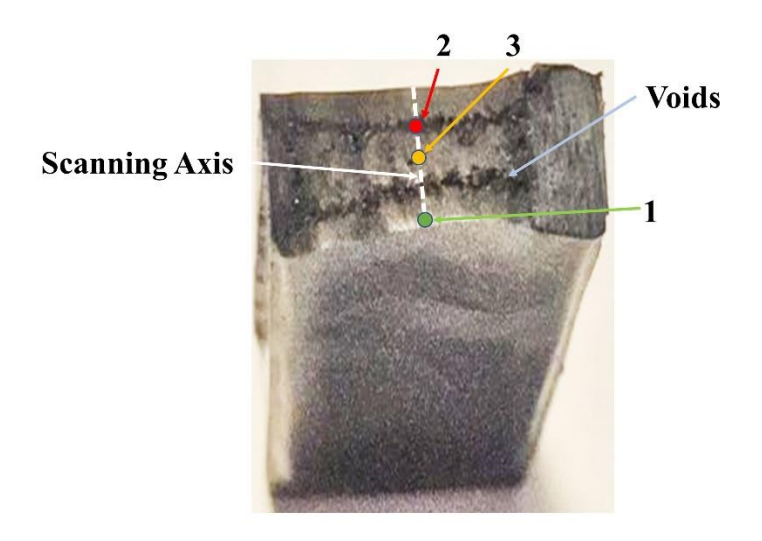


Figure 3-17: IZOD impact fracture surface for LA-ICP-MS test

Table 3-5 shows the Fe₃O₄ concentration in ABS samples across the cross-section. Points 1 and 3 represent the edge and center of the sample cross-section respectively. Point 2 represents the material near the visible voids due to degradation. Table 3-5 summarizes the results, and shows that Fe₃O₄ concentration is the highest nearby the voids and lowest towards the edge of the sample.

Table 3-5: Fe₃O₄ concentrations along the cross section of IZOD fracture surface

Point of Interest	Weight Percentage of Fe ₃ O ₄ (%)
Point 1 (At sample edge)	6.7
Point 2 (Void/Degradation spot)	34
Point 3 (At center)	25

Since the voids are only observed in EM heated samples and not in oven heated samples, it is evident that they are caused by local polymer degradation resulting from one or more of the electromagnetic heating mechanisms. The rectangular pattern suggests that the voids could be a result of Joule heating because of the skin effect associated with this heating mechanism. Under

this hypothesis, the eddy current skin is formed below the surface because of the mold-flow artifacts that result in a higher Fe₃O₄ particle concentration. The current skin is formed at a depth which is as outward as possible while still having the necessary Fe₃O₄ percolation to sustain eddy currents. Furthermore, fe₃O₄ clusters near the voids as seen in the SEM image strengthens this hypothesis (Figure 3-18).

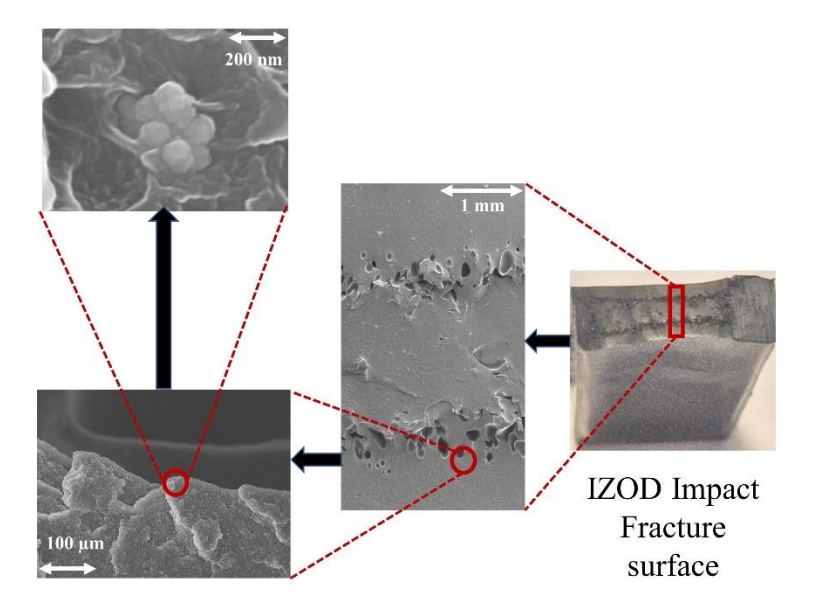


Figure 3-18: IZOD Impact fracture surface of reversible PNCs (ABS +16wt.% FMNP) subjected to EMI heating

Although previous studies [11] have suggested that hysteresis heat loss is the most dominant heating mechanism in polymer nanocomposites exposed to EM radiations, the contribution of Joule's heating cannot be neglected in polymer nanocomposites. Joule heating is more likely to occur if the nanoparticles are not well dispersed within the polymer matrix. One way to limit the Joule's heating in PNCs under EM fields is to chemically treat the nanoparticles so that they repel each other. Although multiple modes of heating can cause severe thermal degradation, it can be useful for certain application that needed rapid heating.

3.5. Conclusions

This work studied the thermal degradation of ABS/Fe₃O₄ polymer nanocomposite under electromagnetic induction heating and its effect on mechanical properties.

The results of this study demonstrate that repeated EM heating of PNCs, even with the temperature maintained at the processing point, introduce thermo-oxidative degradation and deteriorate toughness of the polymer by 40 percent. However, the tensile modulus and yield strength are not significantly degraded in the repeated heating cycles. Longer exposure time to EM radiations resulted in high temperatures and deteriorate both the tensile and IZOD impact properties of the PNC's. FTIR results showed degradation of ABS polymer even when the bulk temperature reached it's processing temperature due to electromagnetic induction heating.

The void pattern found within the fracture surfaces suggests that eddy current Joule heating might be the dominant heating mechanism. Scanning electron microscopy and Laser ablation inductively coupled mass spectroscopy (LA-ICP-MS) confirmed the presence of mold-flow artifacts that could force the eddy current path and possibly cause the structured void patterns observed.

REFERENCES

REFERENCES

- 3-[1] Pielichowski K, NjugunaJames. Thermal Degradation of Polymeric Materials. Rapra Technology Limited; 2005.
- 3-[2] Suzuki M, Wilkie CA. The thermal degradation of acrylonitrile-butadiene-styrene terpolymei as studied by TGA/FTIR. Polym Degrad Stab 1995;47:217–21. doi:10.1016/0141-3910(94)00122-O.
- 3-[3] Chrissafis K, Bikiaris D. Can nanoparticles really enhance thermal stability of polymers? Part I: An overview on thermal decomposition of addition polymers. Thermochim Acta 2011;523:1–24. doi:10.1016/j.tca.2011.06.010.
- 3-[4] Suzuki M. The thermal degradation of acrylonitrile-butadiene-styrene terpolymer as studied by TGA/FTIR 1995;47:217–21.
- 3-[5] Zong R, Hu Y, Liu N, Wang S, Liao G. Evaluation of the thermal degradation of PC/ABS/montmorillonite nanocomposites. Polym Adv Technol 2005;16:725–31. doi:10.1002/pat.651.
- 3-[6] Cai JWX. Kinetics study of thermal oxidative degradation of ABS containing flame retardant components 2012:725–32. doi:10.1007/s10973-011-1704-5.
- 3-[7] Triantou MI, Chatzigiannakis EM, Tarantili PA. Evaluation of thermal degradation mechanisms and their effect on the gross calorific value of ABS/PC/organoclay nanocomposites. J Therm Anal Calorim 2015;119:337–47. doi:10.1007/s10973-014-4152-1.
- 3-[8] Tiganis BE, Burn LS, Davis P, Hill AJ. Thermal degradation of acrylonitrile-butadiene-styrene (ABS) blends. Polym Degrad Stab 2002;76:425–34. doi:10.1016/S0141-3910(02)00045-9.
- 3-[9] Gong J, Chen Y, Jiang J, Yang L, Li J. A numerical study of thermal degradation of polymers: Surface and in-depth absorption. Appl Therm Eng 2016;106:1366–79. doi:10.1016/j.applthermaleng.2016.06.114.
- 3-[10] Cervantes-Uc J., Cauich-Rodriguez J., Vazquez-Torres H, Licea-Claverie A. TGA / FTIR study on thermal degradation of polymethacrylates containing carboxylic groups. Polym Degrad Stab 2006;91:3312–21. doi:10.1016/j.polymdegradstab.2006.06.005.
- 3-[11] Bayerl T, Mitschang P. Heating of Polymer-Polymer Composites By Inductive Means. Iccm-Central.Org, 2011, p. 1–6.
- 3-[12] Bayerl T. Application of Particulate Susceptors for the Inductive Heating of Temperature

- Sensitive. Institut für Verbundwerkstoffe GmbH, 2012.
- 3-[13] Bayerl T, Brzeski M, Martı M, Schledjewski R, Mitschang P. Thermal degradation analysis of short-time heated polymers 2015:390–414. doi:10.1177/0892705713486122.
- 3-[14] Manufacturing A, Canada C, Laurent S. Fusion Bonding/Welding of Thermoplastic Composites n.d.;17:303–41. doi:10.1177/0892705704045187.
- 3-[15] Ahmed TJ. Induction welding of thermoplastic composites an overview 2006;37:1638—51. doi:10.1016/j.compositesa.2005.10.009.
- 3-[16] Rudnev V, Loveless D, Cook R, Black M. Handbook of induction heating. Basel: Marcel Dekker AG; 2003.
- 3-[17] Tay TE, Fink BK, S.H.McKnight, S.Yarlagadda, Gillespie JW. accelerated curing of adhesives in bonded joints using induction heating.pdf. J Compos Mater 1999;33.
- 3-[18] Vattathurvalappil SH, Hassan SF, Haq M. Monitoring Residual Strains in Oven-and Induction-bonded Joints. Proc. Am. Soc. Compos. Tech. Conf., 2019. doi:10.12783/asc34/31288.
- 3-[19] Vattathurvalappil SH, Haq M. Experimental and numerical Investigation of Bonded joints subjected to transverse impact loads. SPE ACCE, 2017.
- 3-[20] Vattathurvalappil SH, Haq M. Thermomechanical Characterization of Nano-Fe3O4 Reinforced thermoplastic adhesives and joints. Compos Part B Eng 2019;175:107162. doi:10.1016/j.compositesb.2019.107162.
- 3-[21] Ciardiello R, Belingardi G, Martorana B, Brunella V. International Journal of Adhesion and Adhesives. Int J Adhes Adhes 2019;89:117–28. doi:10.1016/j.ijadhadh.2018.12.005.
- 3-[22] Verna E, Cannavaro I, Brunella V, Koricho EG, Belingardi G, Roncato D, et al. Adhesive joining technologies activated by electro-magnetic external trims. Int J Adhes Adhes 2013;46:21–5. doi:10.1016/j.ijadhadh.2013.05.008.
- 3-[23] Faraday M. On the magnetization of light and the illumination of magnetic lines of force c. 1. c. 1. R Soc 1846.
- 3-[24] Rudolf R, Mitschang P, Neitzel M. Induction heating of continuous carbon-fibre-reinforced thermoplastics. Compos Part A Appl Sci Manuf 2000;31:1191–202. doi:10.1016/S1359-835X(00)00094-4.
- 3-[25] Stoner EC, Wohlfarth E. A Mechanism of magnetic hysteresis in heterogenous alloys 1948;240.
- 3-[26] Néel L. Some theoretical aspects of rock-magnetism. Adv Phys 1955;4:191–243.

- doi:10.1080/00018735500101204.
- 3-[27] Yarlagadda S, BK F, Gillespie JW. Resistive susceptor design for uniform heating during induction bonding of composites. J Thermoplast Compos Mater 1998;11.
- 3-[28] Suwanwatana W, Yarlagadda S, Gillespie JW. Hysteresis heating based induction bonding of thermoplastic composites. Compos Sci Technol 2006;66:1713–23. doi:10.1016/j.compscitech.2005.11.009.
- 3-[29] Zhang XK, Li YF, Xiao JQ. Theoretical and experimental analysis of magnetic inductive heating in ferrite materials. J Appl Phys 2003;93.
- 3-[30] Bayerl T, Schledjewski R, Mitschang P. Induction heating of thermoplastic materials by particulate heating promoters. Polym Polym Compos 2012;20:333–42.
- 3-[31] Vattathurvalappil SH, Haq M. Thermomechanical Characterization of Nano-Fe3O4 Reinforced thermoplastic adhesives and joints. Compos Part B Eng 2019;175. doi:10.1016/j.compositesb.2019.107162.
- 3-[32] Polli H, Pontes LAM, Araujo AS, Barros JMF, Fernandes VJ. Degradation behavior and kinetic study of ABS polymer. J Therm Anal Calorim 2009;95:131–4. doi:10.1007/s10973-006-7781-1.
- 3-[33] Nabiyouni G, Ghanbari D. Thermal , Magnetic , and Optical Characteristics of ABS-Fe 2 O 3 Nanocomposites 2012:1–7. doi:10.1002/app.
- 3-[34] International A. Astm D638. vol. 82. 2016. doi:10.1520/D0638-14.1.
- 3-[35] International A. Astm D256-10. 2014. doi:10.1520/D0256-10.N.
- 3-[36] Vattathurvalappil SH, Haq M. Thermomechanical characterization of Nano-Fe<inf>3</inf>O<inf>4</inf> reinforced thermoplastic adhesives and single lap-joints. Compos Part B Eng 2019;175. doi:10.1016/j.compositesb.2019.107162.
- 3-[37] Shimada J, Electrical T. The Mechanism of Oxidative Degradation of ABS Resin . Part I . The Mechanism of Thermooxidative Degradation 1968;12:655–69.
- 3-[38] Bergstrom J. Mechanics of solid polymers:theory and computational modeling. 1st ed. Amsterdam: Elsevier; 2015.
- 3-[39] Li J, Chen F, Yang L, Jiang L, Dan Y. Spectrochimica Acta Part A: Molecular and Biomolecular Spectroscopy FTIR analysis on aging characteristics of ABS / PC blend under UV-irradiation in air. Spectrochim Acta Part A Mol Biomol Spectrosc 2017;184:361–7. doi:10.1016/j.saa.2017.04.075.
- 3-[40] Salman SR, Al-shama ND. Effect of Thermal Aging on the Optical Properties of ABS Plastics 2006;2559. doi:10.1080/03602559108021000.

- 3-[41] Wyzgoski MG, Wyzgoski MG. Effects of Oven Aging on ABS, Po I n.d.;16:265–9.
- 3-[42] Kinloch AJ, Young R. Fracture behaviour of polymers. Appl Sci Publ London New York 1983. doi:https://doi.org/10.1002/pi.4980160231.
- 3-[43] Dontula N, Ramesh N., Campbell G., Small J., Fricke A. An Experimental Study of Polymer-Filler Redistribution in Injection Molded Parts. J Reinf Plast Compos 1994;13:98–110.
- 3-[44] Dane F, Garnier B, Dupuis T, Lerendu P, -Phap NT. Non-uniformity of the filler concentration and of the transverse thermal and electrical conductivities of filled polymer plates. Compos Sci Technol 2005;65:945–51. doi:10.1016/j.compscitech.2004.10.017.

Chapter 4: Reversible Adhesive Bonded Single Lap Joints ¹

4.1. Abstract

In this work, Acrylonitrile Butadiene Styrene (ABS) was selected as the thermoplastic adhesive and reinforced with 12, 16 and 20 weight percent of ferromagnetic nanoparticles (FMNP) through melt processing to use as adhesives Lap-joints using glass-fiber substrates were bonded using ABS/FMNP films through conventional oven-bonding and induction-bonding techniques, and their effect on resulting joint behavior was studied. Further, effects of O₂-plasma surface treatment and adherent preheating on resulting joints were also studied. Results indicate that joints without O₂-plasma surface treatment led to interfacial failures whereas induction-bonded joints with both O₂-plasma and substrate preheating had 15% higher peak loads relative to oven-bonded joints. Optimization of the induction heating process parameters along with surface functionalization of particles and substrates is essential to fully exploit the benefits offered by these novel thermoplastic adhesives.

4.2. Experimental Methods

4.2.1. Materials

This study used Acrylonitrile Butadiene Styrene (ABS) as the thermoplastic adhesive (CYCOLACTM Resin MG 94, SABIC®). ABS was selected for its excellent toughness provided by the polybutadiene phase grafted to the acrylonitrile styrene matrix. Additionally, ABS provides a good balance between cost, mechanical properties, chemical resistance, ease in processing and aesthetics [1] and is widely used in various domains including automotive, consumer market, electronics and sports industry. The melt temperature provided by the ABS supplier is 240°C and

_

¹ Part of this work has been published in : S. H. Vattathurvalappil, M. Haq, "Thermomechanical characterization of Nano Fe₃O₄ reinforced thermoplastic adhesives and single lap joints", Composites – Part B, 2019, 175, 107162.

was used for all processing in this work. The higher the melt temperature, the better the flow and wettability for joining purposes. The ferromagnetic nanoparticle (FMNP) fillers used were Iron (II, III) oxide (Fe₃O₄, Sigma Aldrich) spherical particles with approximately 50-100 nm in diameter. The adherent used in the single lap joint were commercially available glass-fiber/epoxy (Garolite G-10) with a thickness of 3.2 mm Garolite G-10 was selected as it is effectively isotropic (in-plane), has low thermal expansion, and is dimensionally stable at the ABS processing temperature, while also being electrically non-conductive so that it does not interact to the applied magnetic field during induction heating.

4.2.2. Adhesive Processing and Manufacturing

A total of six ferromagnetic nanoparticle (FMNP) concentrations in ABS were studied in this work, namely: i) neat ABS (0 wt.%), ii) 4 wt.%, iii) 8wt.%, iv) 12wt.%, v) 16 wt.%. and vi) 20 wt.%. First, the ABS pellets were dried for 3 hours at 80°C to remove any residual moisture. A 15 cc. mini-extruder (DSM Netherlands) was used for processing the ABS/FMNP mixtures. The desired quantity of FMNP powder was dry mixed and fed to the DSM extruder barrel that houses two contra screws rotating at 100 RPM. The barrel temperature was maintained at 240°C (melt temperature) and the polymer was mixed for either 3 min. or10 min. Further, molten adhesive was collected as discs and cooled to further create adhesive films by compressing it in a Carver press. Steel spacers of 1mm were used along with a temperature of 150°C and a pressure of ~575 kPa. The resulting films were cut into 25.4 mm x 25.4 mm. squares to be bonded with the adherents. The tensile and impact samples were measured for its dimensional compatibility with ASTM standards and no visible effects of shrinkage or voids were observed after cooling process.

4.2.3. Manufacturing of Single Lap Joints

Oven-Bonding

The single lap joints were manufactured using both induction heating and oven heating methods. In both cases, glass rods of 0.5 mm diameter were used as spacers to provide a uniform bond thickness and the adherents were clamped as shown in Figure 4-1. For thermal bonding, the joints in Figure 1 were placed in a convection oven at 240°C for 15 minutes.

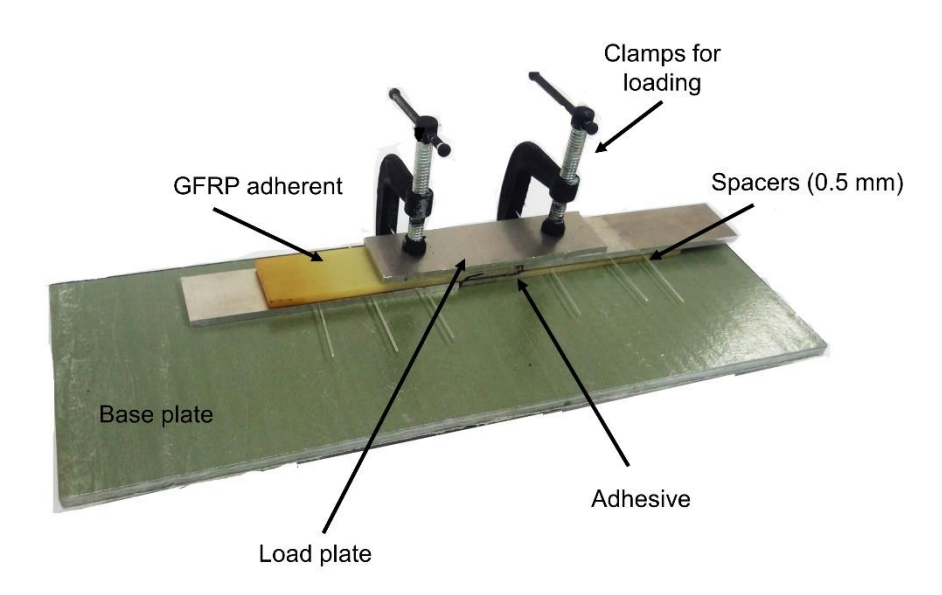


Figure 4-1: Single lap joint fixture for oven heating process

Induction Bonding:

The equipment used for induction bonding in this work was an induction heater (Across International -IHG06A1) which had a maximum input current of 30 A, output frequency of 100-500 kHz and maximum oscillating power of 6.6 kW. The coil used with this system for the induction bonding was obtained from Acroos International (model: IHHC 2x1) and had internal dimensions of 50.8 mm x 25.4 mm. The coil was made of a copper tube with a square cross-section of 6.35 mm x 6.35 mm and had six turns. It should be noted that the heating efficiency will change when the power and frequencies are altered. Hence, in this work 200 kHz and 30 A were

maintained for all adhesive systems to create the initial baseline for induction bonded joints. Figure 4-2 shows the induction system along with the coil used in this work.

A fixture made of non-conductive ceramic that does not interact with electromagnetic radiations was used and is shown in Figure 4-2. The coil used for the induction process has a rectangular cross-section conforming geometrically to the lap-joint profile with outer dimensions of 25.4 mm x 50.8 mm. Guide pins were used to consistently align the substrates and to prevent them from moving during processing. The time required to initiate thermoplastic melt and flow was measured for each adhesive configuration and the results are presented in section 0. Once the top substrate moves to the final thickness that of the spacers, the induction system was turned off and the joint was left to cool back to room temperature.

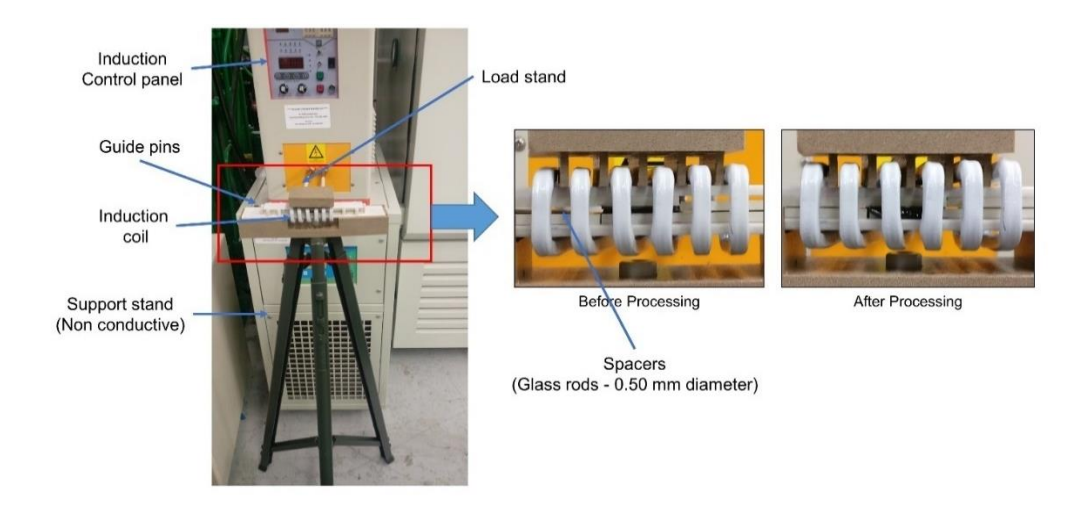


Figure 4-2: Single lap joint fixture for induction heating process

4.2.4. Surface Treatment of Adherents and Adhesive Films

Each adherent was grit blasted with alumina powder having spherical particles with a mean diameter of 50 microns. The adherents were then air blasted followed by solvent cleaning using acetone to prepare for next step in surface treatment, namely O₂ plasma treatment. The bonding area of the adherents was plasma treated by exposure to O₂ plasma for 3 minutes at 275 watts and maintaining the O₂ pressure at 264 mTorr, to create uniform etching of the bond surface. Similar

to the substrates, thermoplastic adhesive films were also O₂ plasma treated. Commercially available thermoplastics are designed for injection molding applications and have proprietary release agents for facile mold-removal. Using such thermoplastic films cannot create structural bonds. Hence, in this work, O₂ plasma was used to etch the surface release agents prior to bonding using similar aforementioned steps for adherents. The effect of surface treatment on resulting joint behavior is discussed in section 3.

4.3. Mechanical Testing Methods

4.3.1. Uniaxial Lap Shear Tests

A load-cell with maximum capacity of 50 kN and a cross-head speed of 5 mm/min. was used as per ASTM standard D5868.

4.4. Monitoring Adhesive Temperature

In order to monitor the thermoplastic processing during the induction process, accurate temperature measurements in the adhesive are needed. While several non-contact infrared temperature sensors are available, they only provide surface temperatures [2]. In order to measure the temperature in the adhesive bond-line, a fiber-optic sensor was placed in the bond-line and time-temperature measurements were recorded during the exposure to electromagnetic radiations. Specifically, a distributed fiber-optic sensor (Luna ODiSI-B) which had a diameter of 1.0 mm was used as shown in Figure 4-3. This system uses the Rayleigh scattering effect in optical fibers to enable continuous measurement of either temperature or axial strain along the entire length of the fiber. The fiber optic sensors were placed along the center and two edges of the adhesive film. Only the center fiber optic sensor was used to determine the heating rate of the adhesive as the edges have boundary condition that can lead to rapid cooling

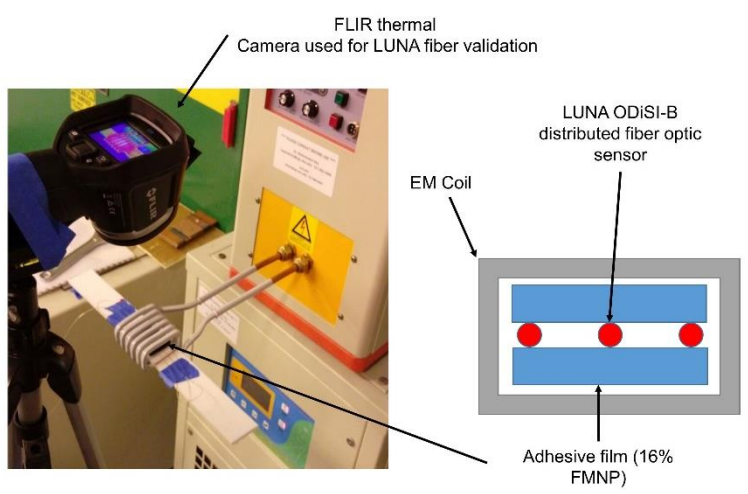


Figure 4-3: Temperature measurement of adhesive under induction heating process

4.5. Results & Discussion

4.5.1. Induction Heating: Processing Time and Temperature Measurements

As described in section 2.6, a distributed fiber-optic sensor (Luna ODiSI-B) was used to measure the temperature in the adhesive bond-line while it was exposed to electromagnetic radiation. The sensor used is capable of measuring temperatures up to 240°C while the range of processing point of the ABS polymer is 200°C to 240°C. In order to compare the heating efficiency of adhesives with varying FMNP, the time required to reach 220°C was considered, and the results are shown in Figure 4-4. The temperature was recorded only at the center point of the adhesive bond-line where it was found to be maximum at any given time.

As expected, it was observed that the time required for adhesive processing drops with increasing FMNP content. The neat ABS polymer used in this work does not react to electromagnetic radiations for up to 300s and hence ignored for this temperature study. Similarly, the non-conductive substrates used in this work do not interact with electromagnetic radiations.

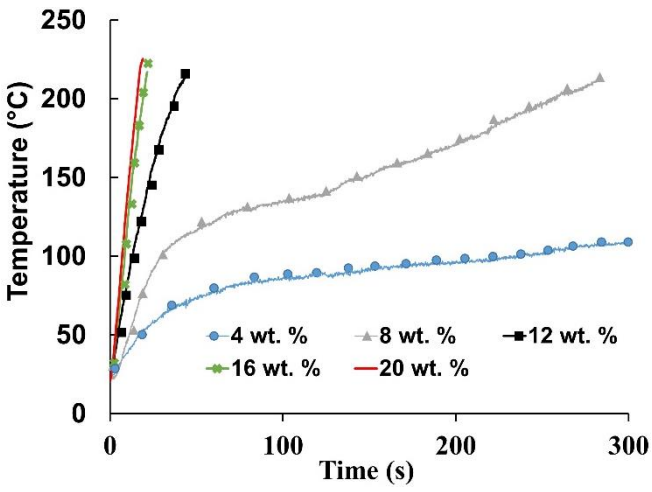


Figure 4-4: Heating rate of adhesives under induction heating process

The induction-based manufacturing of lap-joints was described in section 2.3. One of the major limitations of coil-based induction heating is the non-uniform distribution of the electromagnetic field within the joint/adhesive assembly and is dependent on the coil geometry and material composition of the joint/adhesive [3]. Hence, for any given FMNP concentration, the time required for the adhesive to reach the processing point within the lap-joint assembly was greater than those observed for just adhesives (without substrates). Figure 4-5 provides the manufacturing time for lap-joints, i.e., the time required for electromagnetic exposure such that the adhesive melts and the substrates come into contact with the spacers to achieve the final bondline thickness. This manufacturing time is also compared with the time required to melt the adhesive alone (without substrates) as shown in Figure 4-5. This study on manufacturing time comparison was only done of adhesives with FMNP contents greater than 12 wt.% as lower concentrations have poor electromagnetic response and take longer processing time (see Figure 4-4). Hence, adhesives with 4wt.% and 8 wt.% FMNP were not converted into lap-joints and the resulting mechanical lap-shear behavior was only studied for three adhesive configurations, namely 12 wt.%, 16 wt.% and 20 wt.%.

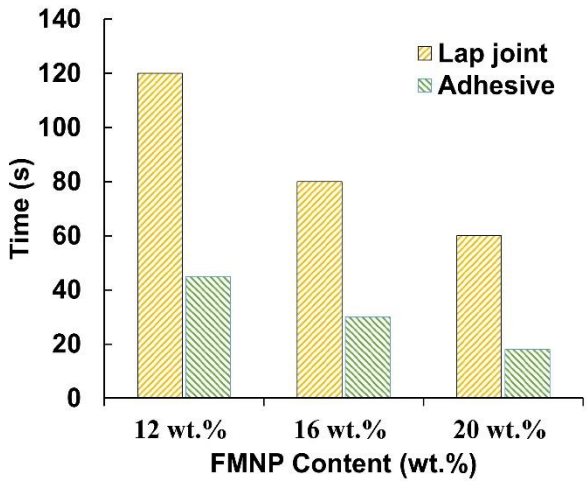


Figure 4-5: Time required for processing FMNP embedded ABS in 'adhesive only (no substrates)' and 'lap-joint assembly' configurations.

4.5.2. Mechanical Testing of Oven Bonded Lap-Joints

Figure 4-6 summarized the average peak loads and displacements at failure in lap-joints with varying FMNP content in ABS adhesive. On average, the displacements at failure increased with increasing FMNP content and the average peak loads remained relatively the same for varying FMNP content. The typical failure surface is shown in Figure 4-6 (b). It can be observed that the failure initiates in the regions of high peel stresses and propagates through the adhesive. The mechanisms controlling the crack movement through the adhesive will govern the behavior of the joint. It also appears from Figure 4-6 (b) that the regions of high peel stresses experience interfacial failure followed by crack passing through the adhesive. The crack resistance mechanisms from the FMNP are present only in the zone where the crack propagates through the adhesive. It appears that the crack pinning around spherical nanoparticles [4] contributes only to the displacement and not the load carrying capacity.

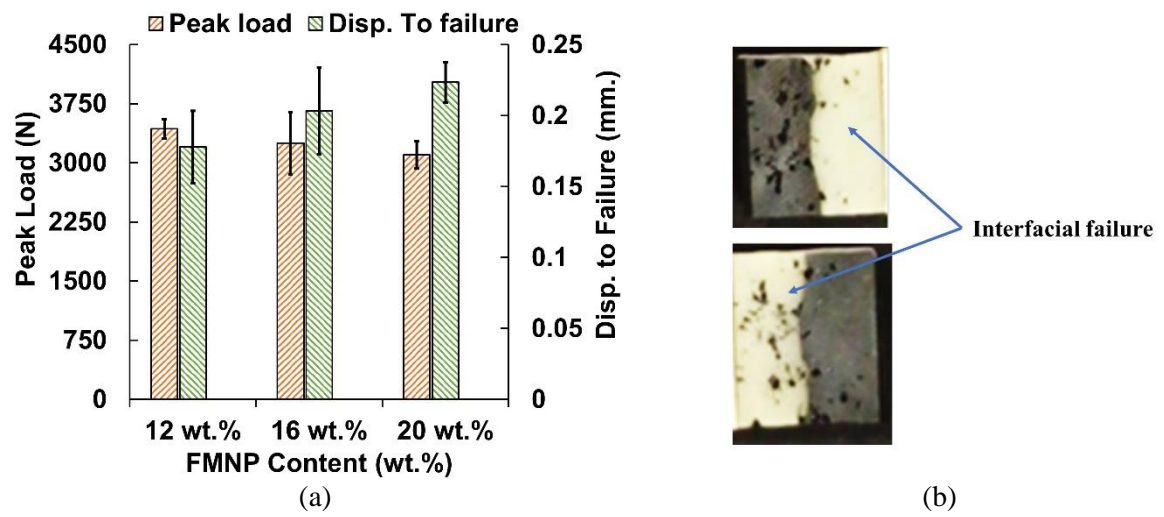


Figure 4-6: Effect of FMNP content in oven bonded joints (a) Peak Loads and Displacements at Failure (b) Failure surfaces of untreated samples

4.5.3. Effect of O₂ plasma surface treatment

The surface preparation of the adherents and manufacturing of adhesive films were described in sections 2.4 and 2.2.1 respectively. These grit-blasted adherents and pressed-films were further exposed to O₂ plasma as explained in section 2.4. This study on O₂ plasma treatment was evaluated for only one case of adhesive, namely ABS with 16 wt.% FMNP. Figure 4-7 shows the comparison of peak loads and displacement at failure for resulting lap-joints with, and without the O₂ plasma treatment. While the average peak loads were similar for both untreated and plasma treated joints, the failure displacements were approximately 6 times higher for plasma treated joints. This indicates an efficient bond with excellent load-transfer. Oxygen plasma treatment improved the surface energy of the adherents and resulted in strong interfacial bonding between the adhesive and the adherents, thereby forcing the failure to happen through the adhesive bondline (and not on interfaces), leading to cohesive failures as shown in Figure 4-7 (b). Since the crack propagates through the adhesive, the nanoparticles may act as crack arrestors/deflectors and further enhance the ductility.

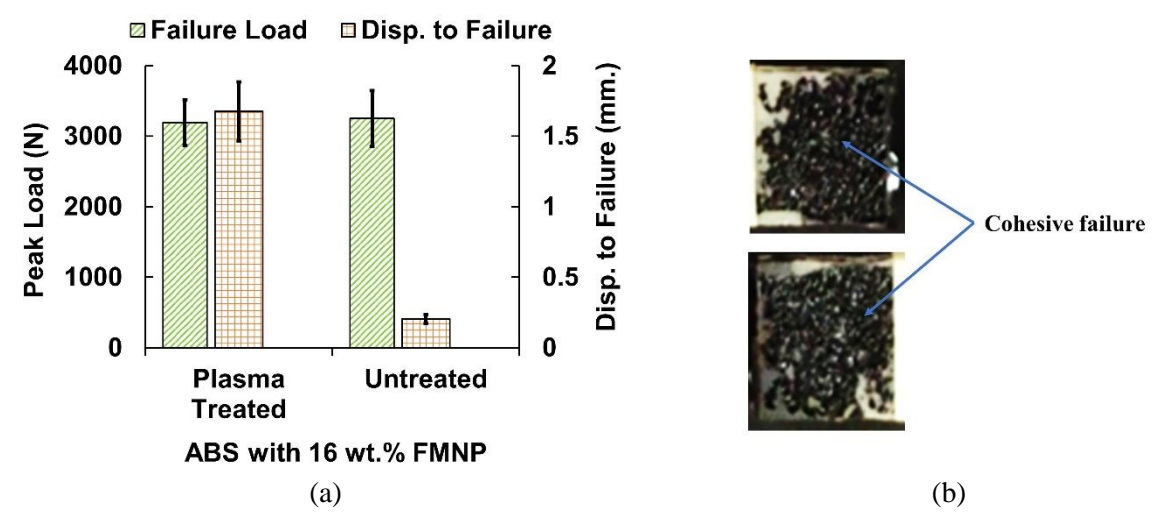


Figure 4-7: Effect of O₂ plasma treatment: a) Peak Loads and Failure Displacements, b) Fracture surface indicating cohesive failure in O₂ plasma treated samples.

4.5.4. Mechanical Testing of Induction Bonded Joints

The previous section focused on oven-bonded joints wherein the assembly of adherents and adhesive were simultaneously heated in a convection oven to create a bonded joint. This section focuses on induction-bonded joints wherein 'just the adhesive' heats up rapidly and the adherents are at room temperature, except near the adhesive interfaces wherein heat-conduction through the adhesive occurs. It has been noted [5] that the thermal conditions on the adhesive/adherent interface are important for formation of the bond. Furthermore, the temperature of the adherent has to be higher than a critical contact temperature to facilitate the formation of a strong bond [6]. The rapid heating of the adhesive and relative lack of heating of the substrate in the induction process in this study, does not allow for proper wettability of the adhesive, as observed from the results. Figure 4-8 a summarizes the average peak loads and displacements at failure for induction-bonded joints with varying FMNP content. While, the average peak loads and displacements at failure showed increasing trend with increasing FMNP content, the failure mode was interfacial as shown in Figure 4-8 b. For a given duration of induction exposure, the adhesives with higher FMNP reached the processing temperature quickly and consequently heated the

substrate, leading to relatively higher peak loads and displacements. One approach is to increase the induction exposure time until a good bond is formed. But, excessive induction exposure can lead to adhesive degradation, and the study of exposure time and its effect of bond quality is beyond the scope of this paper. Another approach is to pre-heat the substrate independently and introduce it into the induction system for bonding. This approach is explained in the next section.

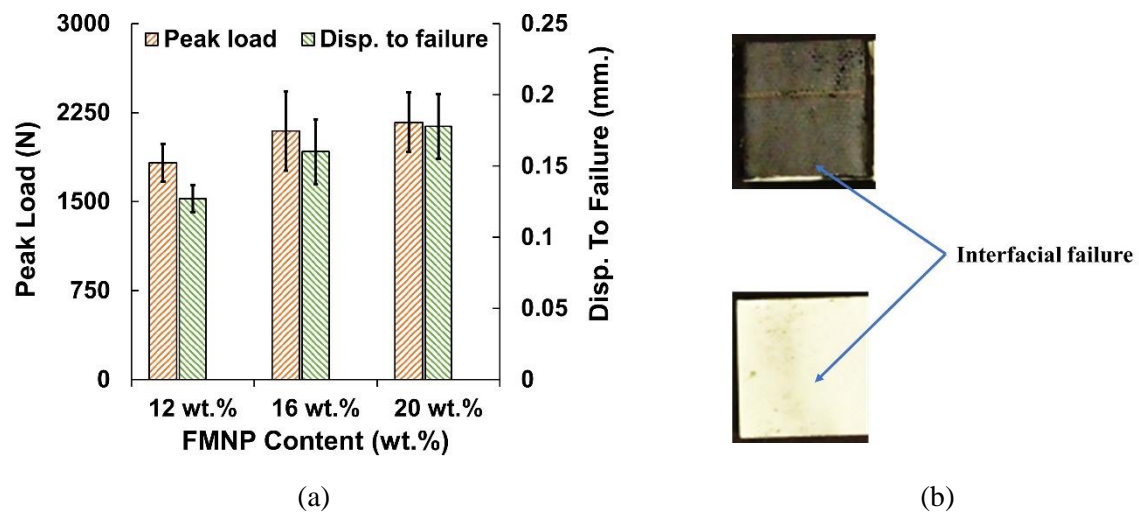


Figure 4-8: (a) Peak Loads and Displacements of induction bonded lap-shear joints with varying FMNP content (b) Typical fracture surface for all induction bonded joints.

4.5.5. Effect of Adherent Preheating

In order to form a strong bond, conditions to have proper wettability of the adhesive to the adherent is essential. While surface preparation techniques are well known, the need for the preheating of the substrate to form a strong bond is relatively not well understood [6]. Treffer et al. [5] provide critical information to understand the need for preheating substrates to create strong bonds in hot-melt adhesives. In short, the contact temperature at the adherent when the hot-melt/thermoplastic is applied should be greater than the polymers solidification point to create a strong bond. In this work, three adherent temperatures (140 °C, 180 °C and 200 °C) were selected such that they were greater than the adhesive (ABS) glass transition temperature (T_g) of 105 °C and below its processing temperature of 200 °C.

Figure 4-9 shows the effect of adherent preheating on lap-shear strengths and failure displacements for ABS adhesives with a constant FMNP content of 16 wt.%. Out of three temperatures, 180 °C showed the best preheating temperature to get the highest peak load and displacement at failure. Overall, for the type of adhesive and adherents studied in this work, adherent preheating resulted in approximately +100% improvement in both average peak loads and displacements to failure.

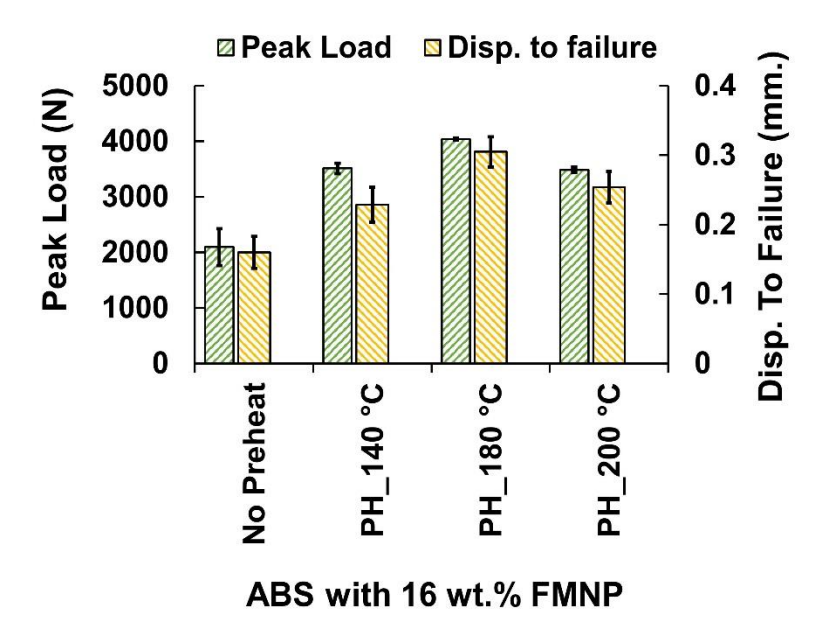


Figure 4-9: Effect of adherent preheating on lap-joint performance. All joints were O_2 plasma treated and had constant FMNP content of 16 wt.%

While it is well understood that higher temperature exposure of ABS adhesive leads to thermal degradation [1], [7], [8], further detailed thermal degradation studies are need to fully understand the electromagnetic heating and degradation of polymers, which is beyond the scope of this work and hence not included. Also, studies on repeated disassembly/re-assembly of joints, polymer degradation due to induction exposure and phenomena controlling their behavior needs to be further evaluated.

4.5.6. Oven vs Induction Joints: A Comparison

Figure 4-10 provides representative force-displacement responses in lap-shear configuration for the five cases of single lap-joints studied in this work. This was done to compare the effect of each parameter studied on the stiffness, strength and ductility of resulting joints. The parameters compared include differences in oven-based and induction-based manufacturing, effect of plasma surface treatment and preheating. The plots are shown with the following nomenclature "Process-Surface Treatment-Preheating". For instance, an induction bonded (IB), plasma treated (PT) and preheated (PH) lap-joint is denoted in Figure 4-10 as IB-PT-PH. Similarly, oven bonding (OB) that do not have preheating are denoted by NH and the joints with no pretreatment are denoted by NP

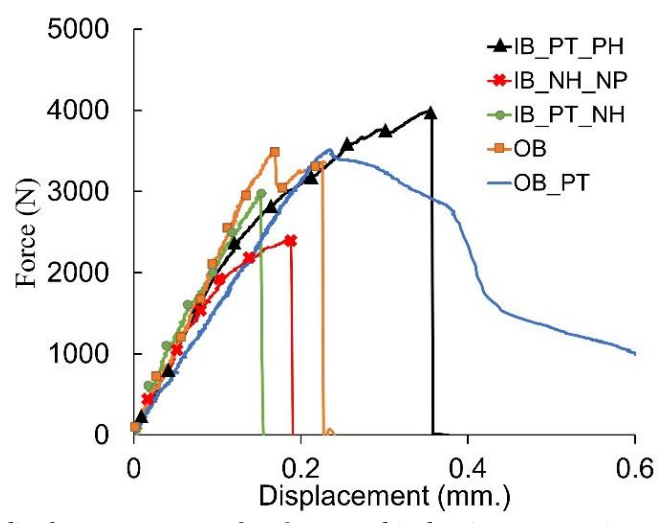


Figure 4-10: Load-displacement curve for Oven and induction comparison. Legend: IB-Induction Bonded, OB-Oven Bonded, PH- preheated, NH- No preheat, PT-Plasma Treated, NP-No plasma treatment

As expected, the lap-joints manufactured with surface treatment performed better than untreated adherent joints. Similarly, preheating the adherend increased both peak load and ductility compared to similar joints that were not preheated. Overall, the induction bonded joints that contained adherends that were neither preheated nor plasma treated exhibited lowest peak loads and ductility. Exposure of ABS+FMNP adhesives to electromagnetic induction results in rapid

heating, flow of adhesive on the substrate. If the substrate is cold, a skin-effect that inhibits bonding occurs resulting in interfacial failures. If the substrate is preheated, the adhesive flows with excellent wettability and results in good bonding. Hence, the induction bonded joints with preheating and surface treatment exhibited the highest shear strengths and ductility. On the other hand, oven bonding using convection heating leads to a gradual heating of the entire joint (adherents + adhesive). The top/bottom and edges of the adherents along with the adhesive edges heat faster than the center of the adhesive. The entire joint is then maintained at the processing temperature until the entire system comes to equilibrium. The flow of adhesive and resulting bonding is not uniform and as instantaneous as observed in induction bonding. This can be one of the reasons for slightly lower shear strengths of oven-bonded joints relative to pre-heated, surface treated induction joints.

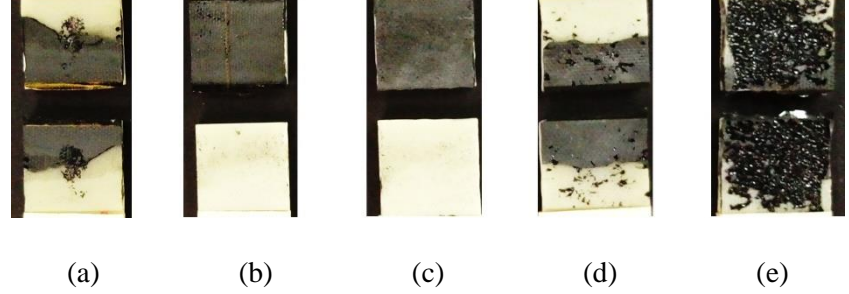


Figure 4-11: Single lap shear test fracture surfaces (a) Induction bonded, preheated and plasma treated (b) Induction bonded joint (no preheat and no plasma) (c) Induction bonded after plasma treatment but no preheat (d) Oven bonded (no plasma treatment) (e) Oven bonded after plasma treated

While, the instantaneous/quick bonding using induction is beneficial for rapid joining, the thermal boundary conditions in induction bonding are significantly different than oven bonding. Induction bonding is instantaneous and introduces a thermal shock due to varying thermal properties of the adherend and the adhesives, leading to thermal locked-in stresses or residual stresses that can impact the strength and ductility of the joints. These thermally induced stresses are expected to be significantly lower in oven-bonded joints due to gradual heating and cooling. Nevertheless, the study of processing and its effect on generation of residual stresses is beyond the

scope of this work. Figure 4-11 shows the representative fracture surfaces for the five joints shown in Figure 4-10. It was observed that induction bonded joints with neither surface treatment nor preheating had interfacial failures (Figure 4-11b). Similarly, for induction bonded joints with no preheating despite plasma treatment had interfacial failures (Figure 4-11e). The induction bonded joints with both surface treatment and preheating showed mixed cohesive-interfacial failures (Figure 4-11a). It should be noted that these joints had the highest peak load and ductility despite partial cohesive failure. The effect of preheating does not matter in oven bonded joints as the whole lap-joint assembly heats up gradually, but the effect of surface treatment is evident from Figure 4-11 (d) and (e). The oven bonded joints with plasma treatment had cohesive failures (Figure 4-11d).

It should be noted that the phenomena of bonding for induction and oven bonding system is very complex and is dependent on many factors including but not limited to surface treatments, mechanical and thermal boundary conditions, additives in the thermoplastic, nanoparticle concentration, etc. and detailed study on each of these parameters is essential to select the right bonding technique for the right application.

4.6. Conclusions

While surface treatment of substrates to increase adhesion is well-established, the additional surface preparation of thermoplastic adhesive film in this work needs further explanation. The commercial thermoplastics are designed for injection molding and have proprietary release agents to enable face demolding. Using such thermoplastics for bonded joints will lead to interfacial failure. Hence, surface treated joints performed better than untreated joints. Similarly, temperature of the substrates when molten adhesive comes into contact with the substrates is vital to create a good bond. Joints with preheated substrates outperformed joints with substrates at room

temperature. The oven bonded joints do not have the preheating constraint as the entire joint assembly heats up uniformly and cools gradually to create the bond. The preheating of substrates is hence required for successful induction bonded joints. The FMNP particles used were nonfunctionalized 'by design' to create a control/benchmark on the behavior of resulting adhesives. Overall, the induction bonded joints decreased the time required to manufacture joints significantly relative to oven bonded joints, thereby reducing the possibility of degradation of the substrates. Statistical tools can further enable finding optimal material configurations that could lead to multiproperty synergistic behavior. Further studies on effect of functionalization of FMNP to increase polymer-particle compatibility and its effect on adhesive and joint properties, induction processing parameters, thermal residual stresses developed due to rapid heating/cooling, and polymer degradation need to be performed to fully exploit the benefits offered by this hybrid material.

REFERENCES

REFERENCES

- 4-[1] H. Polli, L. A. M. Pontes, A. S. Araujo, J. M. F. Barros, and V. J. Fernandes, "Degradation behavior and kinetic study of ABS polymer," *J. Therm. Anal. Calorim.*, vol. 95, no. 1, pp. 131–134, 2009.
- 4-[2] T. Bayerl, "Application of Particulate Susceptors for the Inductive Heating of Temperature Sensitive," Institut für Verbundwerkstoffe GmbH, 2012.
- 4-[3] T. Bayerl and P. Mitschang, "Heating of Polymer-Polymer Composites By Inductive Means," in *Iccm-Central.Org*, 2011, pp. 1–6.
- 4-[4] H. Hu, L. Onyebueke, and A. Abatan, "Characterizing and Modeling Mechanical Properties of Nanocomposites- Review and Evaluation," vol. 9, no. 4, pp. 275–319, 2010.
- 4-[5] D. F. Treffer and J. G. Khinast, "Why Hot Melts Do Not Stick to Cold Surfaces," *Polym. Eng. Sci.*, pp. 1083–1089, 2017.
- 4-[6] J. J. and P. Z. Chenggang Ding, Xu Cui, "Effects of Substrate Preheating Temperatures on the Microstructure, Properties, and Residual Stress of 12CrNi2 Prepared by Laser Cladding Deposition Technique," *Materials (Basel).*, vol. 11, no. 2401, 2018.
- 4-[7] B. E. Tiganis, L. S. Burn, P. Davis, and A. J. Hill, "Thermal degradation of acrylonitrile-butadiene-styrene (ABS) blends," *Polym. Degrad. Stab.*, vol. 76, no. 3, pp. 425–434, 2002.
- 4-[8] G. Liu, Y. Liao, and X. Ma, "Thermal behavior of vehicle plastic blends contained acrylonitrile-butadiene-styrene (ABS) in pyrolysis using TG-FTIR," *Waste Manag.*, vol. 61, pp. 315–326, 2017.

Chapter 5: Computational Modeling of Reversible Adhesives

5.1. Abstract

In this study, a computational framework was developed for reversible adhesives containing multiple reinforcements within the ABS polymer. The effect of particle morphologies, individual concentrations, interphases, dispersion, particle clustering and particle orientations on the tensile modulus were investigated as a part of this work. Two reinforcements considered in this work were Fe₃O₄ nanoparticles (FMNP) and short carbon fibers (SCF). Optical and scanning electron microscopic images were used to aid the realistic/accurate development of representative volume elements (RVES). The elastic modulus of interphase was estimated based on the analytical formulations and was found to be larger than the host polymer. The interphase properties were implemented into the finite element model by defining an interphase region around the nanoparticles. Results from these models were compared with experiments to estimate the thickness of interphase. The results indicated that interphase thickness, aspect ratio and aligned fibers in the loading direction resulted in higher effective tensile modulus of the resulting polymer nanocomposite. Effect of particle clustering was insignificant on effective tensile modulus. The computational models predicted the interphase thickness of both Fe₃O₄ as 40 nm and SCF as approximately 30 nm. The developed computational modeling framework can easily be extended to other polymer nanocomposites containing multiple inclusions.

Keywords—

Nanocomposite, multi-particle reinforcement, Finite element modeling, Representative Volume Element (RVE), Spherical inclusions, Clustering, short carbon fibers

5.2. Introduction

There is a long-standing interest in polymers reinforced with nanoparticles owing to its great potential in development of multi-functional and smart materials. Conductive nano reinforcements in thermoplastic polymers has led to the development of reversible adhesives for rapid bonding and debonding of bonded structures using electromagnetic induction(EM) heating[1-4]. Reversible adhesives which incorporate ferromagnetic nanoparticles (magnetite-Fe₃O₄) and carbon fibers within a thermoplastic, upon exposure to EM radiations heat the surrounding polymer due to eddy current and hysteresis phenomena. Addition of nano/micro particles into the polymer not only increases the conductivity but also improves the effective mechanical properties of the polymer nanocomposite. However, the presence of hybrid (multiple inclusions) particles, clustering/agglomeration of particles and presence of interphase between the polymer and reinforcements increases the complexity in developing a computational framework to predict the effective mechanical properties. The scope of this work was to develop a computational model to predict the elastic modulus of polymer nanocomposites incorporating different material heterogeneities, modeling their interphase, dispersion, clustering and their morphologies (two different length scales).

Several micro-mechanical models are reported in the literature to analyze the mechanical properties of polymer nanocomposites [5–11]. The effective mechanical properties of polymer nanocomposites (PNC) lies in several factors such as polymer reinforcement adhesion, reinforcement/particle stiffness, particle morphology, interphase, particle clustering, voids, etc. All these factors are essential in the development of continuum mechanics-based models.

Quantitative and direct characterization of interphase properties is difficult due to the size of this small zone ($<1\mu$) between the reinforcement and polymer. Investigations of nano

reinforcements on effective composite properties have postulated the presence of interphase region of nanometer thickness between matrix and reinforcements [12][13]. For reinforcements of nanometer scale the contribution of interphase properties to the overall composite property can be significant due to increased interfacial surface area [14][15]. Nano-indentation and atomic force microscopy (AFM) are two important and common tools in the characterization of interphase properties in polymer composites[16–19]. Several closed loop analytical models were developed to tackle the expensive experimental procedures and are described as follows. Saber et al. [20] developed an analytical model to predict the effective average interphase stiffness for spherical reinforcements. However, this model was not used in conjunction with an FE model to study it's effect on effective tensile modulus of the PNC. Alessandro et al. [21] accounted for the presence of interphase around the particles for prediction of effective elastic properties in an FE based model. Although many studies have been conducted to analyze the interphase modulus, to the best of the authors knowledge, studies were the models were validated with experimental data are lacking or non-existent at the time of this work.

One of the most common heterogeneities present in PNC is clustering of nanoparticles also called as agglomeration. The dispersion of nanoparticles is a critical issue for the control of electrical, thermal and mechanical properties in polymer nanocomposites. Several studies were conducted in the past to study the effect of clustering of nanoparticles on the mechanical properties of PNC [5,22–26]. The agglomeration patterns depend on the nanoparticle weight/volume percent, inter particle attraction and particle morphology. The effect of particle agglomeration can be more critical in the plastic deformation and damage initiation[5]. Agglomeration of Fe₃O₄ particles (spherical morphology) in ABS polymer was shown by Vattathurvalappil et al. [3]. Incorporating multiple reinforcements into the polymer (hybrid polymer composites) can significantly improve

the mechanical behavior [27]. Liu et.al [28]. Presented a novel hybrid numerical, - analytical methodology for analyzing the hybrid PNC. Studies on reinforcements of varying size scales, nano- and micro- are very limited.

In this paper, a computational modeling framework was developed to predict the elastic modulus of PNC considering interphase, aspect ratio, clustering and hybrid reinforcements. The aspect ratio, particle shape and particle clustering information's were obtained from electron microscopic observations. An analytical model was used to predict the interphase and further input into the finite element model. The FE model was experimentally validated and used for the numerical characterization of the material beyond the experimental matrix.

5.3. Experimental Details

5.3.1. Materials

Hybrid polymer nanocomposite used in this study consist of acrylonitrile butadiene styrene (ABS) as polymer and two reinforcements namely ferromagnetic nanoparticles (Fe₃O₄) and short carbon fibers (SCF). ABS (CycolacTM Resin MG94) polymer was obtained from Sabic®. Ferromagnetic nano particles (Fe₃O₄), Iron(II,III) oxide of 50-100 nm particle size from Sigma-Aldrich ® was used as one of the reinforcements. Short carbon fibers used in this study were already reinforced in ABS polymer and was purchased as 3D printing filaments from Sigma-Aldrich ® (CarbonX[™] CFR-ABS). These 3D printed filaments consist of 15 wt. % of high modulus short carbon fibers reinforced in ABS (MG 94) polymer. These filaments were further pelletized and mixed with Fe₃O₄ nanoparticles to manufacture hybrid polymer nanocomposites. The composition of all the specimens studied in this work are listed in Table 5-1.

Table 5-1: Specimen compositions investigated, nomenclature used: (ABS/micro-/nano-)

No.	Material	ABS (wt. %)	SCF (wt. %)	F -Fe ₃ O ₄ (wt. %)
	(ABS/micro-/nano-)	((**************************************	(,
1	Neat ABS	100	0	0
2	ABS/0/4F	96	0	4
3	ABS/0/8F	92	0	8
4	ABS/0/12F	88	0	12
5	ABS/0/16F	84	0	16
6	ABS/15CF/0	85	15	0
7	ABS/15CF/4F	81	15	4
8	ABS/15CF/8F	77	15	8
9	ABS/15CF/12F	73	15	12

5.3.2. Manufacturing

Micro-extruder of 15 cc. (DSM Netherlands) was used to manufacture the PNC. At first, the ABS pellets were dried for 3 hours at 80 °C to remove moisture. The required concentration of Fe₃O₄ was dry mixed with the ABS pellets and fed to the extruder barrel that houses two intermeshing conical screws. The barrel was maintained at the processing temperature of ABS (240 °C) and the speed of the conical screws was 100 rpm. The polymer pellets and nanoparticles were mixed for 10 min.

The molten samples from the barrel was then moved into a transfer cylinder which was maintained at the same ABS processing temperature. This molten sample was then pushed into the ASTM closed molds using a pneumatic piston at 100 psi. The tensile test coupons manufactured using this process were compatible with ASTM D 638 type IV standards.

5.3.3. Tensile Tests

Tensile tests were carried out for at least 5 samples in each composition investigated. All tensile tests were carried out according to ASTM D638 standards using a universal testing machine at a constant cross head speed of 5mm/min.

5.4. Micromechanical Modeling of Nanocomposites

The elastic modulus of polymer nanocomposites depends on several factors related to the polymer and reinforcements. Particle loading (weight percent), aspect ratio, particle alignment, clustering and interphase between particles and polymer are some of them. Several models were proposed in the past for the effective prediction of elastic properties in PNC's. However, only few of these models can be applied for spherical reinforcements. According to the reviews carried out on these models[29][30], Mori-Tanaka model based on the Eshelby theory is one of them. However, these models do not account for the presence of interphase. Furthermore, visualization of localized stress/strain behavior is not possible in homogenization models. This study uses the analytical model for interphase properties proposed by Saber et al[31] (section 5.4.1) to predict the interphase modulus and to integrate it into the finite element model to estimate the effective elastic properties of the PNC.

5.4.1. Generalized Effective Interphase Model

The generalized effective interphase model used in this study was based on the three phase analytical model proposed by Saeed Saber-Samandari et al.([32][20]). In this model, the interphase properties are assumed to be varying continuously between the nanoparticle and the polymer as shown in Figure 5-1.

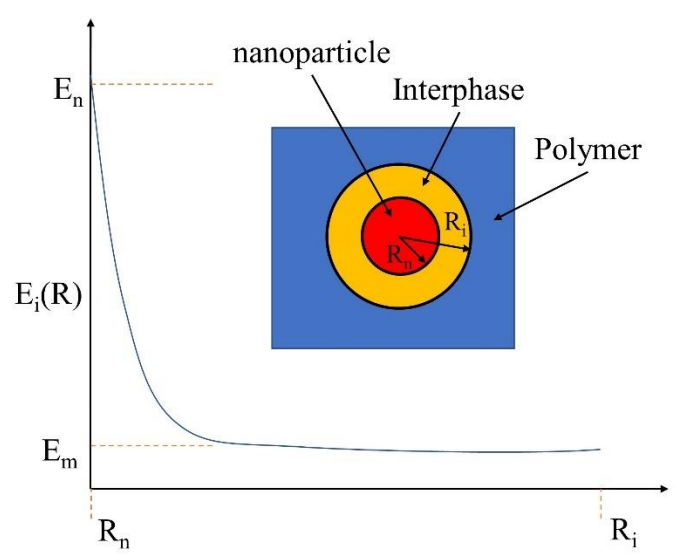


Figure 5-1: Distribution of elastic modulus of interphase region

The elastic modulus of the interphase region was defined by considering radius R as the variable.

The following conditions were adopted to formulate the interphase modulus.

$$E_i(R) = E_n \quad at \ R = R_n \tag{1}$$

$$E_i(R) = E_m \quad at \ R = R_i \tag{2}$$

Where E_i , E_n and E_m are the elastic modulus of interphase, nanoparticle and the matrix. R_n and R_i are the nanoparticle and the interphase radii. Based on equation (1 & 2), saeed et al.[32] suggested the modulus of interphase at any point R can be evaluated by:

$$E_i(R) = E_m(R_i/R) + [(R_i - R)/(R_i - R_n)]^{k/2} [E_n - E_m(R_i/R_n)]$$
(3)

Where k is the interfacial enhancement index which depends on the properties of matrix, nanoparticles, surface treatments on nanoparticles and intercalation/exfoliation of nanoparticles. From equation (3), the average elastic modulus of the interphase region can then be derived to the following equation:

$$E_{i} = 1/(R_{i} - R_{n}) \int_{n}^{i} E_{i}(R) dR$$
 (4)

5.4.2. Development of Representative Volume Element

This section describes the details of finite element modeling performed in this work. The methodology adopted in the development of FE model is shown in Figure 5-2. The finite element models in this study were performed using a material modeling CAE software called Digimat® 2019.0 from MSC Software® [33].

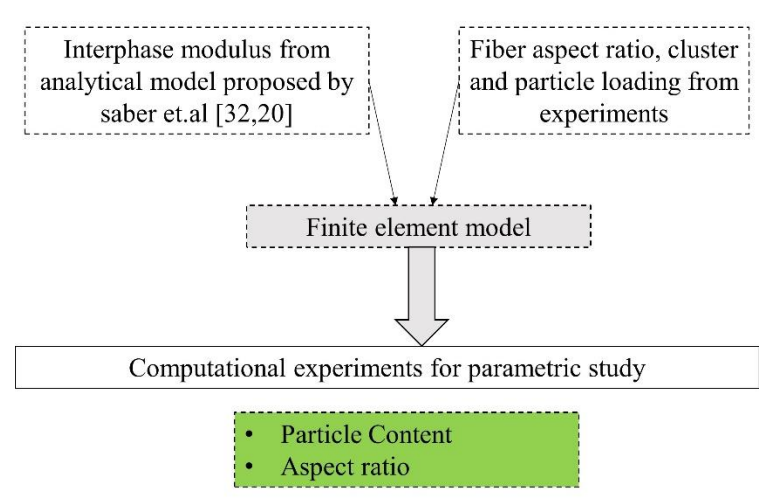


Figure 5-2: Methodology for development of finite element model

Representative volume elements developed for all the compositions were based on experimental measurements and microscopic observations. The aspect ratio, particle clustering, particle size and geometry of reinforcements observed using scanning electron microscopy were used for the design of geometry. From SEM observations the mean aspect ratio of the Fe₃O₄ and SCF particles were determined as 1 and 4.6 respectively. The RVE size for the PNC's were assigned based on the size of Fe₃O₄ (100 nm) and SCF (8 μ diameter). As the particle size difference between Fe₃O₄ and SCF is of order of magnitude difference (Figure 5-3), they cannot be modeled within the same RVE.

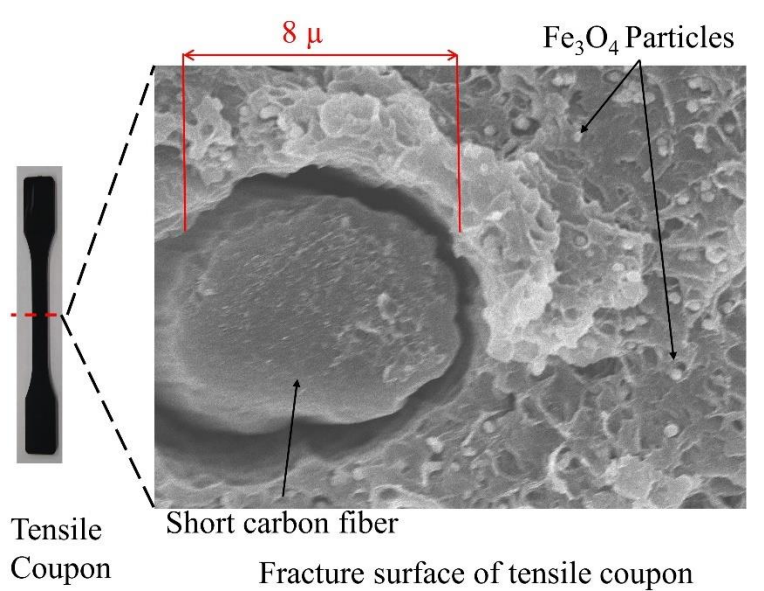


Figure 5-3: Scanning electron microscopy image of tensile coupon (ABS/SCF/Fe₃O₄) fracture surface

The size of 3D RVE cubes for ABS/F and ABS/CF materials were of dimensions 1 μ x 1 μ x 1 μ and 1 mm x 1 mm x 1 mm respectively (Figure 5-4). The geometry of Fe₃O₄ and SCF were defined with spherical and cylindrical morphology and corresponding aspect ratios. The interphase between the particle reinforcements and the polymer was modelled as the outer covering around the particles. The tensile modulus of this intermediate zone was obtained using the analytical model described in section 3.1 and was assigned to the FE model. Particle clusters were defined as relative weight percent of particles present in the RVE. The effect of cluster aspect ratio was changed from 1 to 5 to understand its effect on effective tensile modulus. The interpenetration of interphase coatings was allowed while studying the effect of clustering. The material properties used for ABS polymer and reinforcements in the study are given in Table 5-2. All the RVE's were assigned with periodic boundary conditions to ensure overall compatibility between the nano-/micro-level and macro level. In other words, a macro material can be achieved by repeated nano-/micro- RVE's. In periodic boundary conditions, the flux of the field variable (displacement in this case) is periodic with respect to the faces of the RVE. This was achieved by a large set of

appropriate equations relating the degrees of freedom of the nodes lying in one face to the nodes corresponding to the opposite face.

Table 5-2: Mechanical properties of matrix (ABS), particles (Fe₃O₄ and SCF) and effective interface

Material	Tensile	Poisson's	Aspect	Interphase
	Modulus	ratio	Ratio	Modulus
	(GPa)			(GPa)
ABS	1.95[34]	0.35[35]	-	-
Fe ₃ O ₄	161[36]	0.3[37]	1	Eq. (3)
SCF	238[38]	0.27[39]	4.63	Eq. (3)

In Figure 5-4, the geometry and finite element model of four different RVE's are illustrated. It should be noted that all the RVE geometries and corresponding FE models are not shown in figure 5-4 for brevity. The RVE's were meshed using 4-node linear tetrahedron elements. Two elements were assigned along the interphase thickness. The meshing of particles with interphases are much more challenging when compared with the particles without interphase. This is evident from the highly refined mesh of the RVE's with interphase around the reinforcements (Figure 5-4).

The RVE's were subjected to a small uniform displacement along the x-direction. The volume average stresses and strains were calculated from the displaced RVE to estimate the effective tensile modulus.

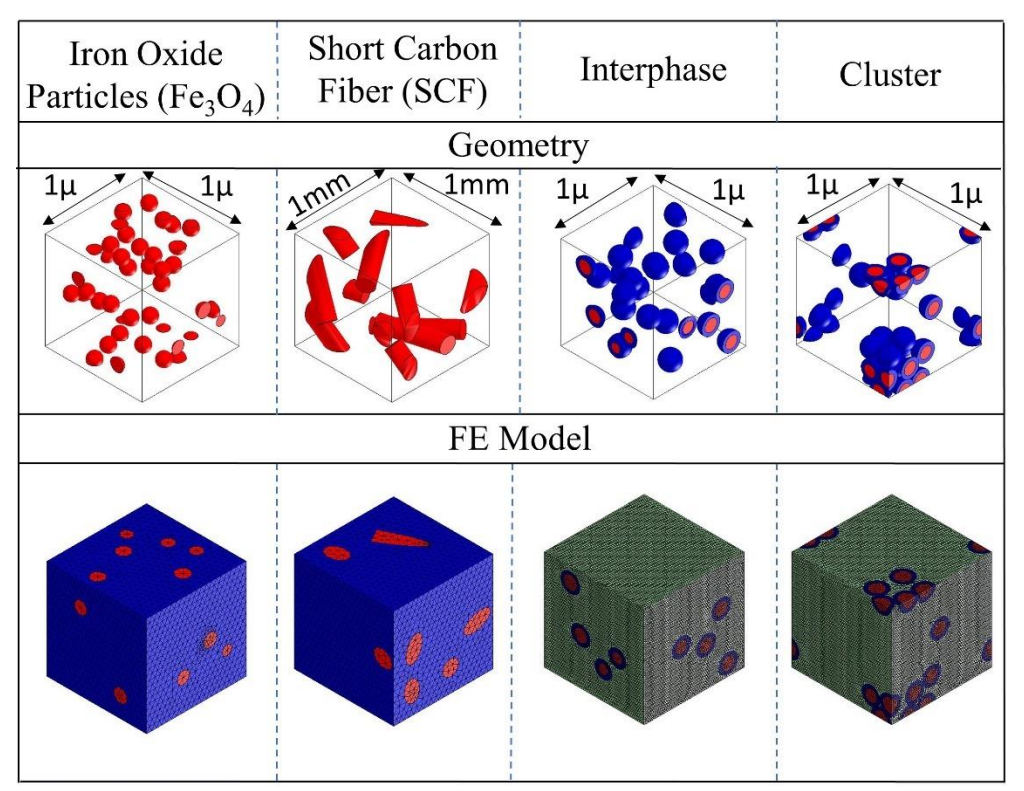


Figure 5-4: Representative volume elements (RVE) and corresponding FE models

5.5. Results and Discussion.

In this section, the effect of different microstructural parameters was investigated based on a series of experiments and computational models.

5.5.1. Determination of Distribution Functions of Short Carbon Fiber

The commercially available ABS/SCF filaments were pelletized during the extrusion process to make the tensile coupons. This pelletization process resulted in different aspect ratios of SCF. Aspect ratio of the fibers is an important input parameter for the determination of tensile modulus. In this study a lognormal mean distribution (Figure 5-5 (b)) was developed for the aspect ratio of SCF based on the fracture surface of the material samples observed using scanning electron microscopy. In lognormal distribution, the logarithm of a random variable is normally distributed. From this, the mean aspect ratio of SCF were measured to be 4.6. It is important to mention about the random orientation of SCF in ABS polymer (Figure 5-5 (a)). This contrasts with the parallel

alignment of SCF in big scale extrusion process[38]. This anomaly can be attributed to the smaller extrusion pressure.

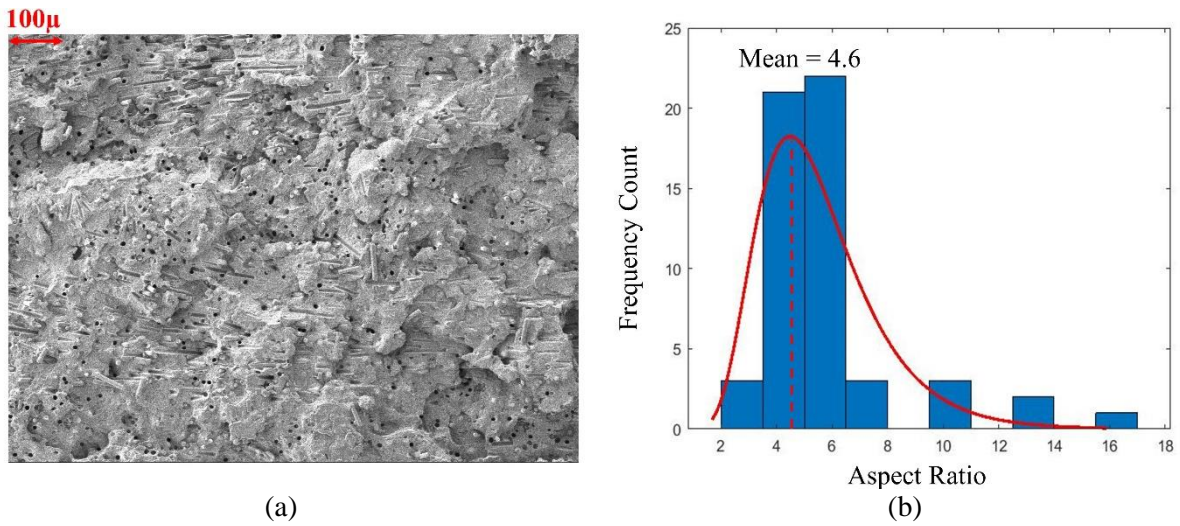


Figure 5-5: (a) SEM image of ABS/CF tensile fracture surface (b) Histogram of SCF aspect ratio

5.5.2. Effect of Interphase Properties

In this section, the effective tensile modulus of interphase was estimated for different interphase thickness values. Further, the effect of these predicted interphase modulus on effective tensile modulus of PNC was evaluated. The interphase modulus was estimated using the formulation described in section 3.1. Figure 5-6 (a) shows the effective interphase modulus for the interfacial zone around SCF and Fe₃O₄ reinforcements with respect to different interfacial thickness. It was evident that average interphase modulus for SCF was greater than Fe₃O₄ at any given thickness. This can be attributed to the inherently higher stiffness and aspect ratio of SCF. The interphase modulus is dependent on parameter 'k' described in the analytical formulation (section 5.4.1). 'k' is the interfacial enhancement index which depends on the properties of matrix, nanoparticles, surface treatments on nanoparticles and intercalation/exfoliation of nanoparticles. In this study we assumed a constant value of k (40) for both the reinforcement as used by Saber et.al. [20]. It is pertinent to mention that the 'k' value can be different in the practical case depending on the adhesion properties of matrix and reinforcement.

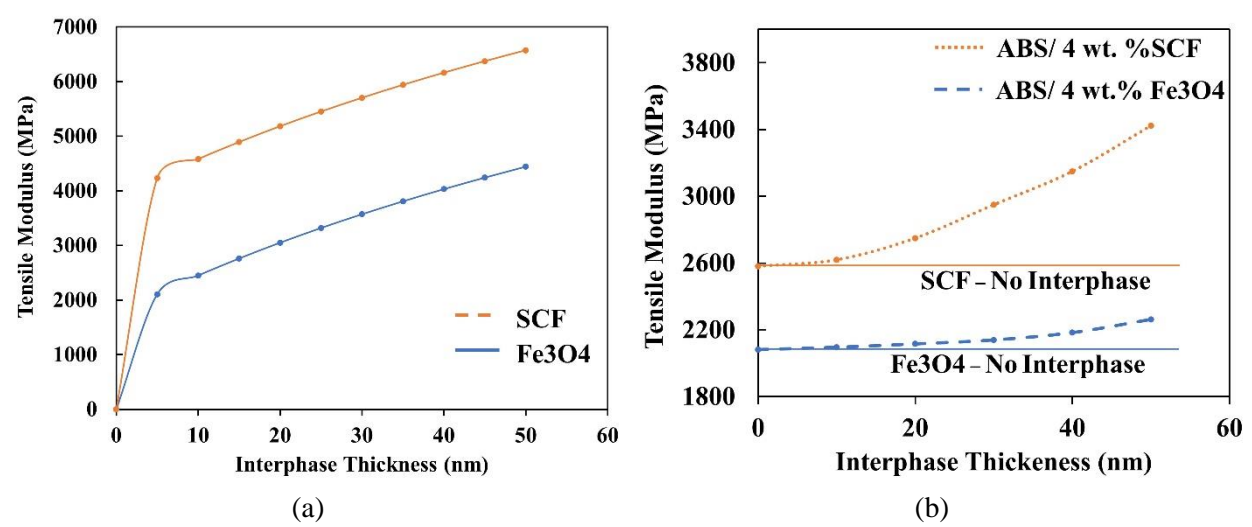


Figure 5-6: (a)Modulus of effective interphase at various interphase thickness (b) Effective tensile modulus polymer nanocomposites

Figure 5-6 (b) shows the effective tensile modulus of ABS / 4wt.% SCF and ABS / 4wt. % Fe₃O₄ composite with various interphase modulus/thickness values as predicted using the analytical model. The RVE's with the smallest particle content was considered for this study to increase computational efficiency. The radius (8μ for SCF and 50nm for Fe₃O₄) and aspect ratio (4.6 for SCF and 1 for Fe₃O₄) of the particles were kept constant. In both cases, the tensile modulus of the particles increased with increase in the interphase thickness. ABS/Fe₃O₄ showed 9 percent increase in tensile modulus whereas ABS/SCF composite showed 132 percent increase. Higher effective modulus in SCF can be attributed to three factors namely interphase modulus, aspect ratio and particle stiffness. On average, the interphase modulus of SCF is ~33 % higher than the Fe₃O₄ particles. As the interphase thickness increases, the weight fraction of interphase in the RVE increases and thereby the effective tensile modulus. Furthermore, higher aspect ratio of SCF augments the effective tensile modulus of ABS/SCF composite.

5.5.3. Effect of Clustering

The extruded PNC samples contained several clusters of Fe₃O₄ particles as shown in Figure 5-7 (a). Figure 5-7 (b) shows the log mean distribution of Fe₃O₄ particle cluster radius in ABS

polymer. It was evident from electron microscopy that there were no particles which were fully dispersed within the polymer. In order to study the effect of clustering 4 different cluster configurations (0 wt.%, 50 wt.%, 75 wt.% and 100 wt.%) were chosen. The mean cluster aspect ratio was kept constant, namely 1 (one) in all the models. This was also evident from the microscopic observations. The RVE chosen to study the effect of cluster contained 4 wt.% of Fe₃O₄ particles. It should be noted that the cluster effect was not studied for SCF. This is because no clusters of SCF were observed in microscopy.

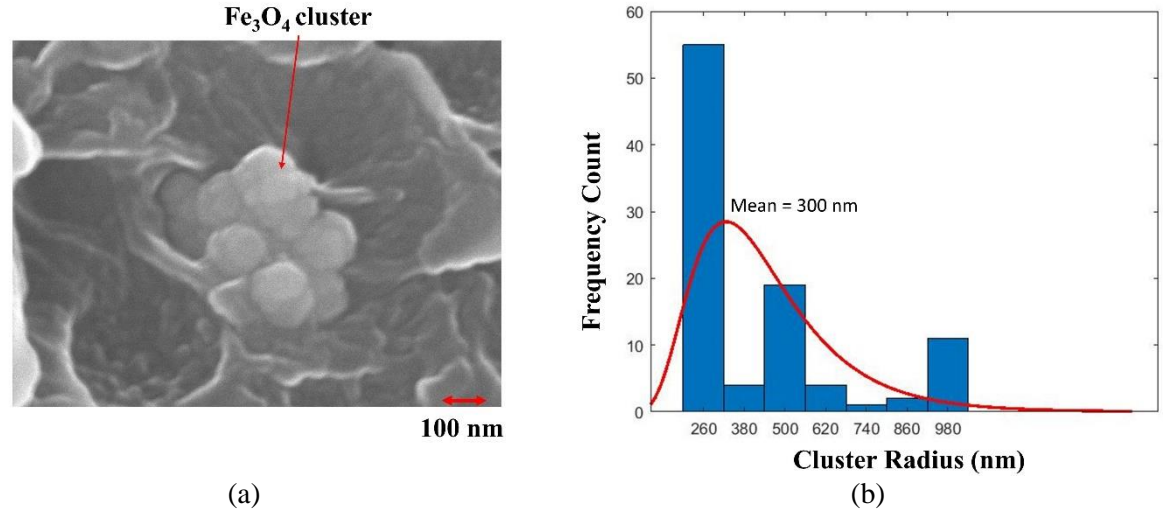


Figure 5-7: Fe₃O₄ cluster (a) cluster models considered for RVE generation (b) Particle cluster observed under scanning electron microscopy

Figure 5-8 (a) shows RVE geometries (with interphase) considered to study the effect of cluster. Effects of clusters were studied with and without interphase. The interphase of 40 nm was selected for this study as obtained from section 5.4.4. It was evident that the effect of cluster configurations with and without interphase were insignificant Figure 5-8 (b). Similar results were reported in earlier work [23]. This can be attributed to the particle morphology and the morphology of the cluster. In all the cluster cases, the aspect ratio of the particles and the cluster remained one. The spherical morphology of the particle limits the efficient load transfer from matrix to particle

and vice versa. As the effect of cluster weight percent was insignificant, 100 wt. % clusters were considered for all the models when compared with experiments.

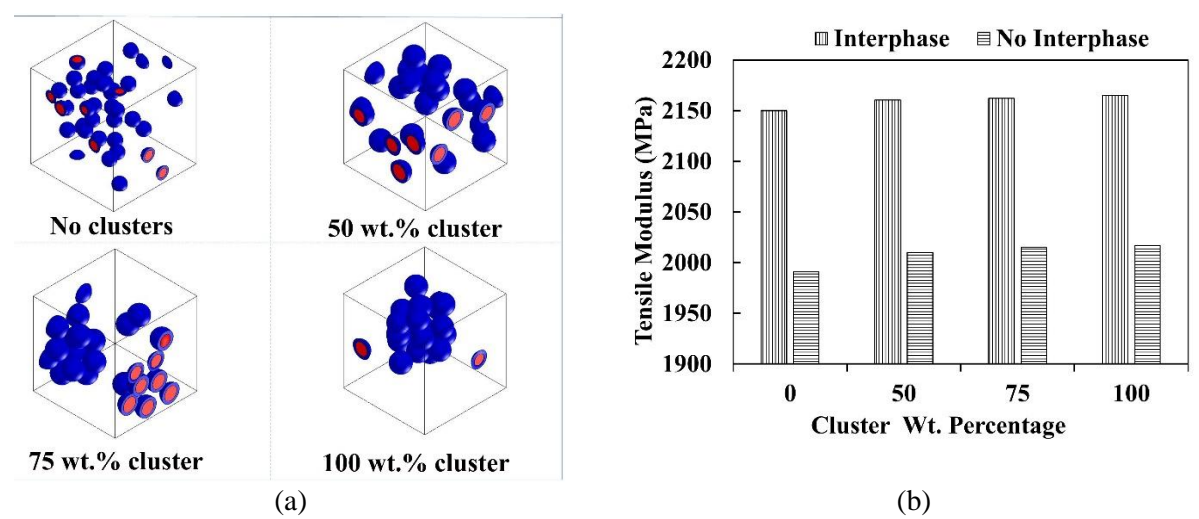


Figure 5-8: Effective tensile modulus of ABS/Fe₃O₄ (a) At Different cluster configurations (b) At different aspect ratio (75 percent cluster)

5.5.4. Comparison with Experimental Results

In this section, the effective tensile modulus from FE models were compared with the experimental results. At first the FE models were developed without the interphase zones. These models account for the aspect ratios (1 for Fe₃O₄ and 4.6 for SCF) and cluster values (100 wt. % with 300 nm radius) obtained from section 4.1 and 4.3. Once the tensile modulus was obtained for PNC without interphase, the interphase thickness was calculated such that the effective tensile modulus of FE predictions matched with experiments. Figure 5-9 shows the effective tensile modulus of ABS/4F, ABS/8F, ABS/12F, ABS/16F and ABS/15CF from experiments and finite element modeling. In experimental testing, ABS with Fe₃O₄ reinforcement showed an increase of 8% in tensile modulus whereas SCF showed 36% increase. Similar results were reported in previous studies[34]. This can be attributed to the higher aspect ratio and stiffness of SCF. The average error between the computational models without interphase and experiments were less than 5%. This 5 % difference was attributed to the contribution of definite presence of an

interphase. In order to match the experimental tensile modulus, an interphase modulus corresponding to 40 nm interphase thickness was essential.

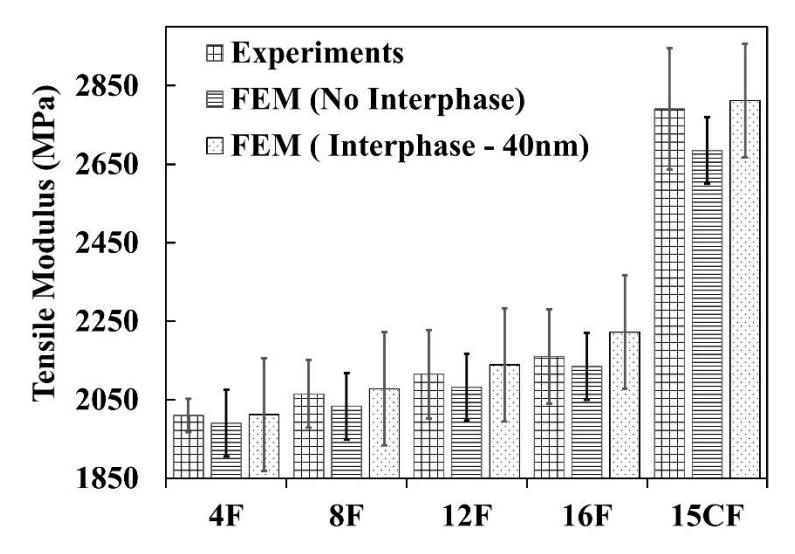


Figure 5-9: Comparison of experimental and FE results of ABS/SCF and ABS/F polymer nanocomposites 5.5.5. Hybrid Reinforcements

As described in section 5.3.2, the SCF reinforcements were in micro scale and the Fe₃O₄ particles were in nanoscale. Hence, the computational difficulties to accommodate both the reinforcements in one single RVE is highly expensive. In this study, a new strategy was framed by analyzing the hybrid reinforced composites using a two-step process. Step 1- ABS with Fe₃O₄ particles were analyzed for effective elastic modulus. The aspect ratio, cluster parameters and interphase thickness obtained from section 5.4.4 were used in this step. In Step 2, the resulting effective modulus from step 1 was input as the matrix modulus in the micro-scale with SCF reinforcements as shown in Figure 5-10 (a). No significant improvement in tensile modulus were observed by adding Fe₃O₄ nanoparticles. As explained in previous sections, this can be attributed to the spherical morphology of Fe₃O₄ particles with an aspect ratio is ~1. The computational models predicted the tensile modulus with less than 5% error without interphase. This 5 % difference was attributed to the contribution of definite presence of an interphase. In order to match

the experimental tensile modulus, an interphase modulus corresponding to 30 nm interphase thickness for SCF was essential.

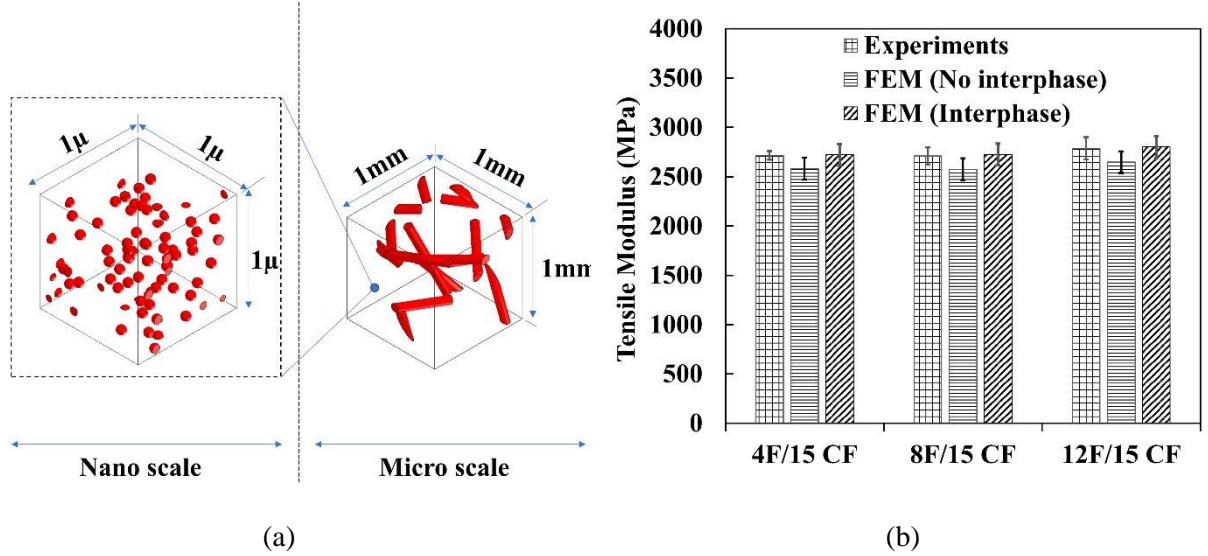


Figure 5-10: (a) Strategy implemented for hybrid reinforced polymer composites (b) Comparison of experimental and FE results of hybrid reinforced composites

These experimentally validated models were used to study the effect of particle content and aspect ratio on effective tensile modulus of PNC's.

5.5.6. Effect of Particle Content

Effect of particle concentration was investigated for both Fe₃O₄ nanoparticles and SCF reinforcements. The interphase regions, aspect ratios and cluster parameters obtained from experimentally validated models were incorporated in this section of computational experiments. The SCF with random and aligned orientations were also investigated. The particle content was varied from 4 wt. % to 16 wt.% and the corresponding tensile modulus was estimated. Figure 5-11 shows that the increase in tensile modulus for ABS/Fe₃O₄ nanocomposite was smaller than short carbon fibers. While 8% change in tensile modulus was recorded for ABS/Fe₃O₄, the random distributed SCF in ABS experienced an increase of 45%. This can be attributed to two factors namely the stiffness of the particles and aspect ratio.

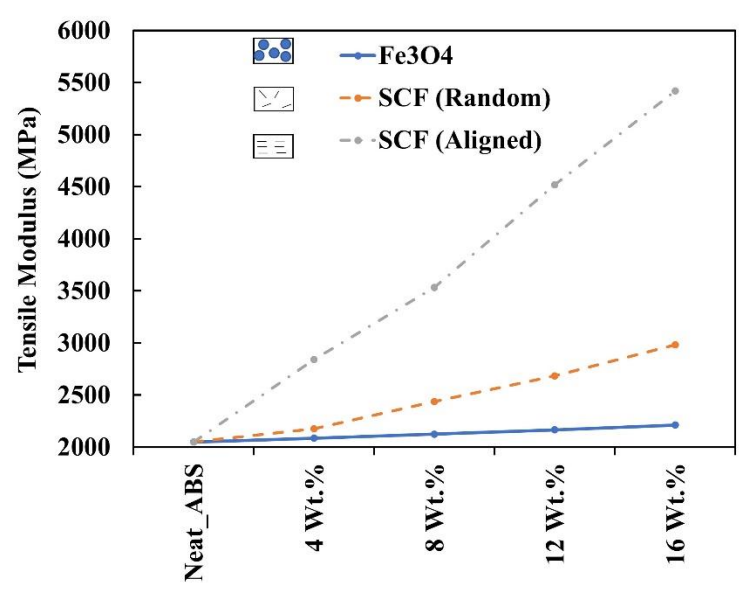


Figure 5-11: Effect of particle content in ABS/Fe₃O₄ and ABS SCF polymer nanocomposites

The stiffness of the SCF reinforcement is higher than those of Fe₃O₄ particles. Hence, the effective tensile modulus of polymer reinforced with SCF will be higher than that of Fe₃O₄ reinforced polymer. Aspect ratio is an important parameter in estimating the tensile modulus of polymer composites. When polymer composites are stretched, the load is transferred from matrix to the fiber through shear stresses generated at the interface and normal stresses at the fiber ends[40][41]. As the aspect ratio increases, the interfacial length also increases. This can lead to higher load bearing capability and thereby increased tensile modulus. However, if the fibers are randomly oriented, the load transfer efficiency is reduced in the loading direction. The SCF aligned in the loading direction increased the tensile modulus by 164 percent by adding 16 wt.% of SCF in the ABS polymer.

5.5.7. Effect of Aspect Ratio

Aspect ratio is an important parameter in determining the mechanical properties of particle reinforced polymer. Fe₃O₄ particles are of aspect ratio 1 and are not considered for this study. Furthermore, the spherical morphology of Fe₃O₄ does not have any significant effect on particle alignment. SCF with minimum number of particles (4 wt. percent) was studied for computational

efficiency. Figure 5-12 illustrates the tensile modulus of ABS/SCF composites with different SCF aspect ratios. Effect of random orientation and fiber alignment (in the loading directions) were also considered as part of this study. The predicted results from finite element model (FE) was also compared with Halpin-Tsai analytical model for the random oriented fibers. According to Tsai and Pagano [41], the composite modulus for randomly oriented fibers can be approximately predicted as,

$$E_{c} = (3/8) E_{L} + (5/8) E_{\tau}$$
(4)

Where E_L and E_{τ} are the longitudinal and transverse modulus of aligned short fiber composites, and can be written as,

$$E_L/E_m = (1 + 2(L/d) \eta_L V_f)/(1 - \eta_L V_f)$$
(5)

$$E_{\tau}/E_{m} = (1 + 2\eta_{\tau} V_{f})/(1 - \eta_{\tau} V_{f})$$
(6)

Where,

$$\eta_{L} = ((E_{f}/E_{m}) - 1)/((E_{f}/E_{m}) + 2(L/d))$$
(7)

$$\eta_{-}\tau = ((E_{-}f/E_{-}m) - 1)/((E_{-}f/E_{-}m) + 2)$$
 (8)

It was evident from Figure 5-12, the tensile modulus increased with increase in aspect ratio for both random oriented and aligned fibers. As the aspect ratio increased, the load transfer between matrix and fibers were enhanced. This can be attributed to long interfacial surface of the fibers that transfer the load through shear stresses[40][41]. The load transfer also happens at the fiber end through normal stresses. In the case of aligned fibers in the loading direction, the interfacial area is much higher and results in a better load transfer, hence higher modulus. For an aspect ratio of 20, the modulus of aligned fiber composite was ~1.8 times higher than the random fiber composite. The Halpin-Tsai model, a commonly used tool agreed well with FE in predicting

the composite tensile modulus for randomly distributed fibers. However, it should be noted that this model does not account for the interphase of the reinforcements.

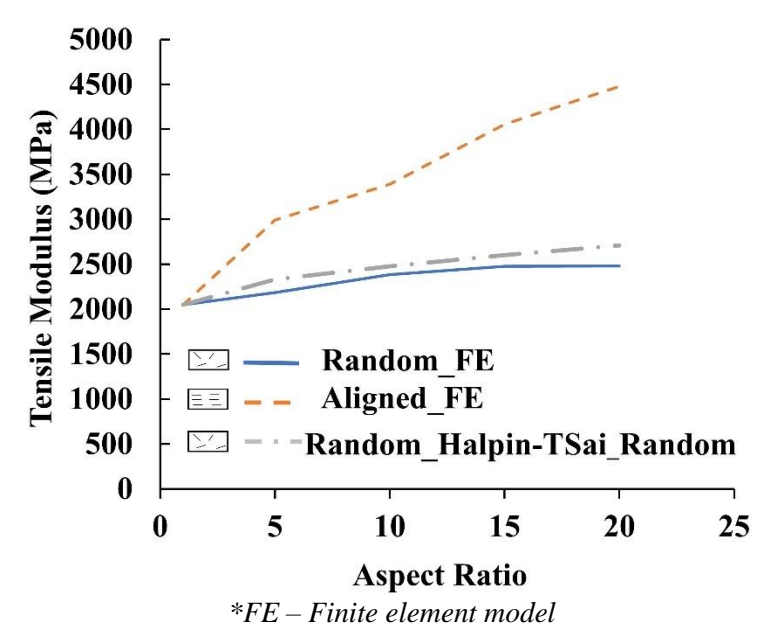


Figure 5-12: Effect of particle alignment and aspect ratio on tensile modulus

5.6. Conclusion

In this study, a computational framework was developed for predicting the tensile modulus by considering the material heterogeneities such as particle clustering, interphase, aspect ratio and hybrid reinforcements at different size scales. The computational models predicted the tensile modulus obtained from the experiments within an error range of 5 percent without an interphase. In order to account for the definite presence of interphase zone, the error range was compensated with an effective interphase modulus. The interphase thickness was estimated as 40 nm and 30 nm for Fe₃O₄ nanoparticles and SCF, respectively. It was observed that the tensile modulus of the polymer nanocomposite is highly dependent on the particle aspect ratio and the particle alignment (for reinforcements with aspect ratio higher than 1). The interphase thickness can increase the effective tensile modulus of the polymer as it increases the volume content of the interphase zone with in the RVE. The effect of clusters was minimal on the effective tensile modulus. Overall, the

developed computational framework can be used as a predictive tool to estimate the elastic tensile properties of the polymer nanocomposites.

REFERENCES

REFERENCES

- 5-[1] Bayerl T. Application of Particulate Susceptors for the Inductive Heating of Temperature Sensitive. Institut für Verbundwerkstoffe GmbH, 2012.
- 5-[2] Verna E, Cannavaro I, Brunella V, Koricho EG, Belingardi G, Roncato D, et al. Adhesive joining technologies activated by electro-magnetic external trims. Int J Adhes Adhes 2013;46:21–5. doi:10.1016/j.ijadhadh.2013.05.008.
- 5-[3] Vattathurvalappil SH, Haq M. Thermomechanical Characterization of Nano-Fe3O4 Reinforced thermoplastic adhesives and joints. Compos Part B Eng 2019;175:107162. doi:10.1016/j.compositesb.2019.107162.
- 5-[4] Verna E, Koricho EG, Spezzati G, Belingardi G, Martorana B, Roncato D, et al. Validation of a New Nano-Modified Adhesive Joining Technology Triggered By Electromagnetic Field, By Testing of a Real Component 2014:22–6.
- 5-[5] Peng RD, Zhou HW, Wang HW, Mishnaevsky L. Modeling of nano-reinforced polymer composites: Microstructure effect on Young's modulus. Comput Mater Sci 2012;60:19–31. doi:10.1016/j.commatsci.2012.03.010.
- 5-[6] Martone A, Faiella G, Antonucci V, Giordano M, Zarrelli M. The effect of the aspect ratio of carbon nanotubes on their effective reinforcement modulus in an epoxy matrix. Compos Sci Technol 2011;71:1117–23. doi:10.1016/j.compscitech.2011.04.002.
- 5-[7] Zare Y. Determination of polymer-nanoparticles interfacial adhesion and its role in shape memory behavior of shape memory polymer nanocomposites. Int J Adhes Adhes 2014;54:67–71. doi:10.1016/j.ijadhadh.2014.05.004.
- 5-[8] Pahlavanpour M, Hubert P, Lévesque M. Numerical and analytical modeling of the stiffness of Polymer-Clay Nanocomposites with aligned particles: One- and two-step methods. Comput Mater Sci 2014;82:122–30. doi:10.1016/j.commatsci.2013.09.038.
- 5-[9] Bhuiyan MA, Pucha R V., Worthy J, Karevan M, Kalaitzidou K. Understanding the effect of CNT characteristics on the tensile modulus of CNT reinforced polypropylene using finite element analysis. Comput Mater Sci 2013;79:368–76. doi:10.1016/j.commatsci.2013.06.046.
- 5-[10] Mortazavi B, Bardon J, Ahzi S. Interphase effect on the elastic and thermal conductivity response of polymer nanocomposite materials: 3D finite element study. Comput Mater Sci 2013;69:100–6. doi:10.1016/j.commatsci.2012.11.035.
- 5-[11] Chicot D, Roudet F, Zaoui A, Louis G, Lepingle V. Influence of visco-elasto-plastic properties of magnetite on the elastic modulus: Multicyclic indentation and theoretical

- studies. Mater Chem Phys 2010;119:75–81. doi:10.1016/j.matchemphys.2009.07.033.
- 5-[12] K Dusek. Advances in Polymer Science II. Springer Berlin Heidelberg; 1985.
- 5-[13] Drzal LT. The role of the fiber-matrix interphase on composite properties. Vacuum 1990;41:1615–8. doi:10.1016/0042-207X(90)94034-N.
- 5-[14] Brown D, Mélé P, Marceau S, Albérola ND. A molecular dynamics study of a model nanoparticle embedded in a polymer matrix. Macromolecules 2003;36:1395–406. doi:10.1021/ma020951s.
- 5-[15] Díez-Pascual AM, Naffakh M, Gómez MA, Marco C, Ellis G, Gonzlez-Domínguez JM, et al. The influence of a compatibilizer on the thermal and dynamic mechanical properties of PEEK/carbon nanotube composites. Nanotechnology 2009;20. doi:10.1088/0957-4484/20/31/315707.
- 5-[16] Schöneich M, Zamanzade M, Stommel M. Fiber-matrix interphase in applied short glass fiber composites determined by a nano-scratch method. Compos Sci Technol 2015;119:100–7. doi:10.1016/j.compscitech.2015.10.004.
- 5-[17] Griepentrog M, Krämer G, Cappella B. Comparison of nanoindentation and AFM methods for the determination of mechanical properties of polymers. Polym Test 2013;32:455–60. doi:10.1016/j.polymertesting.2013.01.011.
- 5-[18] Sattari M, Naimi-Jamal MR, Khavandi A. Interphase evaluation and nano-mechanical responses of UHMWPE/SCF/nano- SiO2 hybrid composites. Polym Test 2014;38:26–34. doi:10.1016/j.polymertesting.2014.06.006.
- 5-[19] Molazemhosseini A, Tourani H, Naimi-Jamal MR, Khavandi A. Nanoindentation and nanoscratching responses of PEEK based hybrid composites reinforced with short carbon fibers and nano-silica. Polym Test 2013;32:525–34. doi:10.1016/j.polymertesting.2013.02.001.
- 5-[20] Saber-Samandari S, Afaghi Khatibi A. Evaluation of elastic modulus of polymer matrix nanocomposites. Polym Compos 2007;28:405–11.
- 5-[21] Pontefisso A, Zappalorto M, Quaresimin M. An efficient RVE formulation for the analysis of the elastic properties of spherical nanoparticle reinforced polymers. Comput Mater Sci 2015;96:319–26. doi:10.1016/j.commatsci.2014.09.030.
- 5-[22] Néel L. Some theoretical aspects of rock-magnetism. Adv Phys 1955;4:191–243. doi:10.1080/00018735500101204.
- 5-[23] Ayyar A, Crawford GA, Williams JJ, Chawla N. Numerical simulation of the effect of particle spatial distribution and strength on tensile behavior of particle reinforced composites. Comput Mater Sci 2008;44:496–506. doi:10.1016/j.commatsci.2008.04.009.

- 5-[24] Tszeng TC. The effects of particle clustering on the mechanical behavior of particle reinforced composites. Compos Part B Eng 1998;29:299–308. doi:10.1016/S1359-8368(97)00031-0.
- 5-[25] Yu M, Zhu P, Ma Y. Effects of particle clustering on the tensile properties and failure mechanisms of hollow spheres filled syntactic foams: A numerical investigation by microstructure based modeling. Mater Des 2013;47:80–9. doi:10.1016/j.matdes.2012.12.004.
- 5-[26] Segurado J, González C, LLorca J. A numerical investigation of the effect of particle clustering on the mechanical properties of composites. Acta Mater 2003;51:2355–69. doi:10.1016/S1359-6454(03)00043-0.
- 5-[27] Sandler JKW, Pegel S, Cadek M, Gojny F, Van Es M, Lohmar J, et al. A comparative study of melt spun polyamide-12 fibres reinforced with carbon nanotubes and nanofibres. Polymer (Guildf) 2004;45:2001–15. doi:10.1016/j.polymer.2004.01.023.
- 5-[28] Liu H, Catherine Brinson L. A hybrid numerical-analytical method for modeling the viscoelastic properties of polymer nanocomposites. J Appl Mech Trans ASME 2006;73:758–68. doi:10.1115/1.2204961.
- 5-[29] Bernardo LFA, Amaro APBM, Pinto DG, Lopes SMR. Modeling and simulation techniques for polymer nanoparticle composites A review. Comput Mater Sci 2016;118:32–46. doi:10.1016/j.commatsci.2016.02.025.
- 5-[30] Raju B, Hiremath SR, Roy Mahapatra D. A review of micromechanics based models for effective elastic properties of reinforced polymer matrix composites. Compos Struct 2018;204:607–19. doi:10.1016/j.compstruct.2018.07.125.
- 5-[31] Saber-Samandari S, Afaghi-Khatibi A. Evaluation of elastic modulus of polymer matrix nanocomposites. Polym Compos 2007;28:405–11. doi:10.1002/pc.20322.
- 5-[32] Saber-Samandari S, Afaghi Khatibi A. The Effect of Interphase on the Elastic Modulus of Polymer Based Nanocomposites Saeed Saber-Samandari 1,. Key Eng Mater 2006;312:199–204. doi:10.4028/www.scientific.net/KEM.312.199.
- 5-[33] Digimat(2019.1) MSC Software Belgium SA. 2019.
- 5-[34] Vattathurvalappil SH, Haq M. Thermomechanical Characterization of Nano-Fe3O4 Reinforced thermoplastic adhesives and joints. Compos Part B Eng 2019;175. doi:10.1016/j.compositesb.2019.107162.
- 5-[35] SABIC. CYCOLAC TM Resin MG94UAmericas: Commercial. 2016.
- 5-[36] Doraiswami M. ELASTIC CONSTANTS OF MAGNETITE, PYRITE AND CHROMITE. Proc Indian Acad Sci 1947;A28:413–6.

- 5-[37] Chicot D, Mendoza J, Zaoui A, Louis G, Lepingle V, Roudet F, et al. Mechanical properties of magnetite (Fe3O4), hematite (α-Fe2O3) and goethite (α-FeO·OH) by instrumented indentation and molecular dynamics analysis. Mater Chem Phys 2011;129:862–70. doi:10.1016/j.matchemphys.2011.05.056.
- 5-[38] Fu SY, Feng XQ, Lauke B, Mai YW. Effects of particle size, particle/matrix interface adhesion and particle loading on mechanical properties of particulate-polymer composites. Compos Part B Eng 2008;39:933–61. doi:10.1016/j.compositesb.2008.01.002.
- 5-[39] Krucinska I, Stypka T. Direct measurement of the axial poisson's ratio of single carbon fibres. Compos Sci Technol 1991;41:1–12. doi:10.1016/0266-3538(91)90049-U.
- 5-[40] Cox HL. The elasticity and strength of paper and other fibrous materials. Br J Appl Phys 1952;3:72–9. doi:10.1088/0508-3443/3/302.
- 5-[41] Zhao P, Ji S. Refinements of shear-lag model and its applications. Tectonophysics 1997;279:37–53. doi:10.1016/S0040-1951(97)00129-7.
- 5-[42] Halpin JC, Pagano NJ. The Laminate Approximation for Randomly Oriented Fibrous Composites. J Compos Mater 1969;3:720–4. doi:10.1177/002199836900300416.

Chapter 6: Multi-Scale Modeling of Bonded Joints Using Reversible Adhesives

6.1. Introduction

The objective of the work was to develop a computational modeling scheme for bonded joints using reversible adhesives and manufactured using EMI heating technique. The overall scheme of the multi-scale modeling strategy adopted in this work is shown in Figure 6-1. The macro structure considered in this study was a single lap bonded joint. The micro-macro behavior of the single lap bonded joints was studied using the following steps.

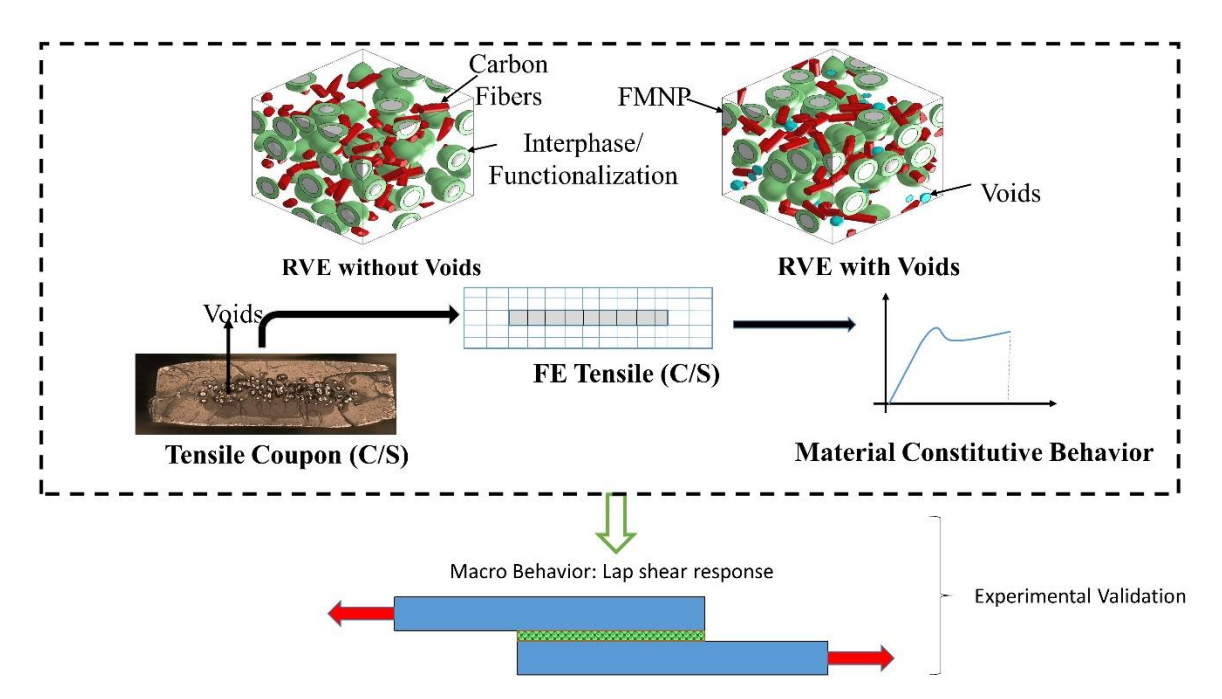


Figure 6-1: Overall approach of multi-scale modeling for bonded joints manufactured using EMI heating

a) The homogenized linear elastic material properties for reversible adhesives under EMI heating was obtained from the micromechanical model (chapter 4). The material properties consist of elastic modulus and Poisson's ratio. A homogenized material constitutive law was developed in the microscale to feed (input) as a macroscopic adhesive property in the bonded joints.

b) This macro structure (single lap bonded joint) was developed and analyzed using a commercial finite element software, namely ABAQUS ®. Experimental validation of the model was performed using a Quasi-static single lap shear test.

6.2. Finite Element Model

The finite element model of single lap joint and bond overlap region is shown in Figure 6-2. The adherents made of glass fiber reinforced plastics (Garolite [1]) were of dimensions 101mm x 25.4 mm x 3.2 mm. Tabs made of Garolite were also included in the model. The adhesive thickness of 0.5 mm corresponds to the thickness used in experimental testing (chapter 5). The tensile modulus of Garolite were experimentally determined as ~20 GPa [1]. A rigid tie constraint contact model was applied between the adhesive and adherent surfaces. This contact ensures that there is no slip between the tied surfaces.

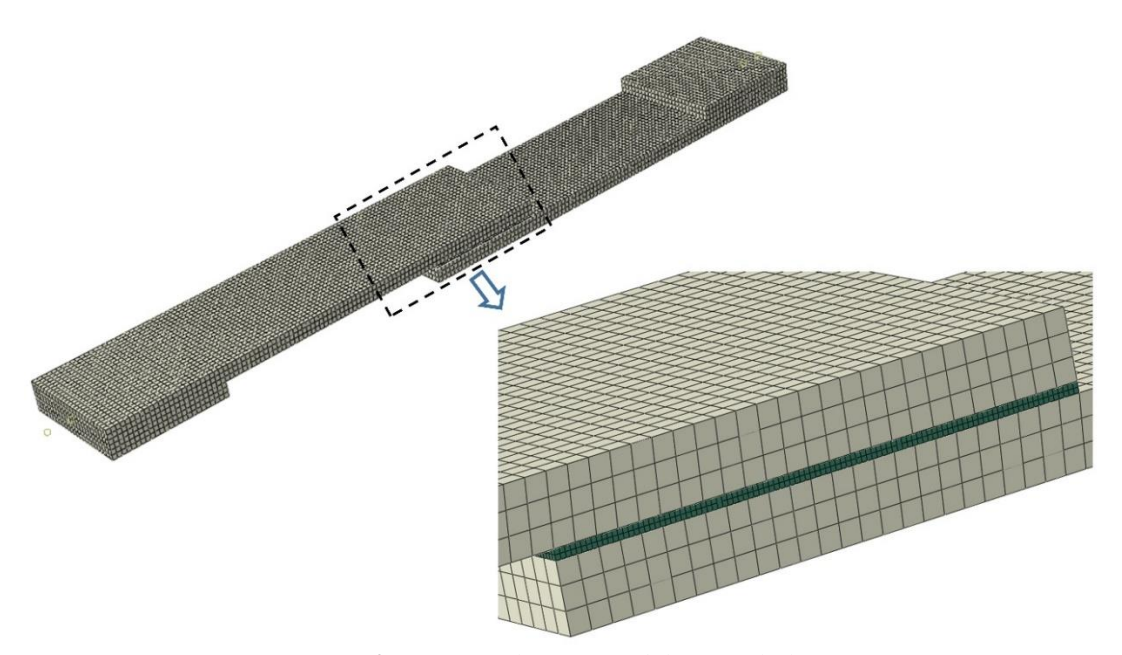


Figure 6-2: Finite element model of single lap joint

All the components were modeled using 8-noded linear brick, reduced integration, hourglass controlled elements (C3D8R). The FE model was fully constrained at one end and the other end was constrained along the transverse direction (both translation and rotation). This is to

arrest the out of plane translation and rotation in the non-symmetrical loading axis in the bonded joints. The lap joint model was subjected to displacement of 0.2 mm as this was the maximum displacement observed experimentally.

It is important to mention that only linear static response of the bonded joint was captured in this study. In order to capture the failure, plasticity and damage models for both adherents and adhesives are to be developed. Furthermore, the cohesive behavior at the interface between adherents and adhesive is to be characterized. This was considered to be beyond the scope of this work and is recommended as one of the important future direction resulting from this work.

6.3. Results & Discussion

Figure 6-3 shows the force-displacement response (lap-shear) obtained from experiments and multi-scale predictions. The adhesive considered for this work had 16wt.% Fe₃O₄ in ABS. In comparison with experiments, the multi-scale predictions were accurate for up to 1000 N. It should be noted that the damage initiates locally, around the nanoparticles and accumulates as the load increases. This increasing accumulation of damage introduces non-linearity at the macro-/large-scale. As the load further increases, these local damages will coalesce and form micro-cracks, which then combine to form a macro-crack and eventual failure. As seen in Figure 6-3, the multi-scale predictions slightly overpredict the response compared to experiment at higher load (>1000 N). Despite the slight overprediction, the multi-scale simulations agreed with the experimental response with an error of less than 5%. Overall, this approach can easily be translated to other heterogeneous materials and structures. Future work should focus on incorporation of material non-linearity and failure models.

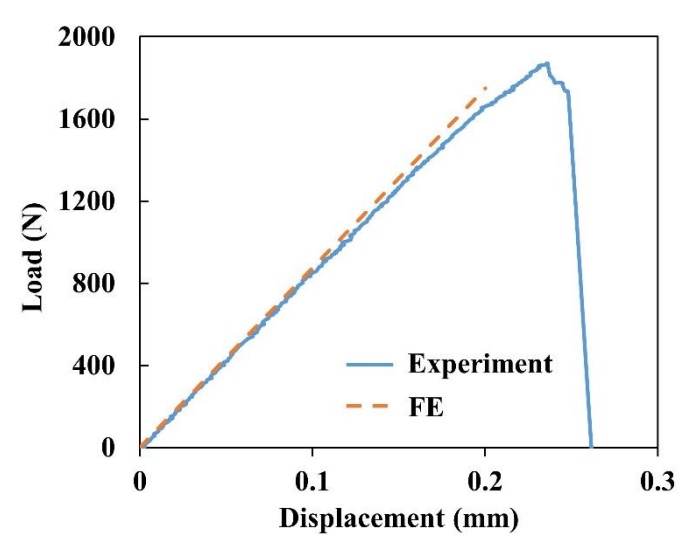


Figure 6-3: Force-displacement curve of single lap bonded joints manufactured using ABS adhesive reinforced with 16wt.% fe $_3O_4$

REFERENCES

REFERENCES

6-[1] Ravi-Chandar K, Satapathy S. Mechanical Properties of G-10 Glass – Epoxy Composite. 2007.

Chapter 7: Measurement of Processing Induced Residual Strains in Reversible Bonded Joints

7.1. Abstract

Differential thermal expansion of bonded joint constituents results in residual stresses within the adhesive and at the bi-material interfaces, which can significantly reduce the strength of the resulting joints. In this work, experimental strains were recorded during both the heating and cooling cycles of electromagnetic (EM) induction bonded and oven bonded joints. The fiber optic sensors that use distributed sensing technology and provide strain measurements at every 1.2 mm along the length of the sensor were placed with in the adhesive during the bonding process. A parabolic strain distribution was observed between the edges and midpoint of the adhesive bondline at the edges of joints in joints manufactured from oven bonding technique. Furthermore, the magnitude of strains developed in the geometrical center of adhesive bondline through EM bonding was three times that of the oven bonded joints due to the difference in the thermal boundary conditions of the two processes. The study showed that the EM bonding results in increased thermal residual strains despite of its other processing advantages such as rapid heating and lower energy consumption. Further studies are necessary to fully quantify the residual strains developed during the processing thereby aid in better design of both the processing and structural parameters. Introduction

The process of bonding in adhesive joints involves heating (processing temperature of adhesive) and subsequent cooling (room temperature) resulting in differential contraction of adhesive joint constituents that leads to residual strain/stress formation and premature failure of bonded joints[1–4]. Existing analytical modes cannot accurately predict the joint behavior without incorporating processing induced strains. The residual stresses can be defined as stresses that exist

in a material in the absence of external loading. Although several residual strain measurement techniques are available, it is not feasible to employ these techniques for measurement within the relatively small adhesive bondline. These challenges are not limited to existing joining techniques but can affect performance evaluation of new joining techniques. One such technique is the reversible adhesives technique. Thermoplastic adhesives reinforced with conductive nanoparticles allow for selective heating of adhesives enabling facile assembly and re-assembly (hence reversible) when exposed to electromagnetic (EM) radiations[5][6]. EM bonding technique allows for rapid and localized heating within the bondline. Nevertheless, relative to the conventional oven bonded joints, the rapid increase in temperature and subsequent cooling to room temperature induces residual stresses within the adhesive and at the bi-material interfaces, which can significantly reduce the strength of the resulting joints. This study was focused on measuring the residual strains in EM bonding technique and comparing with the conventional oven bonding technique using distributed fiber optic sensors, to study the formation of processing induced residual strains.

Although several studies were reported on induction bonded joints [5,7,8], the process induced residual strains were not addressed in this relatively novel bonded joining technique. The difference in thermal boundary conditions in both oven and induction bonded joining technique can result in significant change in the development of residual strains in the adhesive bondline. One of the simplest and conventional procedure to measure processing induced residual strains is to measure the curvature of the bonded structure during processing. This measured deflections can be used to calculate the stresses and strains[9]. A good summary of experimental techniques to determine the residual stresses in polymer matrix composite are reported in [10][3], wherein they have classified it into two parts: Destructive and non-destructive techniques. Raman spectroscopy

and embedded fiber optic sensors can be considered as two optimum non-destructive residual strain measurement techniques as they do not require complex mathematical formulation other than calibration curves [1].

The goal of this work was to measure the axial residual strains present in the geometrical center of the adhesive along the bondline due to the two different processing techniques, namely oven and EM bonding. Amorphous thermoplastic polymer, ABS (Acrylonitrile Butadiene Styrene) reinforced with iron oxide (Fe₃O₄) nanoparticles was used as an adhesive to bond glass fiber reinforced polymer (GFRP) composite adherends. An optical fiber sensor was embedded within the adhesive to measure the temperature and axial strains along the adhesive bondline at every 1.2 mm length during the bonding process. The process induced axial residual strains measured from both the techniques were then compared to understand the advantages offered by both the joining technique.

7.2. Experimental Methods

7.2.1. Materials

The adhesive used for joining the single lap joint substrate was made using an amorphous thermoplastic polymer, acrylonitrile butadiene styrene (ABS, CYCOLACTM Resin MG 94) which was reinforced with ferromagnetic nanoparticles (FMNP, 50-100 nm, Sigma Aldrich). The adherends of the single lap joint were made using glass fiber reinforced plastics (GFRP, Garolite G-10). GFRP was selected as it does not react to EM exposure thereby allowing for selective heating of the adhesive.

7.2.2. Adhesive Processing and Manufacturing

The adhesive was manufactured by the extrusion process using a DSM 15cc mini extruder. Prior to the extrusion process, ABS pellets were dried for 3 hours at 80°C to remove any moisture content. The dry mixed ABS was fed to the DSM extruder barrel that houses two contra screws rotating at 100 RPM. The barrel temperature was maintained at 240°C (melt temperature) and the polymer was mixed for 10 minutes. The extruder was used to make tensile and impact samples, as well as the adhesive 'films' to be used in single lap joint manufacturing. The adhesive collected from the DSM extruder was compression molded using a carver press to obtain the thin adhesive films. The temperature was maintained at 150 °C (beyond the glass transition of ABS) for 5 minutes. Steel spacers of 1 mm were used for consistent adhesive thickness.

7.2.3. Oven and Electromagnetic Induction Joining Technique

Single lap joints were processed using both Induction heating and oven heating methods. Glass fiber rods of 0.50 mm diameter was used as spacers to provide uniform bond line thickness. The joints were processed at 240°C for 30 minutes in the oven. A custom-built induction fixture (Figure 7-1) was used for the induction heat joining process. All elements in the fixture were made of non-conductive ceramic to prevent EM interaction. Guide pins were employed to prevent the substrates movement while processing.

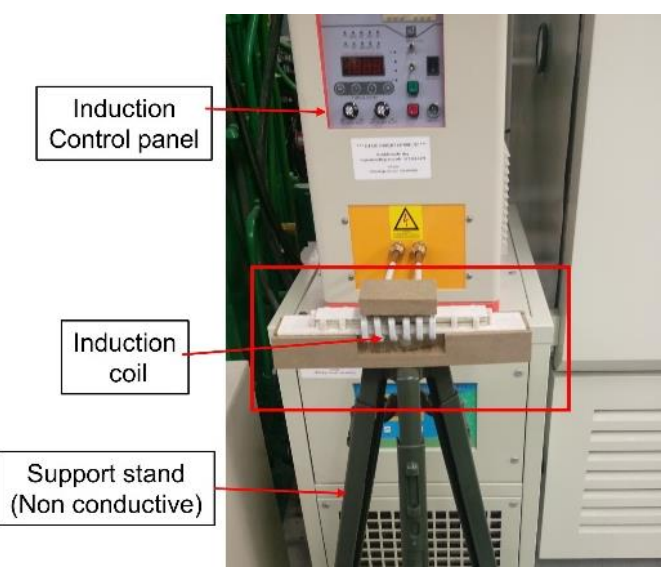


Figure 7-1: Electromagnetic Induction machine for single lap joint manufacturing

In order to have consistent thermal boundary conditions for both techniques studied in this work, a support fixture as shown in Figure 7-2 was used with the aim of minimizing the surface contact from another material during the cooling phase. The sharp pins not only minimized surface contact but also allowed for repeatable air flow and ambient conditions for both techniques.

7.2.4. High Definition Fiber Optic Sensors

In order to measure the temperature and/or strain in the adhesive, a distributed fiber optic sensor was placed along the adhesive bondline of single lap joints as shown in Figure 7-2. This system uses Rayleigh scattering effect in optical fibers and enables continuous measurement of temperature and strain at every 1.2 mm of the fiber length.

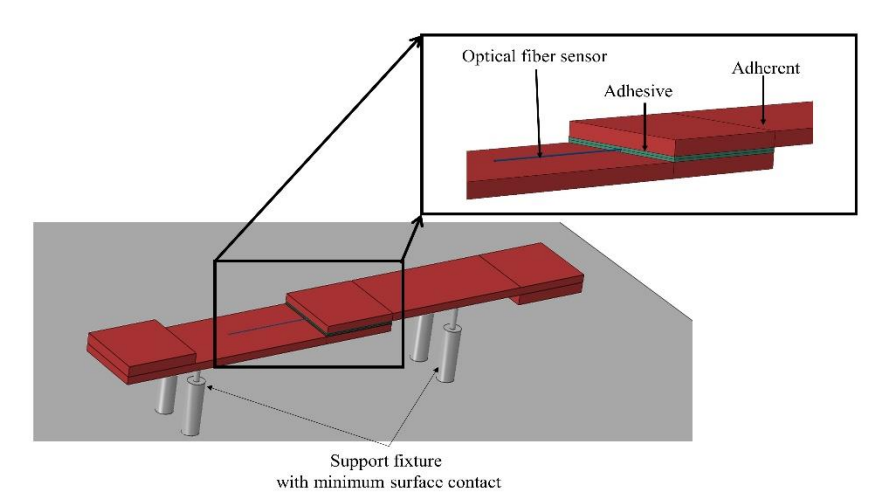


Figure 7-2: Schematic of the support fixture for cooling and the optical fiber sensor in the adhesive bondline

7.3. Results & Discussion

The experimental measurements of process induced residual strains for two different manufacturing process will provide valuable input for developing accurate models and design tools. In this work, a single lap joint was considered for the experimental study as an initial launch pad due to its simplicity prior to exploring other joint configurations. In order to better understand the development of residual strains developed in the adhesive the following key parameters must be understood:

1. Stress-free temperature

Stress - free temperature is an important parameter in residual strain calculation of amorphous thermoplastic polymers. This is the threshold temperature below which the polymer starts to solidify, and the residual stress starts to build. This has been reported to be around the glass transition temperature [11]. Beyond the stress-free temperature, elemental articles (atoms and molecules) break the bonds and can move freely in the material. Dynamic mechanical analyzer (DMA) test was conducted on the adhesive to determine the stress-free temperature. The storage modulus was found to be zero approximately at 120°C. As such, the strains measured in the

adhesive bondline beyond the stress-free temperature was not considered in the residual strain measurement study.

2. Temperature vs. cooling time along the bondline

The cooling rate (temperature vs. time) along the bondline was also experimentally recorded and provides the exact time at which various locations in the bondline reach the stress-free temperature. This allows for better understanding of residual strain development as cooling happens.

3. Strain vs. cooling time along the bondline

The axial residual strain experienced by the optical fiber sensor (Total measured strain) was recorded throughout the curing process. The adhesive strain was calculated from total measured strain by deducting the contribution of strain due to optical fiber sensor material.

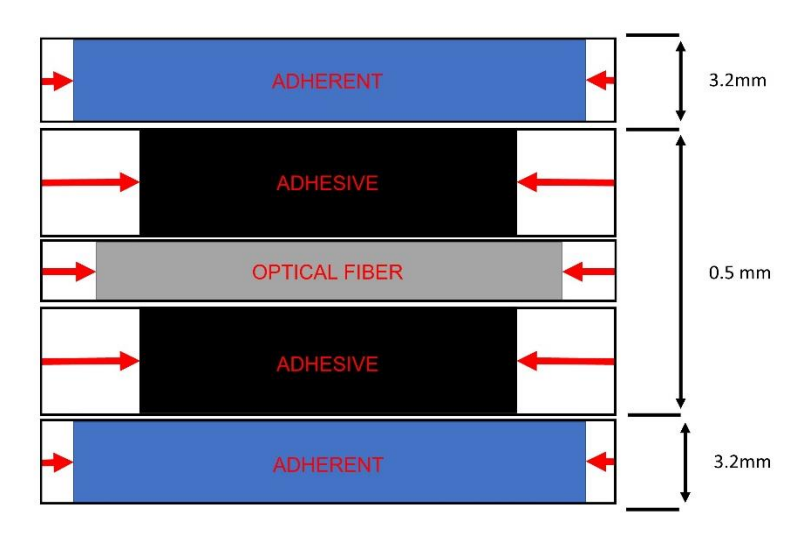


Figure 7-3: Schematic of the bonded overlap region. The red arrows indicate varying contraction upon cooling of each constituent in its free state.

The strains developed in the adhesive will be affected by the presence of the adherent and optical fiber sensor due to the mismatch in their coefficients of thermal expansion. However, strain/stress values at the edges are zero due to the edge boundary condition. Following assumptions were incorporated in calculating the axial residual strains within the adhesive.

- 1. Perfect bonding between the optical fiber sensor and the adhesive.
- 2. Influence of adherent was not accounted while calculating the axial residual strains in the adhesive.
- 3. The z-direction/through thickness strains were not considered and the axial residual strains were assumed to be the same throughout the adhesive thickness.

7.3.1. Cooling Rate Measurements in Oven and Induction Bonded Joints

The temperature in the adhesive bondline just prior to placing on the support fixture (see Figure 7-2) for cooling is shown in Figure 7-4. The x-axis represents the adhesive bondline length of 25 mm and the y-axis denotes the temperature in the adhesive bondline

In oven bonding, the adhesive, adherends and surroundings are uniformly heated to the processing temperature of 200 °C. Hence, the bond-line temperature was a constant throughout the bondline including the edges. In the case of EM bonding, while the adhesive heats up, the edges of the joint are exposed to ambient conditions. Hence the average temperature at the edges is lower than that of the center. In addition, the magnetic field strength is also stronger in the center and weakens near the edges of the coil.

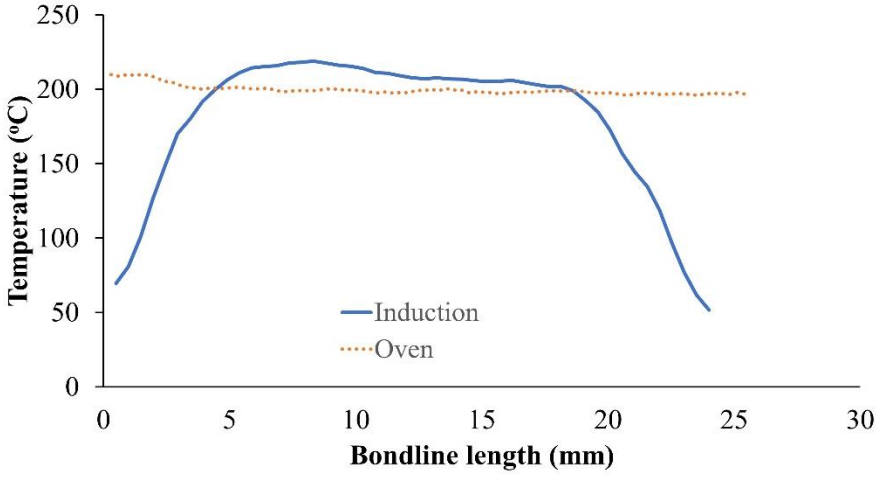


Figure 7-4: Temperature along the adhesive bondline prior to start of cooling cycle

As explained earlier and shown in Figure 7-4, the thermal boundary conditions and phenomena near the edges of induction bonded system are complex and hence the cooling time comparison was carried out at the geometric center of the adhesive bondline, and is shown in Figure 7-5.

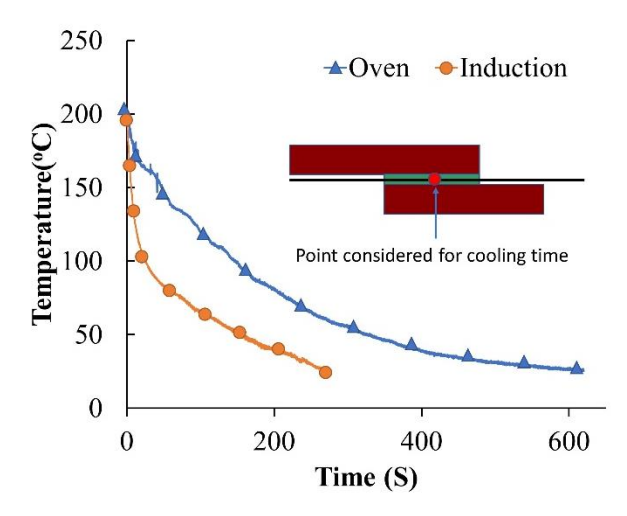


Figure 7-5: Time-temperature plots for oven and induction bonded joints measured at the geometrical center of the adhesive bondline during the cooling process

The cooling rate observed in EM bonded joints was approximately two time faster than the oven heating technique. This rapid cooling in this heating technique can be attributed to the thermal boundary conditions. In oven bonding, the adherents were in thermal equilibrium with the adhesive, i.e, at 200 °C. Hence, when cooling starts, the adherends and the adhesive all have to cool gradually. In EM heating, the adhesive heats rapidly to reach 200 °C. The boundary/interface of the adherent with the adhesive experiences conduction from the adhesive, whereas the bulk of the adherent is at room temperature. Hence, the cooling is much faster in EM bonded joints. However, this rapid cooling can result in larger residual strains in the adhesive bondline.

7.4. Residual Strain Measurements

In parallel to the cooling rate measurement, the axial strains experienced by the material of the optical fiber were also measured. The experimentally measured strains cannot be directly considered as residual strains developed in the adhesive as the contribution from the sensor and adherent need to be removed from the total measured strain as shown below:

$$\in_{Total/Measured} = \in_{Optical\ fiber} + \in_{Adhesive} + \in_{Adherent}$$
 (1)

The influence of the adherent is neglected for simplicity and equation (1) can be written as;

$$\in_{Total/Measured} = \in_{Optical\ fiber} + \in_{Adhesive}$$
 (2)

Residual strains introduced in any material subjected to thermal loads can be calculated as follows

$$\epsilon = \alpha \Delta T$$
(3)

Where α is the thermal expansion coefficient and ΔT is the temperature change encountered by the material.

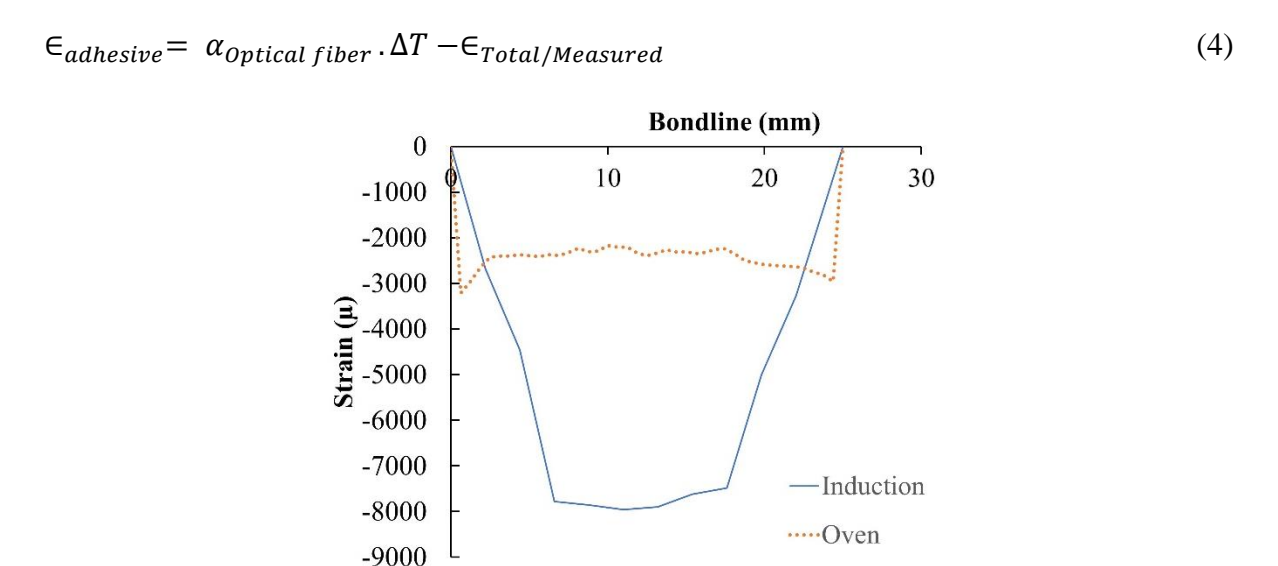


Figure 7-6: Axial residual strain along the adhesive geometrical center in oven and induction bonded single lap joints

The axial residual strains along the adhesive bondline, developed at the end of curing cycle (cooling until room temperature) for oven and induction bonded joints is shown in Figure 7-6. The strains and stresses are always zero at the edge. A parabolic curve was observed towards the edge in oven bonded joints. The axial strains values towards edge was approximately ~1.5 times more than the center of the bondline. This can be attributed to the sudden cooling of the edges which

was exposed to the environment. This can exacerbate the peel stresses during the single lap shear test and leads to premature failure. In the case of induction bonded joints, the edge strains cannot be compared to that of the oven bonded joints as the temperature did not reach the processing point. The axial residual strains at the center of adhesive bondline in EM bonded joints was ~3 times that of the oven bonded joints. This can be attributed to the rapid cooling of the adhesive bondline. The edge effects in induction bonded joints and the temperature at the edges not reaching the processing point can significantly affect the behavior of resulting joints. A detailed study on EM interaction of the adhesive, preheating of adherents and its effect on resulting material and structural behavior is needed to fully understand these EM bonded joints. Nevertheless, the approach used in this work to experimentally measure processing induced strains can aid in better optimizing the EM bonding process.

7.5. Conclusion

In this work, the axial residual strains developed in the adhesive bondline during the curing process were measured using an optical fiber sensor for two adhesive bonding techniques: (1) Oven and (2) Electromagnetic Induction. The strains at the geometrical center of the adhesive bondline was selected for comparison as the edges had complex thermal boundary conditions. The cooling rate of EM induction bonded joints were ~2 times faster than that of the oven bonded joints. The axial residual strains at the geometrical center in EM bonded joints were ~3 times that of the oven bonded joints. The parabolic increase in residual strains towards the edges in the case of oven bonded joints can be detrimental as it can exacerbate the peel stresses and can lead to premature failure. The study showed that, EM bonding can lead to severe thermal residual strains in the adhesive bondline during the processing despite of its other processing advantages. A detailed study on EM interaction of the adhesive, preheating of adherents and its effect on resulting

material and structural behavior is needed to fully understand these EM bonded joints.

Nevertheless, the approach used in this work to experimentally measure processing induced strains can aid in better optimizing the EM bonding process.

REFERENCES

REFERENCES

- 7-[1] Parlevliet PP. Residual Strains in Thick Thermoplastic Composites an Experimental Approach door. 2010.
- 7-[2] Parlevliet PP, Bersee HEN, Beukers A. Residual stresses in thermoplastic composites A study of the literature Part I: Formation of residual stress 2006;37:1847–57. doi:10.1016/j.compositesa.2005.12.025.
- 7-[3] Parlevliet PP, Bersee HEN, Beukers A. Residual stresses in thermoplastic composites-A study of the literature-Part II: Experimental techniques. Compos Part A Appl Sci Manuf 2007;38:651–65. doi:10.1016/j.compositesa.2006.07.002.
- 7-[4] Parlevliet PP, Bersee HEN, Beukers A. Residual stresses in thermoplastic composites a study of the literature . Part III: Effects of thermal residual stresses 2007;38:1581–96. doi:10.1016/j.compositesa.2006.12.005.
- 7-[5] Vattathurvalappil SH, Haq M. Evaluating healing behavior of thermoplastic adhesive bonded joints subjected to transverse impact loads. SPE ANTEC, 2019.
- 7-[6] Ciardiello R, Belingardi G, Martorana B, Brunella V. International Journal of Adhesion and Adhesives. Int J Adhes Adhes 2019;89:117–28. doi:10.1016/j.ijadhadh.2018.12.005.
- 7-[7] Verna E, Cannavaro I, Brunella V, Koricho EG, Belingardi G, Roncato D, et al. Adhesive joining technologies activated by electro-magnetic external trims. Int J Adhes Adhes 2013;46:21–5. doi:10.1016/j.ijadhadh.2013.05.008.
- 7-[8] Verna E, Koricho EG, Spezzati G, Belingardi G, Martorana B, Roncato D, et al. Validation of a New Nano-Modified Adhesive Joining Technology Triggered By Electromagnetic Field, By Testing of a Real Component 2014:22–6.
- 7-[9] Oel H., V.D F. Stress Distribution in Multiphase Systems: I , Composites with Planar Interfaces 1967;50:542–9.
- 7-[10] Kesavan K, Ravisankar K, Parivallal S, Sreeshylam P. Non destructive evaluation of residual stresses in welded plates using the barkhausen noice technique. Exp Tech 2005;29:17–21.
- 7-[11] Kim K-S, Hahn H, Croman R. The Effect of Cooling Rate on Residual Stress in a Thermoplastic Composite. J Compos Technol Res 2010;11:47. doi:10.1520/ctr10151j.

Chapter 8: Healing Potential of Bonded Joints Using Reversible Adhesive

Abstract—

Impact loads transferred to the bondline of adhesive joints can result in damage of the bond and significantly decrease their load carrying capacity. If the damage in the adhesive layer can be healed or reversed, such losses in structural behavior can be recovered. One such healing technique can be implemented in the use of thermoplastic 'reversible adhesives' which are mixed with conductive nanoparticles. Such materials have been shown to heal through exposure to electromagnetic fields, heating the thermoplastic adhesive. In this work, single lap joints were bonded using ABS thermoplastic polymer modified by adding ferromagnetic nanoparticles. The joints were tested under quasi-static tensile loading to determine their baseline performance. Similar joints were then subjected to impact load (10 J) to induce bondline damage. Impacted joints were subjected to quasi-static lap-shear to obtain impact-induced performance. Next, the impacted joints were subjected to electromagnetic fields to heal the damaged adhesive and then subjected to lap-shear tests to obtain the healed performance. A simultaneous study was carried out to heal the impacted samples by heating in a convection oven. The loss in joint strength due to impact and its subsequent recovery due to healing was evaluated. It was found that approximately 92 percent of joint strength was gained through both oven and electromagnetic induction heating. The exposure time to electromagnetic radiations was also optimized and it was found that induction healing is 60 times faster than oven healing.

8.1. Introduction

Meeting customer demands in quality and reducing lead times in maintenance, repair and overhaul (MRO) of vehicular structures is critical for original equipment manufacturers (OEM) in automotive and aerospace industry [1]. With extensive application of bonded joints in structures used in vehicle design and manufacturing, service records attribute more than 50% of structural defects to adhesive bond failures [2]. Removal and repair of damaged bonded assemblies is expensive and, in some cases, not feasible either due to lack of access or risk of potential damage to adjoining structures. Conventional practice of using thermoset polymers as adhesives hinders the disassembly and repair of the joints. An alternative and effective approach is to design adhesives which are reversible, recyclable and can sustain required structural integrity. An effective method of achieving this approach is to disperse conductive particles within a thermoplastic polymer matrix[3]-[9]. These particles can act as heaters when exposed to electromagnetic (EM) radiation leading to melting of the surrounding thermoplastic, the extent of which depends upon the exposure time[3]. This paper attempts to experimentally investigate and quantify the potential of reversible adhesives (RA) to heal or reverse damage within the bondline when activated using EM heating.

Healing/damage reversibility concepts are well known in bulk polymers and their composites[10]. This approach has however rarely been translated to adhesive healing in bonded joints[11]. The most commonly used method used for adhesive bondline healing is microencapsulation approach [12]. One of the earliest works in this regard was done by Jin and his co-workers[13]. The authors dispersed a healing agent and catalyst in a thin epoxy matrix used to join substrates. Upon damage, these capsules burst and release the healing agent which upon coming in contact with the suspended catalyst particles, polymerizes and activates the healing

process. The authors achieved a 56 %, recovery of fracture toughness at room temperature curing. In a later work, Jin et al [14] used the same the same healing concept with an epoxy which cured at relatively higher temperatures. Sepideh et al [15] also explored the micro-encapsulation approach in three different metallic joints and an optimized concentration of amine nano-capsules, a healing efficiency of 85%, was achieved in one configuration. Microencapsulation technique was also followed by Nazrul et al [16], [17]. In both studies, the authors used dual component microcapsules of epoxy resin and polyamine hardener to reinforce the epoxy adhesive. Different emulsification process for preparing the hardener shell were employed in these studies, and a healing efficiency of nearly 90 percent was achieved after first heal. A major drawback of this method is the limitation on the size of the capsules that poses a major challenge for their use in joints. The capsules can act as stress concentrators and effect the structural integrity. At the same time, their size needs to be large enough to provided requisite amount of healing agent in the crack. Furthermore, timely rupture and release of the healing agent is still an evolving science.

Another healing approach in adhesive joints was introduced by Li et al [18]. They proposed a biomimetic two-step self-healing method - close-then-heal (CTH)[19]–[21] - to repeatedly heal adhesively bonded composite joints. The underlying concept of this technique is to close or narrow down the crack and then activate a healing mechanism stimulated by heat. The initial crack closure was achieved by compressing the samples in a steel frame which was placed inside an oven to activate the thermoplastic particles incorporated in the epoxy. The healing cycle was repeated three times and descending efficiencies of 91.34%, 85.65%, and 82.46% were recorded. The authors deduced that no chemical changes took place in the adhesive and the healing process occurred solely due to physical entanglement between the thermoplastic and adhesive molecules, as well as mechanical interlocking at the thermoplastic film/fractured adhesive interface. Halil et al

[22]followed Li's CTH approach to experimentally investigate the self-healing efficiency of an epoxy adhesive. A healing efficiency of 90.166 % was achieved after the first healing and 74.812 % after the second heal. The limitation with this method is that it requires an intimate contact between the cracked surfaces and a heat source. In the experimental works above, ovens were used to prove the base concept however the absence of an intrinsic heat stimuli poses a major challenge to in-situ healing.

Aubert et al [23], introduced a new intrinsic healing approach in bonded joints. The author used a new class of cross-linked polymers capable of healing internal cracks through thermoreversible covalent bonds formation. These reactions, commonly known as called Diels-Adler (DA) reactions, can be activated inside the adhesive at different temperatures depending upon the concentration of cross-linking compound. The author showed excellent reversibility for three heal cycles in his experimental investigation. The only drawback to this approach was that the DA reactions started to occur at 90°C, beyond which the shear strength reduced by a factor of 10³. The bonds were again reformed when cooled below 60°C. The healable joints could therefore not be used high stiffness applications. Bekas et al [24] monitored two self-healing polymeric adhesives using the same approach and showed healing efficiencies as high as 75% can be achieved in the first heal cycle. More recently, Tang et al [25] characterized the healing capability of a vitrimer adhesive having high strength. The covalent bond activation barrier for this adhesive was recorded at 150°C and the first three heal cycles showed an efficiency of more than 80%. The DA approach towards healing is a promising prospect however the low glass transition temperatures of the polymers render them unsuitable for structural and high temperature applications.

Using an alternating magnetic field (EM) heating for joining and healing non-metallic/composite joints presents a very effective alternative to the above approaches. Conductive susceptors dispersed in thermoplastic polymer adhesive can induce localized melting of the polymer when exposed to EM radiation. Through selective heating, these conductive particles can facilitate bonding/de-bonding and healing of the joints. This EM technique offers several advantages such as targeted heating, reduced energy consumption, rapid processing, consistent and optimized product quality and safety[26]–[29]. A typical EM system consists of a power circuit that converts 50/60 Hz AC supply to a frequency range of 10-400 kHz current inside an electromagnetic induction coil to generate a magnetic field within the coil. This EM field induces eddy currents in any conductive work piece placed in or around the coil (Joule heating) in addition to the magnetic hysteresis losses if the work piece has magnetically susceptibility. The combination of these mechanisms were responsible for heat generation within the material bulk volume.

There has been limited research on using conductive/magnetic particles in adhesive bonded joints. Kolbe et al. [30] proposed this concept for thermosets. For thermoplastics, this technique was subsequently used for assembling/disassembling of joints by Verna[6] and Raffaele [7]. However barring one study which the authors presented as a proof of concept [3], electromagnetic induction heating using ferromagnetic nano-particles has not been used for healing structural adhesively bonded joints. The scope of the present work is to understand the healing behavior of a reversible thermoplastic adhesive when exposed to electromagnetic fields. For this work, glass fiber reinforced plastic (GFRP) adherents were bonded using Acrylonitrile Butadiene Styrene (ABS) polymer adhesive mixed with ferromagnetic particles (Fe₃O₄). The joints were heated in an oven and subjected to quasi-static single lap shear strength test to create a baseline. These joints

were then subjected to transverse impact to introduce damage in adhesive bondline and were further tested. Another set of similar impacted joints were healed (using both oven and induction heating) and tested after impact. The loss in strength due to impact, the increase in strength due to healing and their comparison with the baseline has been reported. Further the optimum healing time required for EM healing was estimated based on thermo-mechanical degradation study on the thermoplastic adhesive material.

8.2. Experimental Procedure

8.2.1. Materials

Acrylonitrile Butadiene Styrene (ABS) thermoplastic polymer (CYCOLAC Resin MG 94, SABIC) was used as an adhesive in this study. ABS was selected because of its excellent toughness properties owing to the polybutadiene phase [3]. Additionally, this adhesive has good mechanical properties, resistance to chemical corrosion, low cost and is easy to process [31]. The adhesive was combined with ferromagnetic nanoparticles (Fe₃O₄) using extrusion compounding. These ferromagnetic particles consisted of Iron (II, III) oxide nano powders with sizes ranging from 50-100 nm and an aspect ratio close to 1. Fe₃O₄ concentration at 16 wt. % [3] was chosen for the study for optimized mechanical and EM response. For further reference in this study, the ABS mixed with 16 wt. % Fe₃O₄ would be denoted as RA (reversible adhesive). The adherents were made from commercially available glass/fiber epoxy, Garolite (G-10). The adherent materials was chosen because of its dimensional stability at the ABS processing temperature (240 °C), while also being electrically non-conductive so that it does not interact to the applied magnetic field during induction heating. The schematic representation of the lap joint has been presented in Figure 8-1 below.

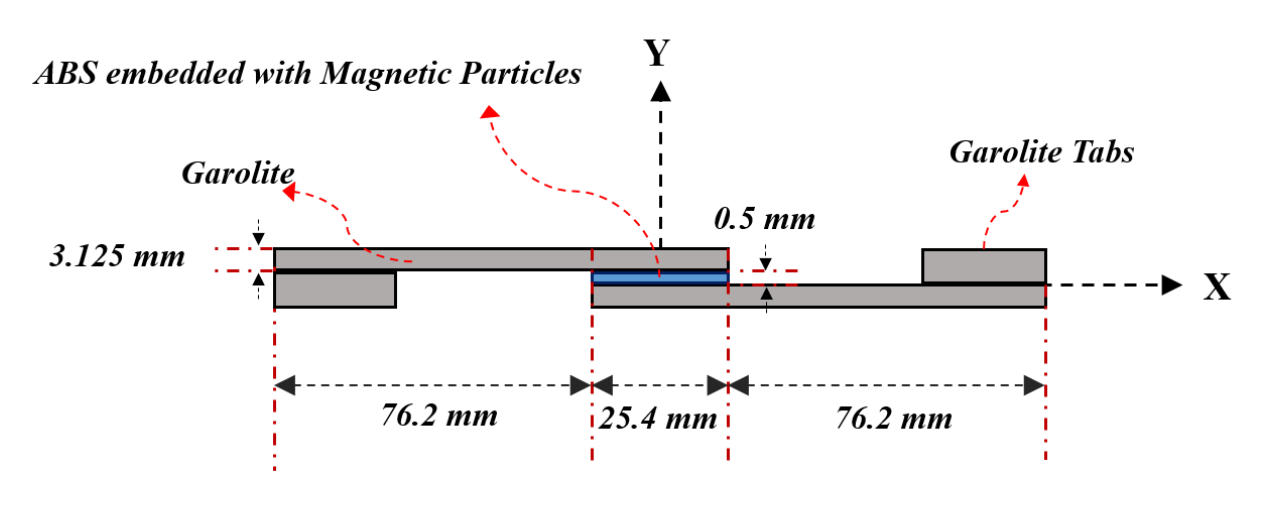


Figure 8-1: Schematic (enlarged) representation of Single Lap Joint

8.2.2. Processing and Manufacturing

The ferromagnetic nano-particles (Fe₃O₄) were mixed in ABS using a DSM Extruder. The ABS pellets were dried for 3 hours at 80°C to remove any moisture content and then dry mixed with 16 wt. % Fe₃O₄ powder. The mixture was fed to the DSM extruder barrel maintained at the melt temperature of ABS (240°C). The melted polymer and nano-particles were mixed in the barrel for 10 minutes using two inter meshing co-rotating screws set at a speed of 100 rpm. The molten mix was collected and then pressed in a Carver press to make adhesive films of 1mm thickness. The resulting films were cut into 25.4 mm x 25.4 mm. squares to be bonded with the adherents. The Garolite adherents bonding surfaces were prepared using grit blasting and plasma treatment. The adherents were grit blasted with alumina powder having spherical particles with a mean diameter of 50 microns. After cleaning the substrates with high pressure air and an acetone solvent, their bonding area was plasma treated by exposure to O₂ plasma. The O₂ pressure was maintained at 264 mTorr for 3 minutes at 275 watts, to create uniform etching of the bond surface.

Joint Manufacturing

All the lap joints were manufactured inside a convection oven. Glass rods of 0.5 mm. diameter were used as spacers to ensure consistent bond-line thickness. A spring clamping system was used to press the joints as they were heated at 240° C for 30 minutes. The clamping fixture was then removed from the oven and allowed to cool down at room temperature, before separating the joints carefully. A total of 20 lap joint samples were manufactured for testing. The final thickness of each substrates was 3.125 mm and final adhesive thickness was 0.5 ± 0.05 mm. as shown in Figure 8-1 above.

8.2.3. Testing Methods

As mentioned in section 2.2.2, a total of 20 single lap joints samples were manufactured using conventional oven heating technique. Quasi-static lap shear tests were carried out on 5 samples to develop a strength baseline. The remaining 15 samples were transversely impacted with constant energy of 10J to create a flaw in the adhesive bond-line and study its effect on lap-shear strengths. Part of the impacted samples (5) were used to study the damaged-induced behavior and the remaining samples (10) were used to heal the damage in RA and study the efficiency of healing through oven and induction heating systems.

Lap Shear Testing

The lap-shear tests were performed using ASTM D5868 standard with a cross-head speed of 5 mm./min. The tests were carried out using MTS 810 which has a load-cell with maximum capacity of 50 kN.

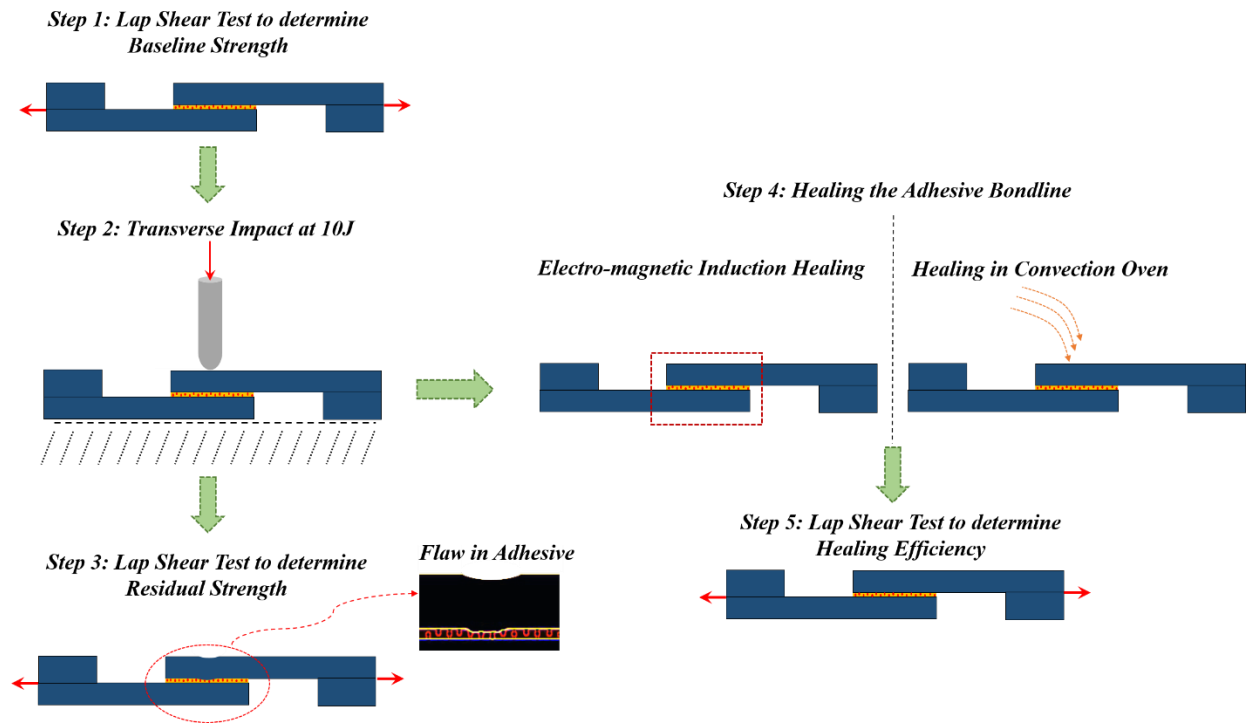


Figure 8-2: Experimental Methodology

Transverse Impact

All 15 samples were transversely impacted at the center of the bonded area using a 12.5 mm hemispherical tup. The testing was carried out using Instron Dynatup 9250HV with an impact energy of 10 J. The schematic of the test and its boundary conditions are shown in Figure 2. Pneumatic brakes were engaged in the system to prevent multiple hits. After impact, five samples were tested in lap-shear configuration to assess an average loss of strength.

8.2.4. *Healing*

Damage induced in adhesive bondline can be healed by re-melting the RA and filling up the micro-cracks/delamination introduced due to the external loads. In this study, two healing mechanisms were investigated, namely electromagnetic induction heating and oven heating.

Electromagnetic Induction Healing

Thermoplastic adhesives can achieve reversibility due to the interaction of embedded conductive nanoparticles with electromagnetic radiation. These nanoparticles act as millions of

nano-heaters to rapidly heat the surrounding polymer allowing dis-assembly and re-assembly. Post impacted bonded joint samples were healed by placing their overlap region inside a magnetic coil as shown in Figure 8-3. The frequency and current of the induction system were set 200 KHz and 30A respectively (maximum potential of the system).

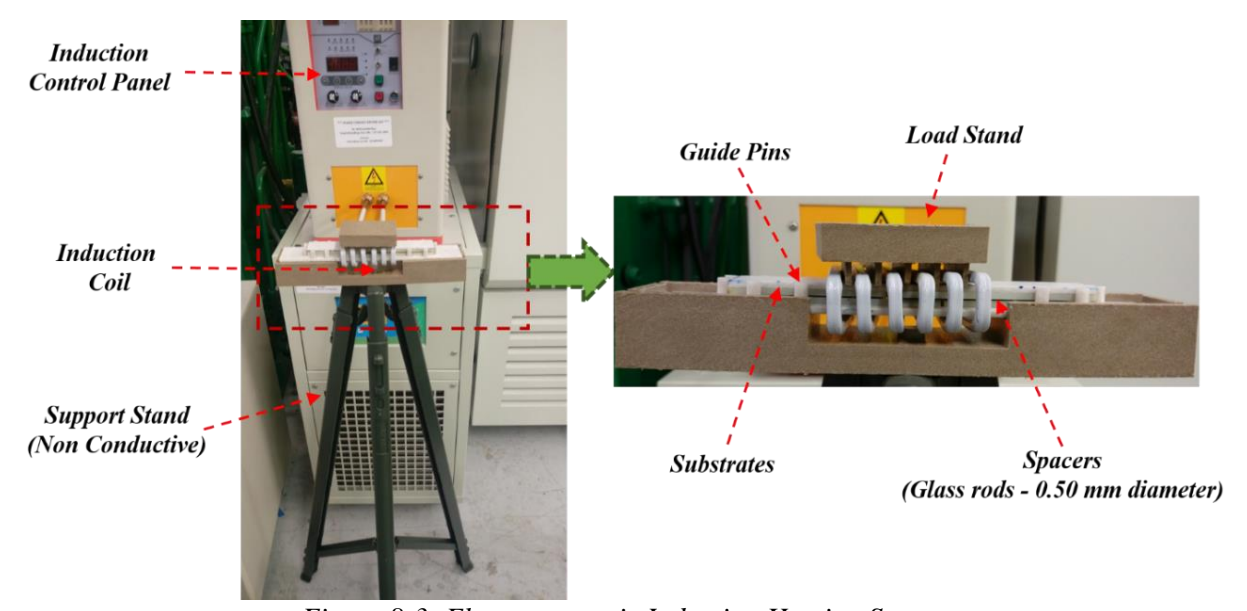


Figure 8-3: Electromagnetic Induction Heating Setup

In order to ensure a firm bond and a uniform RA thickness, the overlap region was firmly fixed using a non-conductive (ceramic) clamping-fixture with 0.5mm diameter glass rods as spacers. These joints were subjected to EM radiations before being allowed to cool down at room temperature. A constant load of 20N was applied on the load stand during the induction heating. After the induction heating process, the healed joints were tested in lap-shear configuration.

Oven Healing

Five post impacted bonded joints were placed inside the convection based oven which was maintained at 240°C. The joints were then allowed to attain thermal equilibrium for 30 minutes before being removed from the oven into ambient atmosphere. The heal strength of the joints were tested once they cooled down to room temperature. It is important to mention here that the oven heal time was optimized by embedding a high resolution distributed temperature sensor inside a

separate yet similar lap joint. Through repeated experimental observations, it was concluded that a heal time of at least 30 minutes was essential for the bulk adhesive to achieve a temperature of 240°C, at which the adhesive completely melts.

8.2.5. Fourier Transform Infrared Testing

An obvious limitation with the EM heating technique is that the heal time has to be precisely optimized so that no localized hotspots can reach temperatures at which the adhesive loses its properties. The deterioration of the RA and heal cycle optimization have been explained in detail in a later section 4.6. To understand the deterioration of RA with respect to different exposure temperatures during the EM induction process, Fourier transform infrared (FTIR) spectroscopy was carried out using FTIR-4600 from JASCO. Square shaped samples of RA having dimensions of 5mm. x 5mm. x 1.5mm (LxWxH) were used in the study and infrared spectra were recorded between spectral ranges of 4000 – 400 cm⁻¹ with a resolution of 0.7 cm⁻¹.

8.2.6. Optical Fiber Temperature Measurement

The spatial time-temperature progression of the RA when subjected to induction heating was monitored by embedding an optical fiber in the bondline. The high resolution distributed optical fiber sensor supported by Luna ODiSI-B platform facilitated in-situ characterization of temperature changes inside the RA. This optical fiber was also used for optimizing the oven heal time as mentioned above.

8.2.7. Thermogravimetric Analysis

A quantitative analysis of mass degradation with temperature in RA was carried out through thermogravimetric analysis (TGA) using TGA Q500 from TA instruments. A 20mg sample of RA was heated under a nitrogen atmosphere from a temperature range of 20°C to 800°C and a ramp rate of 10°C/min to yield the results.

8.3. Results & Discussion

8.3.1. Healing Efficiency

Healing efficiency can be described as the percentage recovery of test material's original (baseline) mechanical properties after it has suffered damage. There are number of studies in literature which used this concept to quantitatively assess the extent of recovery, however characterization of the material response is difficult to compare due to the difference in damage modes (fracture strength, fatigue life, compressive strength after impact (CAI) etc.)[11]. In this study, healing efficiency of the adhesive bondline was measured in terms of load to failure (Maximum load attained before complete joint failure) using lap shear testing based on the methodology defined in section 3.3.

8.3.2. Impact Loading

Reference force and energy curves with time have been shown in Figure 8-4. It can be seen that only a portion of the energy (~75%) was recovered during the impact event. This can be attributed to the plastic deformations in the upper adherent and RA. It is important to mention that the impact was carried out at very low energy to intentionally avoid any major structural damage to the adherents. Upon examination, it was observed that the impacted surface of the upper adherent experienced micro-indentation ~ 0.5mm deep. This plastic indentation can be observed in Figure 8-4 b. The corresponding maximum elastic displacement of the indenter was around 2.14 mm as reported in the load-displacement curve in Figure 8-4 c.

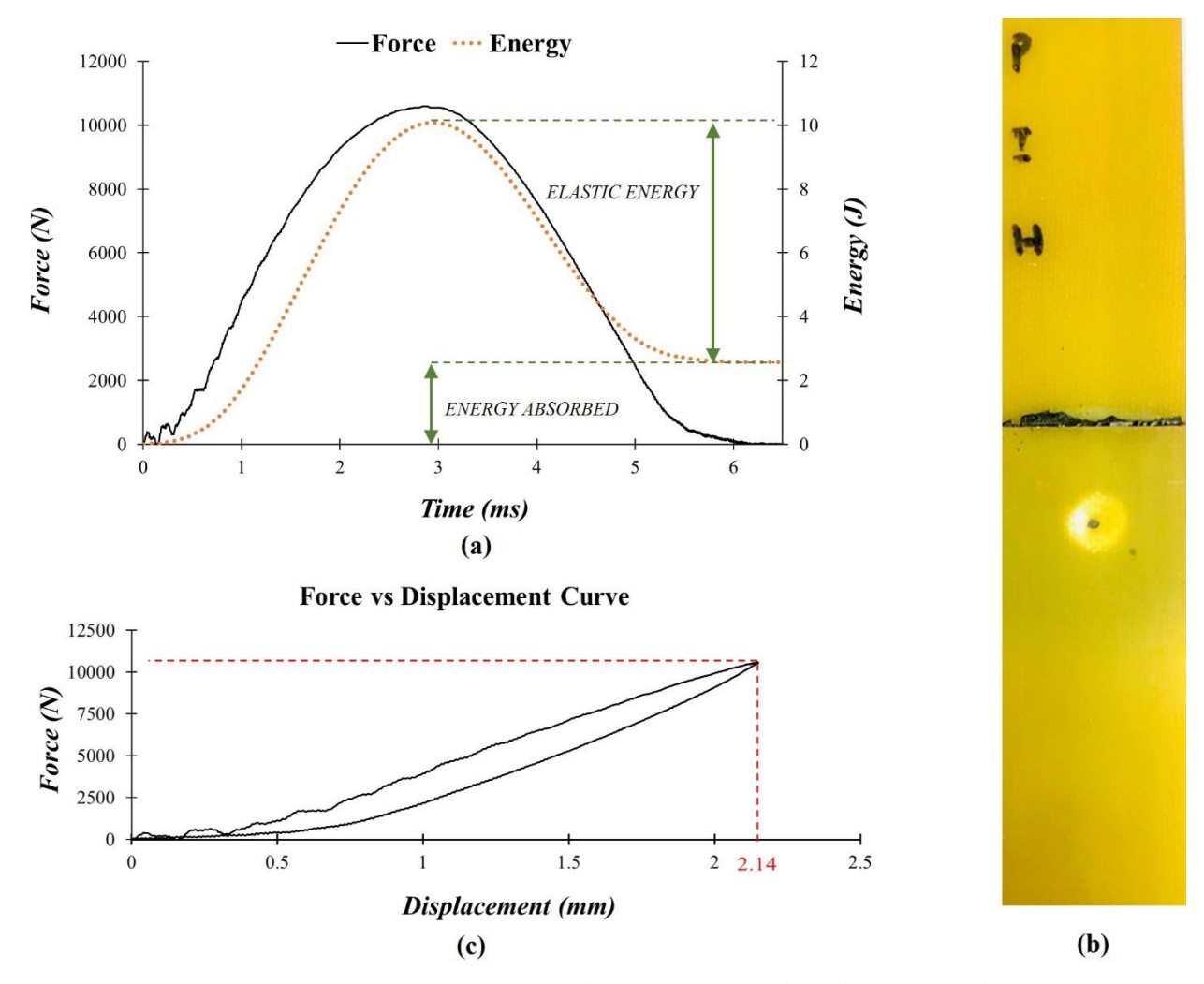


Figure 8-4 (a) Representative curves for Force and Energy vs Time (b) Indentation in the upper substrate (Specimen Top View) (c) Force vs Displacement curve showing the maximum displacement of the tup

8.3.3. Lap Shear Tests

Quasi-static lap shear tests were carried out on baseline, impacted and impacted/healed samples to quantify the healing efficiency. A comparison of the load-to-failure and displacement-to-failure in the aforementioned three cases was performed and is shown in Figure 8-4. As expected, there was a significant reduction in the joint strength after the impact event. It was also observed that both induction and oven heating result in an 'average' increase of load bearing capability and strain-to-failure. The average percentage variation of load and failure strains for the three cases has been detailed in Table 1 below.

8.3.4. Joint Strength

Figure 8-5 shows that although the joint strength reduced sharply due to transverse impact, the damaged samples were able to regain significant residual strength after both healing

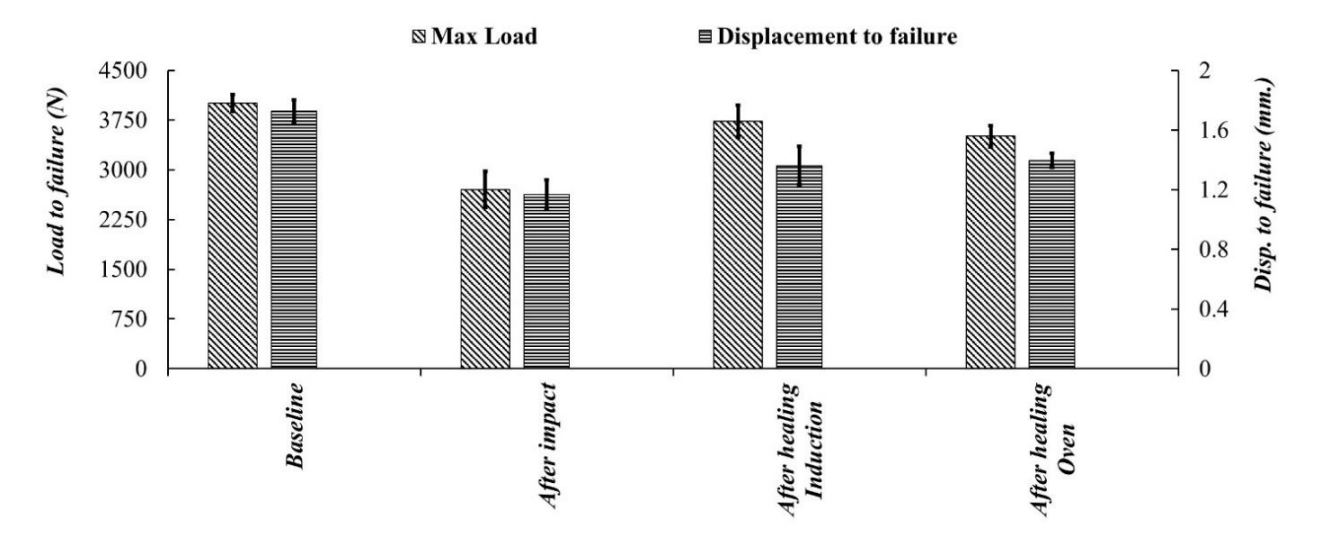


Figure 8-5. Comparison of load and displacement bearing capability in similar joints

processes. It can be seen from Table 8-1 that all healed samples recovered a major portion (~90%) of baseline peak loads. One of the potential causes for loss in joint strength can be attributed to the geometric deformities inflicted to the upper adherent due to the transverse impact load. Although, the impact was performed in a low energy regime, a localized indentation (see Figure 4b) was observed on the surface of the upper adherent. This plastic indent can be directly attributed to energy absorption during the impact event. As can be seen in figure 4a, a part of the energy is absorbed by the joint, while the remaining elastic energy is dissipated. This absorbed energy of impact also forces the adhesive beneath the plastic dent to displace out, a phenomena which the authors have defined as 'shear displacement'. Upon further loading the joint in quasi-static lap shear mode, this shear displacement can be a source of crack initiation in the surrounding RA which may lead to accelerated crack propagation and joint failure.

Table 8-1: Percentage variation of average peak load and displacement

	Average Load to Failure	Avg. Displacement to
	relative to baseline	Failure relative to baseline
After Impact	Reduced by 33 %	Reduced by 32 %
After Healing (Induction)	93% recovered	79 % recovered
After Healing (Oven)	92% recovered	81 % recovered

8.3.5. Joint Toughness

A significant loss in ductility was observed in the impacted samples as can be seen in Figure 8-6, which show a representative comparison of load vs displacement curves for all the cases under consideration in this study. Interestingly enough, this loss of property was not properly recovered even after the healing processes. The impact event caused an average one-third reduction in displacement-to-failure w.r.t baseline samples, which can be attributed to the deformation incurred by the upper adherent during the impact event and the subsequent permanent shear displacement of the adhesive beneath it. Upon healing the impacted samples through both EM and oven, although the damage/micro-cracks in the adhesive was expected to be healed, the physical deformation due to impact is still in existence. This hinders the uniform crack propagation within the bondline and results in premature failure of the joint. A detailed breakdown of post-impact recoverable toughness can be seen in Table 8-1. Both healing processes were only able to recover around ~80% ductility. Another probable cause for reduction in ductility can be attributed to the thermal degradation of RA during induction heat treatment. However as can be seen in Figure 8-6, its effect is minimal.

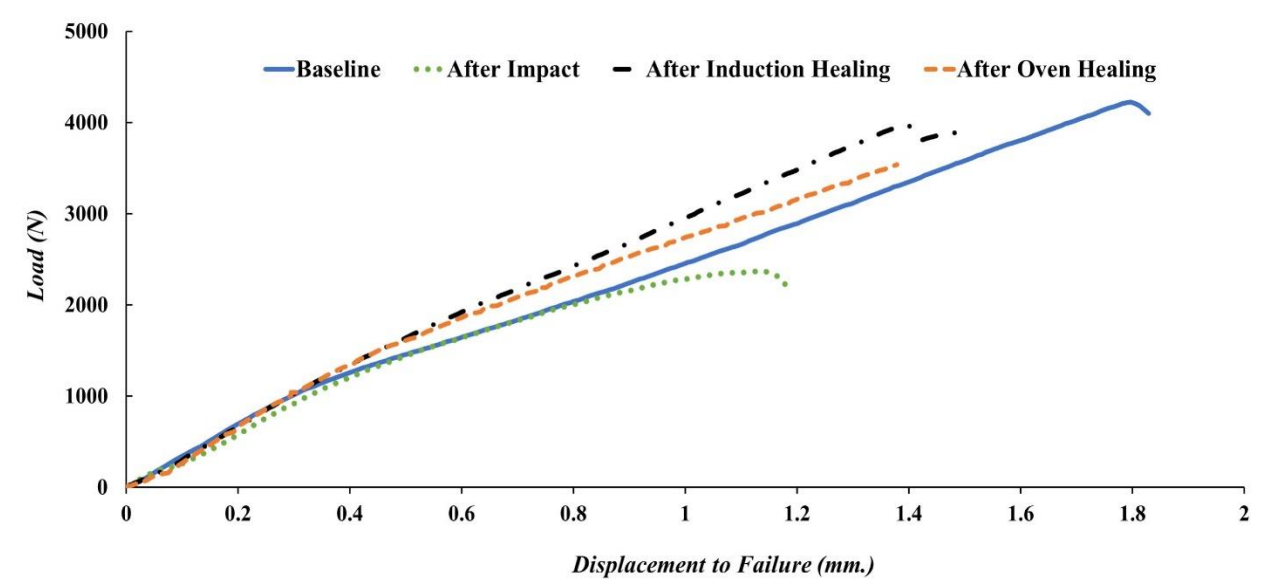


Figure 8-6: Representative Load-Displacement Curves for different cases

8.3.6. Optimum Healing Time for Electromagnetic Heating

A critically important parameter which drives the healing efficiency in RA is the temperature exposure time. As described in section 1, electromagnetic induction heating is an intrinsic heating mechanism in which the conductive susceptors heat the surrounding polymer upon exposure to EM radiation. Optimizing healing time to ensure that the magnetic particles do not become overheated therefore becomes paramount. The optimum healing time required for induction healing depends on a number of parameters;

- 1. Weight percentage of conductive particles
- 2. Melting temperature of thermoplastic
- 3. Size of the defect (induced by out of plane impact at 10 J)
- 4. EM parameters such as frequency, power, current and shape of the coil
- 5. Thermo-oxidative degradation of host polymer

Considering that the first four parameters were constant throughout, the optimum healing time for EM heating was optimized based on thermo-oxidative degradation of the ABS polymer, using FTIR. Thermal degradation in RA was observed after exposing it to 240 °C, 315 °C, 350 °C

and 370 °C. The time required by the adhesive bondline to reach these temperatures was measured using a high-resolution optical fiber sensor. The technique has been described in detail in Vattathurvalappil [3], [5], [33] and provides in-situ temperature variation with time in the RA bondline.

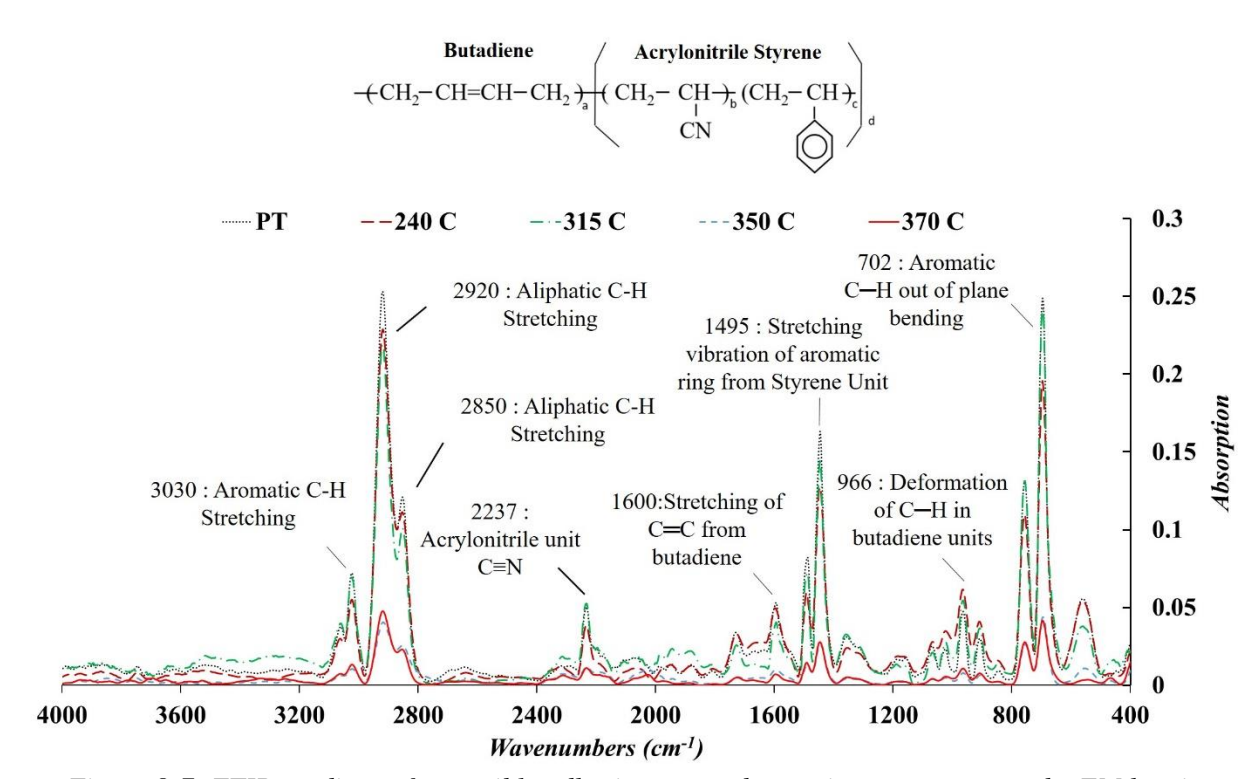


Figure 8-7: FTIR readings of reversible adhesive exposed to various temperatures by EM heating

The selection of above-mentioned temperatures were based on the output of TGA carried out to determine different temperatures at which ABS mass degradation occurs. The first temperature point (240°C) was selected as the processing point of ABS [34]; 315 °C and 350 °C were the 1% and 2% mass degradation temperatures and 370 °C was the onset degradation temperature of ABS polymer[35]. Figure 8-7 shows different infrared (IR) absorption peaks, marked by unique wave numbers, each representing different molecular constituents in RA. Here, pre-heat treatment (PT) represents the adhesive samples prior to the induction heating. It can be seen that at higher temperatures (350 °C and 370 °C), the magnitude of the absorption peaks reduced reduces significantly (~75%). This steep decline in the peaks is indicative of the thermal

degradation experienced by RA at these temperatures. Interestingly, the samples exposed to 240°C were also affected by EM heating technique which probably accounts for some loss of ductility experienced in the oven healed samples. Also, the peaks at 315 °C follow nearly the same path as that of the peaks observed at melting temperature. Among the three monomers - acrylonitrile, butadiene and styrene – which constitute the RA, butadiene is widely understood to be the critical monomer responsible for the loss in ductility/toughness [32], [36], [37]. As shown in Figure 8-7, peaks corresponding to peaks 966 and 1600 represents the butadiene units in FTIR. At higher temperatures, these peaks flatten out which results in loss of ductility. It therefore becomes paramount that the RA is exposed to EM radiations only for a limited time, such that the localized hot spots which develop due to magnetic induction do not reach temperatures where surrounding butadiene matrix completely degrades. Through careful experimentation and subsequent toughness characterization of reversible ABS, the optimized heal time was set as 30 seconds. Under the current configuration, this exposure time allowed for appropriate healing efficiency and reasonable loss in ductility. It is important to note that while both EM and oven heating resulted in similar recovery of joint strength and ductility, the time taken by EM heating was significantly less - 60 times quicker than the oven heating time. It is also important to note, that unlike EM heating, the temperature remains the same at every point in the material inside an oven. However, the polymer can still degrade if the exposure time is not controlled for an extended duration, even if the temperature is lower than its processing point [32].

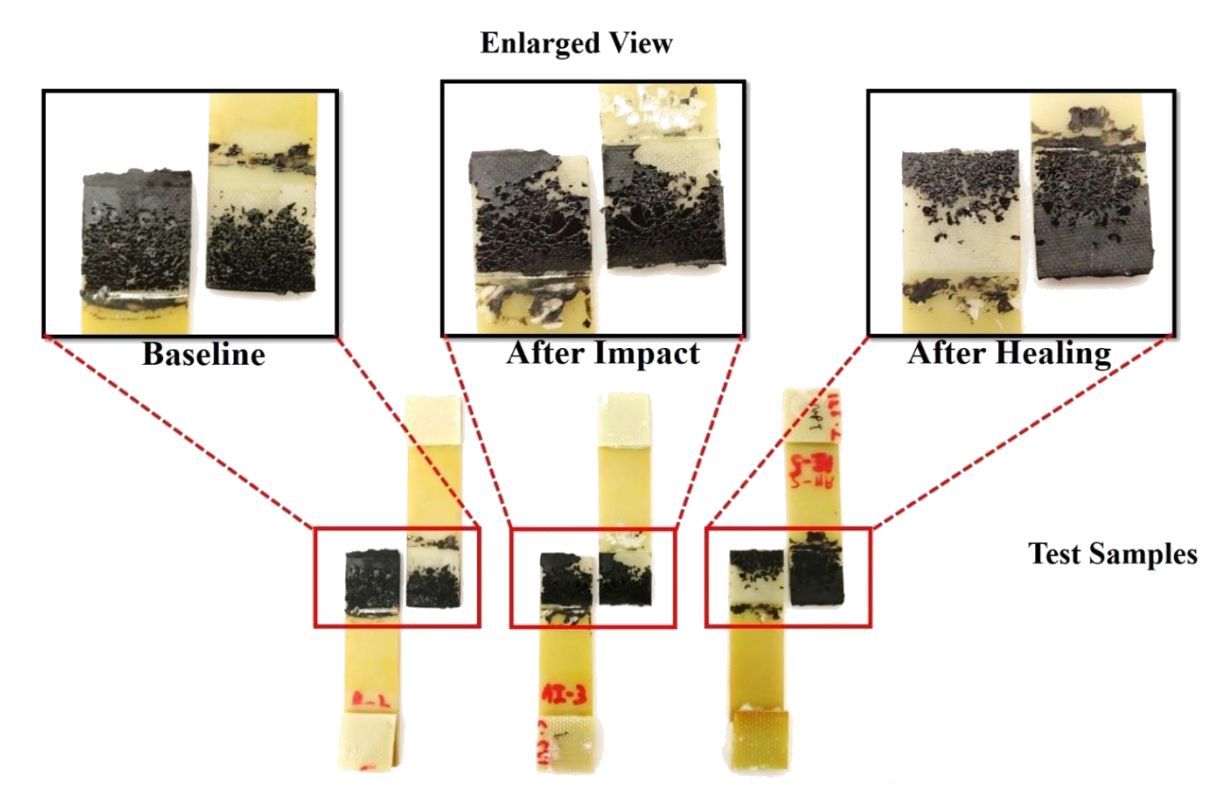


Figure 8-8: Fracture surfaces in baseline, impacted and induction healed adhesive joints 8.3.7. Fracture Analysis

The fracture surfaces of representative joints for baseline, impacted and impacted/induction healed joints are shown in Figure 8-8 above. In all the cases, a cohesive failure of the joints was observed. In the induction healed joints however, the embrittlement of RA caused by thermal degradation results resulted in lesser cohesiveness. This signifies the fact that even with optimized heating, it is virtually impossible to prevent the formation of high temperature localized hot spots in the RA.

8.4. Conclusions

In this study, the concept of healing in joints bonded using 'reversible adhesive' was investigated using electromagnetic induction and oven heating techniques. Healing efficiency was assessed on the recovery of baseline joint strength. Although full recovery was not possible due to permanent indentation on the upper adherent and shear displacement of adhesive beneath it, the

healing efficiency was consistently above 92% in both induction and oven healed specimens. The healing process was also shown to have a detrimental effect on the ductility of the reversible adhesive. FTIR, TGA and optical fiber temperature measurements techniques were used to optimize the heal time for EM technique based on thermo-oxidative degradation of the adhesive. The induction heal time was 60 times lesser than required in oven healing for the same values of joint strength and toughness. Incorporating non-destructive tools and numerical modeling in conjunction the healing process would provide valuable insight in better understanding the behavior of these novel joints. Nevertheless, the results in this work show promise in the healing ability of the reversible adhesives.

REFERENCES

REFERENCES

- 8-[1] P. Ayeni, T. Baines, H. Lightfoot, and P. Ball, "State-of-the-art of 'Lean' in the aviation maintenance, repair, and overhaul industry," *Proc. Inst. Mech. Eng. Part B J. Eng. Manuf.*, vol. 225, no. 11, pp. 2108–2123, 2011.
- 8-[2] M. Davis and D. Bond, "Principles and practices of adhesive bonded structural joints and repairs," *Int. J. Adhes. Adhes.*, vol. 19, pp. 91–105, 1999.
- 8-[3] S. H. Vattathurvalappil and M. Haq, "Thermomechanical characterization of Nano-Fe3O4 reinforced thermoplastic adhesives and single lap-joints," *Compos. Part B Eng.*, vol. 175, Oct. 2019.
- 8-[4] S. H. Vattathurvalappil and M. Haq, "Experimental And Numerical Investigation Of Bonded Joints Subjected To Transverse Impact Loads," in *SPE ACCE*, 2017.
- 8-[5] S. H. Vattathurvalappil, S. F. Hassan, and M. Haq, "Monitoring Residual Strains in Ovenand Induction-bonded Joints," 2019.
- 8-[6] E. Verna *et al.*, "Adhesive joining technologies activated by electro-magnetic external trims," *Int. J. Adhes. Adhes.*, vol. 46, pp. 21–25, 2013.
- 8-[7] R. Ciardiello, G. Belingardi, B. Martorana, and V. Brunella, "Physical and mechanical properties of a reversible adhesive for automotive applications," *Int. J. Adhes. Adhes.*, vol. 89, pp. 117–128, Mar. 2019.
- 8-[8] T. Bayerl, Application of Particulate Susceptors for the Inductive Heating of Temperature Sensitive Polymer-Polymer Composites. Kaiserslautern: Institut f. Verbundwerkstoffe, 2012.
- 8-[9] T. Bayerl, R. Schledjewski, and P. Mitschang, "Induction Heating of Thermoplastic Materials by Particulate Heating Promoters," *Polym. Polym. Compos.*, vol. 20, no. 4, pp. 333–342, May 2012.
- 8-[10] P. Zhang and G. Li, "Advances in healing-on-demand polymers and polymer composites," *Progress in Polymer Science*, vol. 57. Elsevier Ltd, pp. 32–63, 01-Jun-2016.
- 8-[11] M. D. Banea, L. F. M. Da Silva, R. D. S. G. Campilho, and C. Sato, "Smart adhesive joints: An overview of recent developments," in *Journal of Adhesion*, 2014, vol. 90, no. 1, pp. 16–40
- 8-[12] S. R. White *et al.*, "Autonomic healing of polymer composites," *Nature*, vol. 409, no. 6822, p. 794, 2001.

- 8-[13] H. Jin, G. M. Miller, N. R. Sottos, and S. R. White, "Fracture and fatigue response of a self-healing epoxy adhesive," *Polymer (Guildf).*, vol. 52, no. 7, pp. 1628–1634, Mar. 2011.
- 8-[14] H. Jin *et al.*, "Fracture behavior of a self-healing, toughened epoxy adhesive," *Int. J. Adhes. Adhes.*, vol. 44, pp. 157–165, 2013.
- 8-[15] S. Khoee and Z. Kachoei, "Design and development of novel reactive amine nanocontainers for a self-healing epoxy adhesive: Self-repairing investigation using the lap shear test," *RSC Adv.*, vol. 5, no. 27, pp. 21023–21032, 2015.
- 8-[16] N. I. Khan, S. Halder, and M. S. Goyat, "Effect of epoxy resin and hardener containing microcapsules on healing efficiency of epoxy adhesive based metal joints," *Mater. Chem. Phys.*, vol. 171, pp. 267–275, Mar. 2016.
- 8-[17] N. I. Khan, S. Halder, and M. S. Goyat, "Influence of dual-component microcapsules on self-healing efficiency and performance of metal-epoxy composite-lap joints," *J. Adhes.*, vol. 93, no. 12, pp. 949–963, Oct. 2017.
- 8-[18] G. Li, G. Ji, and O. Zhenyu, "Adhesively bonded healable composite joint," *Int. J. Adhes. Adhes.*, vol. 35, pp. 59–67, Jun. 2012.
- 8-[19] G. Li and N. Uppu, "Shape memory polymer based self-healing syntactic foam: 3-D confined thermomechanical characterization," *Compos. Sci. Technol.*, vol. 70, no. 9, pp. 1419–1427, 2010.
- 8-[20] W. Xu and G. Li, "Constitutive modeling of shape memory polymer based self-healing syntactic foam," *Int. J. Solids Struct.*, vol. 47, no. 9, pp. 1306–1316, 2010.
- 8-[21] G. Li and D. Nettles, "Thermomechanical characterization of a shape memory polymer based self-repairing syntactic foam," *Polymer (Guildf)*., vol. 51, no. 3, pp. 755–762, 2010.
- 8-[22] H. Özer and E. Erbayrak, "Experimental Investigation on the Self-Healing Efficiency of Araldite 2011 Adhesive Reinforced with Thermoplastic Microparticles," in *Adhesives Applications and Properties*, InTech, 2016.
- 8-[23] J. H. Aubert, "Thermally removable epoxy adhesives incorporating thermally reversible Diels-Alder adducts," *J. Adhes.*, vol. 79, no. 6, pp. 609–616, 2003.
- 8-[24] D. G. Bekas *et al.*, "Self-healing polymers: Evaluation of self-healing process via non-destructive techniques," *Plast. Rubber Compos.*, vol. 45, no. 4, pp. 147–156, Mar. 2016.
- 8-[25] J. Tang, L. Wan, Y. Zhou, H. Pan, and F. Huang, "Strong and efficient self-healing adhesives based on dynamic quaternization cross-links," *J. Mater. Chem. A*, vol. 5, no. 40, pp. 21169–21177, 2017.
- 8-[26] A. Manufacturing, C. Canada, and S. Laurent, "Fusion Bonding/Welding of Thermoplastic

- Composites," vol. 17, no. July 2004, pp. 303–341.
- 8-[27] T. J. Ahmed, "Induction welding of thermoplastic composites an overview," vol. 37, pp. 1638–1651, 2006.
- 8-[28] V. Rudnev, D. Loveless, R. Cook, and M. Black, *Handbook of induction heating*. Basel: Marcel Dekker AG, 2003.
- 8-[29] T. E. Tay, B. K. Fink, S.H.McKnight, S.Yarlagadda, and J. W. Gillespie, "accelerated curing of adhesives in bonded joints using induction heating.pdf," *J. Compos. Mater.*, vol. 33, no. 17, 1999.
- 8-[30] J. Kolbe *et al.*, "Curable bonded assemblies capable of being dissociated." Google Patents, 04-Aug-2009.
- 8-[31] H. Polli, L. A. M. Pontes, A. S. Araujo, J. M. F. Barros, and V. J. Fernandes, "Degradation behavior and kinetic study of ABS polymer," *J. Therm. Anal. Calorim.*, vol. 95, no. 1, pp. 131–134, 2009.
- 8-[32] B. E. Tiganis, L. S. Burn, P. Davis, and A. J. Hill, "Thermal degradation of acrylonitrile-butadiene-styrene (ABS) blends," *Polym. Degrad. Stab.*, vol. 76, no. 3, pp. 425–434, 2002.
- 8-[33] S. F. Hassan, S. H. Vattathurvalappil, and M. Haq, "Effect of Cooling Rate on Curing Induced Thermal Strains in Bonded Joints," 2019.
- 8-[34] SABIC, "CYCOLAC TM Resin MG94UAmericas: Commercial," 2016.
- 8-[35] R. Zong, Y. Hu, N. Liu, S. Wang, and G. Liao, "Evaluation of the thermal degradation of PC/ABS/montmorillonite nanocomposites," *Polym. Adv. Technol.*, vol. 16, no. 10, pp. 725–731, 2005.
- 8-[36] J. Shimada and T. Electrical, "The Mechanism of Oxidative Degradation of ABS Resin. Part I. The Mechanism of Thermooxidative Degradation," vol. 12, pp. 655–669, 1968.
- 8-[37] J. Bergstrom, *Mechanics of solid polymers:theory and computational modeling*, 1st ed. Amsterdam: Elsevier, 2015.

Chapter 9: Summary and Conclusions

9.1. Summary

Thermoplastic adhesives reinforced with conductive nanoparticles (reversible adhesives) allow for selective heating of thermoplastics through coupling with electromagnetic (EM) radiations via non-contact methods. This allows for increasing the adhesive temperature above the processing temperatures in a short duration which upon cooling forms a structural bond. Hence this process is attractive as it enables quick assembly, removal and re-assembly of joints without the need to heat the entire component. An integrated experimental and numerical characterization approach was developed in this work, leading to prediction of the global structural response of a single-lap joint based upon the local/micro-mechanical modeling. The influence of material heterogeneities and EMI heating was studied and implemented in the material scale of the multiscale model. The thermo-mechanical degradation during the adhesive manufacturing and its effect on reversibility and mechanical properties was also studied. The bonded joints manufactured using reversible adhesives also exhibited a potential to heal the damage induced in the bondline. Healing was done through exposure of the joint to EM radiations after the impact/damage event. Various surface techniques and concentrations of FMNP and SCF were studied to understand the best performance for bonded joints. The numerical models were experimentally validated. These experimentally validated simulations (EVS) act as a powerful prediction and design tool to explore the design space beyond the experimental matrix explored in this work. Furthermore, the measurement and understanding of manufacturing induced residual strains in the computational model makes it more realistic in performance prediction and design of bonded joints. In addition to reversible bonding, the healing potential of the reversible adhesives upon controlled exposure

of electromagnetic radiation creates infinite opportunities in automotive, aerospace and defense sectors as it enables rapid maintenance and repair without any removal of components.

Overall, a successful computational scheme that was experimentally validated at each length scale was developed to predict the behavior of complex, multi-particle reinforced, reversible adhesives and resulting joints. This computational framework also acts as a robust design tool and database generator for a wide-range of joints. Overall, the approach taken in this work can be extended to the development of other complex materials and structures such as those performed in this work

9.2. Research Finding's

9.2.1. Development of Reversible Adhesives

- Reversible adhesives were manufactured using ABS (acrylonitrile butadiene styrene) thermoplastic reinforced with Fe₃O₄ nanoparticles and short carbon fibers. This work studied the influence of Fe₃O₄ and short carbon fibers on mechanical behavior of reversible adhesives. Also, the heating response of reversible adhesives upon exposure to EM radiation was also characterized. While the adhesive used in this work was ABS, the approach is thermoplastic independent, indicating that any thermoplastic reinforced with the right conductive particles and exposed to the right electromagnetic radiations can be processed using the approach proposed in this work. With that said, the dispersion, chemical functionalization, thermo-mechanical properties and degradation characteristics will change depending on the thermoplastic polymer selected.
- With the use of fiber-optic sensors, the minimum concentration (percolation limit) of FMNP in ABS to interact to electromagnetic radiation was 8 wt.%. Nevertheless, this will vary with the choice of thermoplastic. Similarly, lower concentrations will take a much

longer time which will be impractical and higher concentrations can lead to embrittlement and loss in mechanical properties.

9.2.2. Bonded Joints Using Reversible Adhesives

- Glass fiber reinforced substrates were bonded using reversible adhesives by electromagnetic induction heating. While the surface treatment of substrates to increase adhesion is well-established, the additional surface preparation of thermoplastic adhesive film in this work needs further explanation. The commercial thermoplastics are designed for injection molding and have proprietary release agents to enable face demolding. Using such thermoplastics for bonded joints will lead to interfacial failure. Hence, O₂ plasma treatment of adhesives films was performed to etch the surfactant and release agents away to have a strong bond with the substrates.
 - Similarly, the temperature of the substrates when molten adhesive comes into contact with the substrates is vital to create a good bond. A molten adhesive in contact with a cold surface/substrate will create a skin-effect inhibiting the polymer flow leading to kissing bonds and interfacial failure. Joints bonded with preheated substrates outperformed joints bonded with substrates at room temperature. The joints manufactured in convection oven (and not EM heating) do not have the preheating constraint as the entire joint assembly heats up uniformly and cools gradually to create the bond. The preheating of substrates is hence required for successful induction bonded joints. The FMNP particles used were 'asreceived' and were not functionalized. This was 'by design' to create a control / lower limit to thermo-mechanical properties of resulting adhesives and joints. Any functionalization and enhancements in dispersion will only advocate for better reversible adhesive and joints.

Overall, the induction bonded joints decreased the time required to manufacture joints significantly relative to oven bonded joints, thereby reducing the possibility of degradation of the substrates. Computational framework developed in this work along with statistical tools can further enable finding optimal material configurations that could lead to multiproperty synergistic behavior.

9.2.3. Thermo-Mechanical Degradation of Reversible Adhesives Subjected to EM Heating

- This work studied the thermal degradation of ABS/Fe₃O₄ polymer nanocomposite (PNC) under electromagnetic induction heating and its effect on mechanical properties.
- The results of this study demonstrated that repeated EM heating of PNCs, even with the temperature maintained at the processing point, introduces thermo-oxidative degradation and deteriorates the toughness of the polymer by 40 %.
- However, the tensile modulus and yield strength were not significantly degraded in the repeated heating cycles. Longer exposure time to EM radiations resulted in high temperatures and deteriorated both the tensile and IZOD impact properties of the PNC's.
- FTIR results showed degradation of ABS polymer even when the bulk temperature reached its processing temperature (240 °C) due to electromagnetic induction heating. This was attributed to the phenomena wherein the bulk temperature is within 240 °C but the local temperature in the vicinity of nanoparticles far exceeds 240 °C thereby leading to degradation.
- The void pattern found within the fracture surfaces suggests that the eddy current/ Joule heating might be the dominant heating mechanism. Scanning electron microscopy and laser ablation inductively coupled mass spectroscopy (LA-ICP-MS) confirmed the presence of mold-flow artifacts wherein the concentration of nanoparticles was lower at the edges of

the sample and higher at the center of the sample. Hence, when the electromagnetic radiation is applied, the region in the sample wherein the concentration of the particles is large enough to form eddy currents within the agglomerated particles interacts to the radiations causing a so-called skin-effect. This leads to the structured void patterns observed.

9.2.4. Computational Modeling

- In this study, a computational framework was developed for reversible adhesives containing multiple reinforcements within the ABS polymer. The effect of particle morphologies, individual concentrations, interphases, dispersion, particle clustering and particle orientations on the tensile modulus were investigated as a part of this work. Additionally, two reinforcements were considered in this work, namely Fe₃O₄ nanoparticles (FMNP) and short carbon fibers (SCF).
- Optical and scanning electron microscopic images were used to aid the realistic/accurate development of representative volume elements (RVES).
- Additionally, an interphase region was created and modeled based upon the earlier work
 reported in literature. The elastic modulus of interphase was estimated based on the
 analytical formulations and was found to be larger than the host polymer. The interphase
 properties were implemented into the finite element model by defining an interphase region
 around the nanoparticles.
- The computational models predicted the tensile modulus obtained from the experiments within an error range of 5 percent.

- A multi-scale modeling approach was developed wherein the structural (macroscale)
 behavior of a single lap-joint bonded with reversible adhesive was predicted by detailed
 modeling at the lower (material level) scale.
- The multi-scale model predicted the linear-elastic response of a lap-joint containing ABS/16 wt.% FMNP adhesive. The multiscale predictions agreed (100%) with the experiments up to a load of 1000 N and slightly overpredicted beyond that point.
- Despite the slight overprediction, the multi-scale simulations agreed with the experimental response with an error of less than 5%.
- Overall, this approach can easily be translated to other heterogeneous materials and structures. Future work should focus on incorporation of material non-linearity and failure models.

9.3. Research Needs

9.3.1. Nanoparticle Dispersion Studies

Dispersion of nanoparticles in polymer matrix is important to reduce the clustering and associated stress concentration with it. Dispersed nanoparticles can also help reduce/eliminate eddy current/ Joule heating and enable controlled hysteresis mode of heating.

9.3.2. Processing Induced Behavior of Bonded Joints

This work addressed some issues dealing with processing induced residual strains in single lap joints. Nevertheless, there is a need for better understanding on the EM interaction of the adhesive and the substrates. A coupled electromagnetic and mechanical behavior based multiphysics simulations can enlighten some of the underlying phenomena. For instance, a computational model for the prediction of residual strain development in bonded joints manufactured using EM heating can help predict joint failure more accurately.

9.3.3. Incorporation of robust failure models in the computational framework

This work focused on development of robust representative volume elements (RVEs) that incorporated all heterogeneities, their morphology, interphases and distribution as 'realistic' to the 'real' material as possible. These RVEs were then experimentally validated and used in the multiscale framework to predict the macro-structural behavior of lap-joints. This multi-scale framework focused only on linear-elastic behavior. Future work should focus on incorporation of material non-linearities and failure models.